CRANFIELD UNIVERSITY
Escuela Técnica Superior de Ingeniería de Bilbao
UPV/EHU

Fernando LARTATEGUI ATELA

AIRCRAFT PERFORMANCE WITH ONBOARD WATER CONDENSED FROM ENGINE CORE EXHAUST FOR CONTRAIL PREVENTION

Comportamiento de aeronaves transportando agua condensada del escape para prevenir la formación de estelas

SCHOOL OF AEROSPACE, TRANSPORT AND MANUFACTURING
Thermal Power MSc

MSc THESIS
Academic Year: 2015 - 2016

UPV/EHU Supervisor: Dr C. Pinto
Cranfield Univ. Supervisors: Prof P. Pilidis & Dr D. Nalianda
August 2016

CRANFIELD UNIVERSITY

SCHOOL OF AEROSPACE, TRANSPORT AND MANUFACTURING
Thermal Power MSc

MSc Thesis

Academic Year 2015 - 2016

Fernando Lartategui Atela

Aircraft Performance with Onboard Water Condensed from Engine Core Exhaust for Contrail Prevention

Supervisors: Prof P. Pilidis & Dr D. Nalianda
August 2016

This thesis is submitted in partial fulfilment of the requirements for the degree of Master of Science

© Cranfield University 2016. All rights reserved. No part of this publication may be reproduced without the written permission of the copyright owner.

ABSTRACT

Aviation industry has experienced a constant growth over the last decades, and forecasts suggest that this trend will continue. This is not attractive from an environmental point of view due to the increasing contribution of aviation to Global Warming. Significant research has been done on aircraft emissions. It suggests that the impact of contrails and aircraft induced cirrus formed by water vapour within the engine might be significant enough to be a concern.

Consequently, several contrail avoidance strategies have been designed during the last two decades, but they all present the same drawback: a fuel overconsumption. One of these strategies consists in condensing the water vapour within the engine, so that it can be stored on the aircraft or released into the atmosphere in a controlled manner. This technique is the basis of the current work.

The aim of this study is to investigate the feasibility of storing water onboard and establish the effects it may have on aircraft performance. To assess the penalties of the technique, an analytical model of the aircraft capable of water storage was developed. Once the penalties were determined, the net balance between the positive effect of contrail prevention and the negative effect of the additionally emitted CO_2 is calculated.

From these analyses, it was concluded that if contrails are avoided in 2020 a 40-50% reduction in total aviation radiative forcing could be achieved in 2050 due to this contrails prevention technique. However, the water-carrying aircraft experienced a 23.23% range reduction for the same fuel and a 17.35% fuel burn penalty for the same range in comparison to the design point of the baseline aircraft.

Keywords:

fuel burn penalty, global warming, payload, radiative forcing, range, reduction, water storage

ACKNOWLEDGEMENTS

I would like to express my most sincere gratitude to those who accompanied me during this exciting adventure with a special mention.

A very special thanks to my supervisors Dr Devaiah Nalianda and Prof Pericles Pilidis for their guidance through my MSc thesis, and for helping me when I was lost. The Global Warming meetings were precious and a steady source of motivation and ideas.

I would also like to express my gratitude to the PhD student Sarah Qureshi for the help and inspiration provided during all this project.

The valuable conversations with Prof Riti Singh about Global Warming and Global Cooling are gratefully acknowledged too.

I would also want to thank the support received from Dr Theoklis Nikolaidis, who helped me with the engine creation using Turbomatch.

Additionally, I would also want to acknowledge to my group colleagues Shaila Baghail and Ahmed Mahmoud, with whom I share ideas for the common interest.

Finally, I have to mention and express my gratitude to my family, friends and especially, to my beautiful girlfriend, Oli, who supported me during this adventure.

TABLE OF CONTENTS

LIST OF FIGURES

LIST OF TABLES

NOMENCLATURE

SYMBOLS

C_D	Drag coefficient	[-]
C_{D0}	Profile drag coefficient	[-]
C_{Dl}	Lift dependent coefficient	[-]
C_L	Lift coefficient	[-]
c_p	Specific heat capacity	[J/(kg K)]
D	Drag	[N]
G	Slope of the mixing line	[-]
g	Gravity acceleration	[m/s^2]
h	Altitude	[m]
L/D	Lift to drag ratio	[-]
M	Mach number	[-]
M_d	Molar weight of the droplet	[kg/mol]
P	Stagnation pressure	[Pa]
Q	Net calorific value per mass of fuel	[J/kg]
R	Ideal gas constant	[J/(mol K)]
r_d	Droplet radius	[m]
S	Wing reference area	[m^2]
T	Stagnation temperature	[K]
TAS	True Airspeed	[m/s^2]
W	Weight	[kg]
γ	Ratio of specific heat	[-]
γ_t	Surface tension	[N/m]
Δ	Variation	[-]
ε	Water vapour-to-air molar mass ratio	[-]
η	Overall engine efficiency	[-]
λ	Climate feedback parameter	[(K m^2)/W]
ρ	Density	[kg/m^3]

SUBSCRIPTS AND SUPERSCRIPTS

A/C	Aircraft
amb	Ambient conditions
cri	Critical conditions
d	Droplet
eng	Engine
exh	Exhaust conditions
LW	Long-wave
s	Saturation conditions
seg	Cruise segment
surf	Earth surface conditions
SW	Short-wave
w	Water

LIST OF ABBREVIATIONS

AAGR	Average Annual Growth Rate
AIC	Aircraft Induced Cirrus
Avtur	Aviation turbine fuel
BPR	Bypass Pressure Ratio
CCC	Committee on Climate Change
CEEC	Clean Exhaust Engine Concept
CH_4	Methane
CO_2	Carbon dioxide
COT	Combustor Outlet Temperature
DP	Design Point
EASA	European Aviation Safety Agency
EI	Emission index (Subscripts of water and CO2 are not included)
Ex	Excel output
GHG	Greenhouse gas
GTP	Global Temperature Potential
GTPP	Global Temperature Potential (Pulsed emissions)
GTPS	Global Temperature Potential (Sustained emissions)
GW	Global Warming
GWP	Global Warming Potential
H_2O	Water or Water Vapour
He	Hermes input
HP	High Pressure
ICAO	International Civil Aviation Organization
IP	Intermediate Pressure
IPCC	Intergovernmental Panel on Climate Change
LOSU	Level Of Scientific Understanding
LP	Low Pressure
NO_x	Nitrogen Oxides (NO & NO_2)
O_3	Ozone
OD	Off Design Point
PR	Pressure Ratio
RF	Radiative Forcing

RFI	Radiative Forcing Index
RH	Relative Humidity
RR	Rolls-Royce
S/L	Sea Level
SAE	Society of Automotive Engineers
SFC	Specific Fuel Consumption
T/O	Take off

1 INTRODUCTION

1.1 Evolution of civil aviation

During the 20th-century, civil aviation experienced an extraordinary growth and development. This growing trend has continued over the last decades. According to reference (Lee et al. 2009), the Average Annual Growth Rate (AAGR) in passenger traffic was 5.3% between 2000 and 2007, what resulted in a 38% increase in passenger traffic in that period. Analysing some future scenarios, the expected AAGR in passenger traffic between 2015 and 2034 is 4.6%, what would double air traffic from 2015 to 2030 (Airbus 2015). During the period 2030-2040, AAGR is expected to moderate to 4% as stated in reference (ICAO 2013b).

Although air traffic growth is positive for Aviation Industry, it presents some environmental challenges. To help avoid those issues, the technology of the jet engines evolves year after year resulting in more efficient, cleaner and quieter engines. As a result of the effort of Engine Manufacturers, aircraft engines have become 75% quieter and 80% more energy efficient over the last 50 years (ICAO 2013b). Despite this significant improvement, the growth of air traffic is greater than the reduction of aircraft emissions. Therefore, aircraft environmental impact is expected to increase in the following years. In fact, aviation emissions growth is predicted to be around 70% by 2020 and 200-300% by 2050 taking the year 2006 as a baseline (Runge-Metzger 2011).

One of the most notable environmental impacts of aviation is linked to the Global Warming produced by the Greenhouse Effect. Aircraft engines emit CO_2 and H_2O as a consequence of the combustion of fossil fuels, which are major contributors to the Greenhouse effect.

1.2 Aircraft environmental impact

The environmental impact of Aviation is specially reflected on atmospheric pollution. The atmosphere is a protective layer of air that shields cosmic radiation coming from the Sun. This cosmic radiation increases the temperature of the atmosphere because some of the air molecules, mainly carbon dioxide and water vapour, absorb and emit thermal radiation. The effect of preventing thermal

radiation from leaving the Earth's atmosphere is known as Greenhouse Effect The gases that enhance this effect are consequently known as Greenhouse Gases (GHG): water vapour (H_2O), carbon dioxide (CO_2), Methane (CH_4) and Nitrous Oxide (N_2O) (BEACON n.d.).

After the industrialisation process started in 18th-century, the concentration of Greenhouse Gases has increased at an accelerated rate, as shown in Figure 1-1. As a consequence, global mean temperature experienced an accelerated rise, increasing in 0.6-0.9ºC between 1906 and 2005. In addition, the rate of temperature has almost doubled from 1960 to 2010 (Riebeek 2010). The increase on the average temperature of the Earth is known as Global Warming.

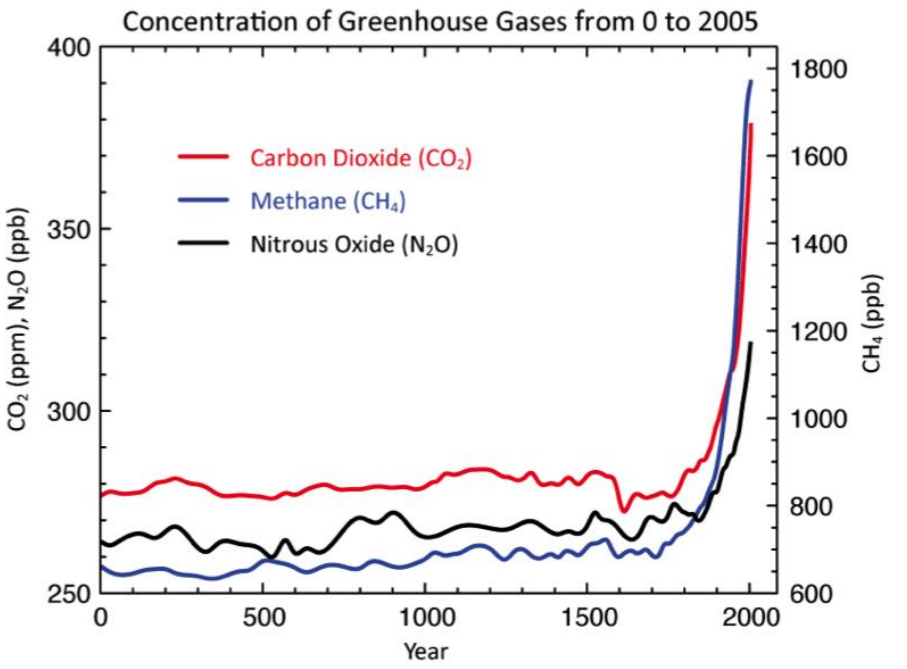

Figure 1-1: CO_2, CH_4 and N_2O concentrations from year 0 to 2005 (IPCC 2007)

Aviation has also contributed to this effect due to the emissions of CO_2 and water vapour, and the contrail and aircraft induced cirrus clouds formation.

Carbon dioxide and water vapour are combustion products of the typical aviation fuel, the kerosene. Both gases are relatively strong greenhouse gases. According to reference (ICAO 2013b), the aviation emissions of CO_2 are currently about 2% of all anthropogenic carbon dioxide emissions.

The direct contribution of CO_2 to Global Warming is much more significant than water vapour's in the upper troposphere, because of the larger emission index and longer residence time of CO_2. However, water emitted in the stratosphere can have longer residence times than troposphere water, which precipitates relatively shortly after being emitted. Additionally, water plays an essential role in contrails' and cirrus clouds' formation, which have a significant effect on Global Warming.

The formation of contrails and induced cirrus clouds is influenced by many effects, such as chemical reactions in the plume, ice microphysics, wake dynamics, state of the atmosphere, atmospheric dispersion rates and engine technology (Noppel 2007).

For contrails formation, water vapour emissions react in the aircraft plume producing ice crystals. These particles have two effects: reflecting cosmic radiation back to space and scattering long-wave radiation, coming from Earth's surface, back to the ground. In average, as the backscattering of terrestrial radiation is greater than the reflection of cosmic radiation, contrails contribute to Global Warming.

There are two kinds of contrails, persistent and non-persistent. If they persist in the upper troposphere, they can spread out horizontally by wind shear forming a contrail cirrus cloud. The impact of cirrus clouds into Global Warming has a great uncertainty and at present, it cannot be accurately estimated. Some recent studies suggest that contrail cirrus impact may be significant enough to be a concern (Burkhardt and Kärcher 2011).

Because of the big impact these gases have on Global Warming, significant research on techniques to avoid them has been conducted recently. To reduce CO_2 and water vapour emissions, more efficient engines are required. This way, they would burn less fuel and produce less CO_2 and water vapour. There are other techniques, such as CO_2 filters, that are being investigated. The motivation for these efforts has been double: on one hand, ethics oblige the companies to do their best on avoiding aircraft environmental impact; on the other hand, the

legislation on CO_2 emissions is getting more severe and establishes strict limits for CO_2 emissions

For contrail and cirrus clouds prevention, on the contrary, there is not any current legislation. Thus, the amount of research on contrail and cirrus clouds avoidance has been significantly lower.

1.3 Project context

To fill in this gap, the Propulsion Centre of Cranfield University has formed a research group that focuses its efforts on analysing techniques to reduce the environmental impact of civil aircraft by preventing contrails, in foresight of future legislation on the field. This MSc project is part of this research group.

Several studies have been carried out in order to analyse the impact of contrails and induced cirrus on Global Warming and then, how to reduce that effect. In the last few years, different technologies have been created to reduce contrail formation, and also, to prevent it.

Reference (Noppel 2007) discusses several contrail avoidance strategies and also proposed a novel engine configuration using an intercooled recuperated engine. This engine had an additional heat exchanger attached for exhaust water vapour condensation.

Additionally, reference (Qureshi 2016) develops the design of a device for the purpose of aero engine exhaust water vapour condensation. It involves the condensation and separation of the water vapour from the core exhaust emission as well as water collection within the engine. This device enables the collection of all the water produced from the fuel combustion process.

The contrail avoidance technique considered by these two investigations is based on water condensation and collection from engine core exhaust. Then, that water could be stored on the aircraft or released into the atmosphere (Noppel, Lucisano, and Singh 2009). For this study, the case of storing all the water produced by fuel combustion during cruise is considered, assuming that this water is released at a

lower altitude after cruise phase is completed. The condensed water is assumed to be stored in the fuel tanks separated from the fuel by a membrane.

This strategy, apart from the technical challenges addressed by reference (Qureshi 2016), implies significant changes on aircraft performance, as the weight of the aircraft will increase during cruise, instead of decreasing.

Current aircraft are designed to experience a weight reduction during cruise as a consequence of burning the fuel. The weight affects the drag of the aircraft. During cruise, the thrust produced by the engines needs to be equal to this drag. To produce thrust the engines need to burn fuel. As a consequence, drag decreases with weight during cruise, resulting in reduced thrust requirements and fuel consumption. This way, the weight of the aircraft defines how much fuel is needed to complete a mission, or how long this mission can be. Then, the implications of increasing the weight by storing the condensed water are sensed in two ways:

- The reduced range for a given amount of fuel
- The augmented fuel consumption for a given range

The research questions of the present project are defined attending to these challenges of the water storage technique. Firstly, the investigation of the feasibility of storing water onboard during cruise and establish the effects it may have on aircraft performance has to be carried out. Secondly, once this analysis is performed, the benefit of the elimination of the contrail regarding Global Warming reduction has to be evaluated.

1.4 Aims and methodology

The main purpose of this thesis is to analyse the changes in aircraft performance due to the inclusion of the contrail prevention technique based on collection and storage of water produced during fuel combustion. Once this analysis is carried out, the secondary aim can be addressed. This consists on an assessment of the net Global Warming benefit obtained by eliminating contrails and induced cirrus, considering the additional CO2 produced by the technique. If the net benefit

results positive, the environmental feasibility of this contrail avoidance method could be proved.

The methodology to fulfil these aims comprises the following steps:

- Achieve a good understanding of contrail formation.
- Obtain a baseline model of a three-spool high bypass turbofan engine inspired by the Rolls-Royce Trent 900 using the engine performance software Turbomatch.
- Obtain the baseline model of a large wide-body aircraft inspired by the Airbus A380 using the aircraft performance software Hermes.
- Create the aircraft model carrying water based on the aircraft inspired by Airbus A380 using the software Matlab.
- Conduct an aircraft performance analysis between both aircraft models and study the range reduction and the fuel burn penalty due to the water storage technique.
- Select a method to measure the Global Warming impact.
- Assess the environmental effect of the contrail prevention technique.

1.5 Thesis structure

The present thesis is divided into 6 chapters. This first chapter has briefly introduced the topic and the objectives of the current project. Chapter 2 reviews the fundamental science and technology related to the Global Warming impact of contrail avoidance techniques. Chapter 3 provides the methodology followed to create the aircraft and engine baseline models.

In chapter 4 the methodology to study the aircraft performance due to the water storage is detailed. It is followed by the explanation of the Global Warming analysis. Chapter 5 shows the results of the the implementation of the water storage technique. In addition, a discussion of the results is included. Finally, in chapter 6 the conclusions and future work on this topic are detailed. The appendices contain the input codes of Turbomatch and Hermes, and additional information about the Global Warming analysis.

2 LITERATURE SURVEY

This chapter reviews the fundamental science and technology related to the Global Warming impact of contrail avoidance techniques. Due to the complexity and multidisciplinary character of the topic, the key elements of contrails and Global Warming are presented so that contrail avoidance strategies can be understood correctly.

2.1 Contrails

Condensation trails, commonly known as contrails, are thin artificial clouds produced by jet engines on the aircraft path under certain conditions. The contrail is the most visible aircraft effect of aircraft on the atmosphere, and for this reason, they were first observed as early as 1919. But they were not studied until World War II, as the presence of aircraft was indicated by the formation of contrails (Schrader 1997). Due to the increasing jet traffic, the formation of condensation trails was a common appreciable effect since the 1960s. Concerns over the impact of contrails on the atmosphere and climate arose in the 1990s, what led to numerous researches (Minnis 2003).

2.1.1 Mechanism of formation

The formation process of contrails is influenced by many variables, but the present analysis will focus only on the principal ones, which are state of the atmosphere, chemical reactions in the plume and engine technology. The other variables were mentioned in Section 1.2.

Aircraft jet engines are thermodynamic machines that utilise air as the working fluid, producing the necessary thrust to allow the aircraft for reaching a high altitude and then, sustaining flight at that altitude. Jet engines are based on Brayton thermodynamic cycle. According to this cycle, air enters the engine through the intake, and then it is compressed, mixed with fuel and burnt in the combustion chamber, expanded in the turbines and finally emitted through the nozzle. The shaft power required by the compressors is provided by turbines, which also provide some mechanical power for aircraft electricity generation. The

exhaust gases consist of a hot mixture of incoming air and combustion products, which are ejected at high velocities. The content of some exhaust gases is described in Section 2.3.2.1 defining their corresponding emission index.

Once the exhaust gases get in contact with ambient air, they experience a drastic cooling. This sudden temperature drop can result in a phase change to liquid or solid, depending on pressure and temperature, as illustrated in Figure 2-1. In this figure, different phases are represented as well as their corresponding phase changes. The triple point, in which the three phases coexist, is also included.

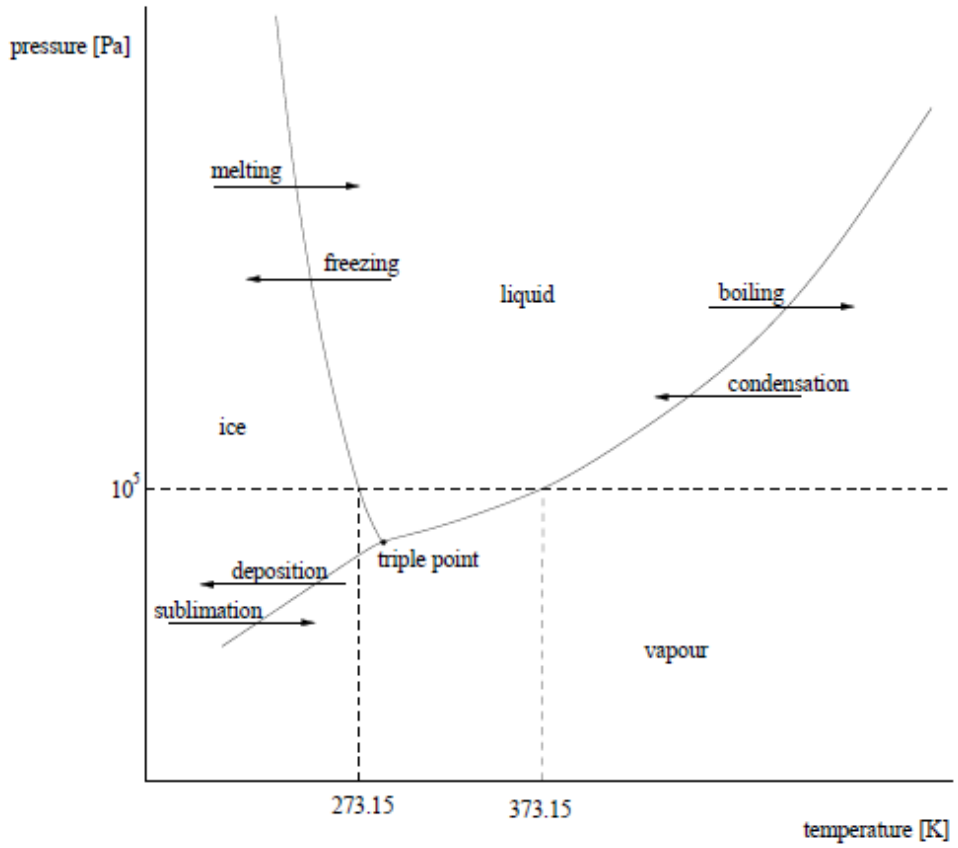

Figure 2-1: Water Phase diagram (Noppel 2007)

The water vapour ejected from the aircraft exhaust can push the local atmospheric content of water over the saturation limit, causing water droplets formation. As droplets are formed, the water molecules attraction, known as capillary force, increases the pressure inside the droplet, changing its phase from liquid to gas, and hence, preventing the formation of droplets. These conditions

enhance the emergence of a supersaturated ambient, in which water in gaseous phase exists, even if temperature and pressure conditions in water phase diagram suggest liquid or solid phase. This supersaturated ambient condition is required for water condensation.

If small particles, such as aerosols, are present in the atmosphere or in the exhaust ejected flow, condensation is promoted due to the increase in the cohesion force between water and the particle. Then, the amount of ambient supersaturation required to enable condensation depends on the size and material of these particles. Equation (2-1) provides a relationship between the amount of supersaturation, molar weight, size and temperature of the water droplet. This equation is known as Kelvin Equation, and its derivation was provided in reference (Galvin 2005). If a more detailed understanding of Kelvin equation is required, refer to (Garrett 2016). The amount of supersaturation is measured using relative humidity (RH), which is the water vapour pressure-to-saturation pressure ratio, as shown in equation (2-2). In a supersaturated ambient, RH is over 100%. If RH is below 100%, the evaporation rate is greater than condensation rate, which results in no water droplets formation (Williams, Noland, and Toumi 2002).

$$P_w = P_s \, exp\left(\frac{M_d}{\rho_d \, R \, T_w} \, \frac{2 \, \gamma_t}{r_d}\right) \quad \textbf{(2-1)}$$

$$RH = \frac{P_w}{P_s} \quad \textbf{(2-2)}$$

In these equations, P_w is the water vapour pressure, P_s is the water saturation pressure, M_d is the molar weight of the droplet, r_d is the radius of the droplet, ρ_d is the density, R is the ideal gas constant, γ_t is the surface tension, and T_w is the water vapour temperature. SI units must be used for all the parameters.

Once ambient supersaturation is achieved, some of the water droplets will freeze into ice crystals due to the low local ambient temperatures and pressures. This effect will eventually form the condensation trail behind the aircraft. The equilibrium between ice crystals, cooled water and water vapour is driven by a thermodynamic process called the Bergeron process. For more details, see

reference (College of Dupage n.d.). Contrails persistence depends on the ambient conditions. If the ambient is supersaturated enough with regard to ice, contrails will persist. The persistence of contrails is explained in more detail in Section 2.1.2.

Figure 2-2: Photo of persistent contrails (Penner et al. 1999)

In conclusion, contrail formation occurs if the mixing process of hot exhaust gases and ambient air reaches a supersaturated state with respect to water, forming liquid drops, which quickly freeze, producing ice crystals (Appleman 1953). Depending on the amount of supersaturation, two kinds of contrails can be formed: persistent and non-persistent contrails. The atmospheric relative humidity is a crucial factor in contrail formation and persistence (Turgut and Rosen 2011). In Figure 2-2, typical persistent contrails can be observed. There are four contrails just behind each aircraft, one per jet engine, and then they mix together.

2.1.2 Contrail prediction

The first studies for predicting the formation of contrails were undertaken independently by E. Schmidt in Germany [1941] and H. Appleman in the USA [1953]. They came up with a criterion that, according to reference (Schrader 1997), is considered even today as the definitive technique to forecast contrails.

This principle is known as the Schmidt-Appleman criteria, and it explains contrail formation using a geometrical approach of the mixing of hot exhaust gases and ambient air on a water phase diagram. Later studies carried out by Schumann [1996] suggested that the saturation requirement established in Schmidt-Appleman criteria is respect to water.

The following assumptions are considered by the Schmidt-Appleman criteria. As their results have been validated, the scientific community has accepted these assumptions (Roig Medina 2014). However, they are considered as limitations of the criteria when applied to real cases (Schumann 1996):

- The water content within the fuel chemical bond is negligible compared to the water produced due to the chemical reaction of fuel combustion.
- The enthalpy content within the fuel chemical bond is negligible compared to the enthalpy produced due to the chemical reaction of fuel combustion.
- Non-air exhaust components, such as aerosols, are neglected with large dilution rates and small relative ambient water vapour content.
- The mixing between hot jet exhaust gases and the atmosphere is adiabatic and isobaric.
- The mixing between water and heat occurs at equal rates.
- Constant gaseous state is assumed during the whole mixing process.
- Constant specific heat capacity value is assumed.

As explained before, Schmidt-Appleman criteria are based on the water phase diagram, which is shown in Figure 2-3. In this chart, water vapour pressure is introduced on the ordinate axis and stagnation temperature in abscissae. Stagnation temperature and water vapour pressure of both engine exhaust gases and ambient air are marked in the graph as point A and B respectively. Stagnation temperature is measured taking the atmospheric frame as reference. Accordingly, the ambient static temperature corresponds to the ambient stagnation temperature. Ambient temperature and pressure calculation at a certain altitude is explained in Section 4.1.2.1. Considering the assumptions stated above, a line joining exhaust (point A) and ambient condition (point B) is

represented on the diagram. This line is known as the mixing line and it illustrates all the intermediate states of the mixing.

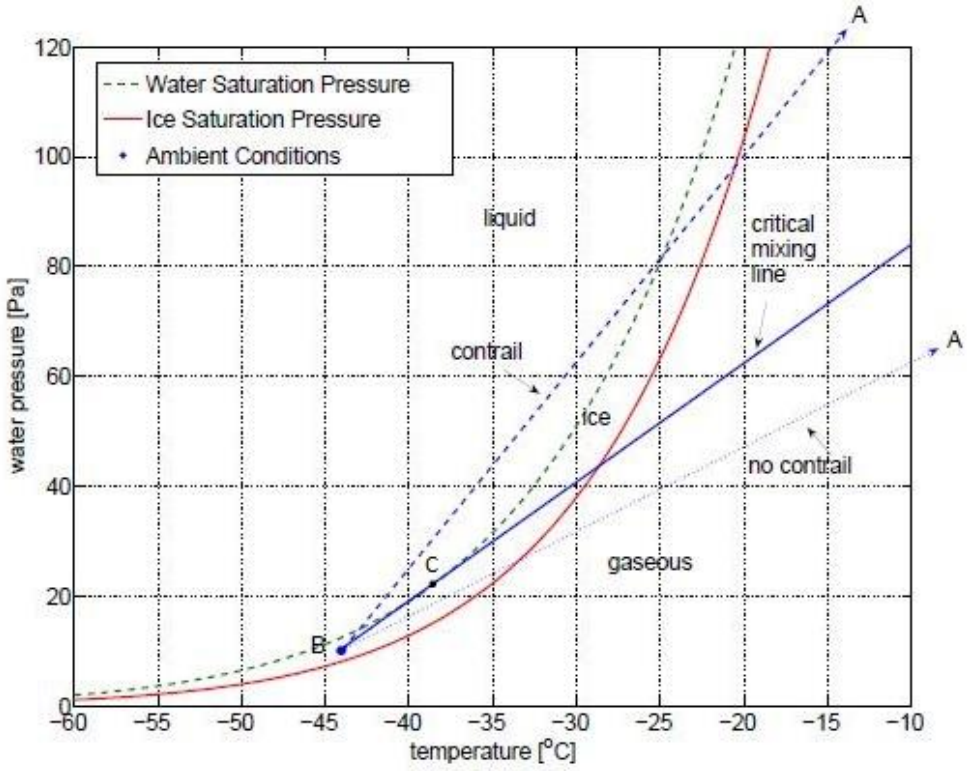

Figure 2-3: Geometrical analysis for contrail formation (Noppel 2007)

Once the ambient point (B) is defined, there are two ways to calculate the slope, G, of the mixing line (Paoli and Shariff 2016).

- If the exhaust conditions are known, the slope is easily defined connecting point A and B in Figure 2-3, as shown in equation (2-3).

$$G = \frac{P_{exh}^{w} - P_{amb}^{w}}{T_{exh} - T_{amb}} \quad \textbf{(2-3)}$$

  In this equation, P_{exh}^{w} and T_{exh} represent the exhaust water vapour pressure and stagnation temperature, while P_{amb}^{w} and T_{amb} are the ambient water vapour pressure and stagnation temperature, which is the same as ambient static temperature.
- Second, if the exhaust conditions are unknown or difficult to define, the slope is calculated considering ambient conditions, fuel energy, engine

emission index of water vapour and engine propulsion efficiency, as shown in equation (2-4). These equations were extracted from reference.

$$G = \frac{c_p^{air}\, EI_w\, P_{amb}}{\varepsilon\, Q\, (1-\eta)} \quad \textbf{(2-4)}$$

In this equation, c_p^{air} is the specific heat capacity of air, EI_w is the water vapour emission index, P_{amb} is the ambient pressure, ε is the water vapour-to-air molar mass ratio, Q is the net calorific value per mass of fuel, and the quantity η represents the overall engine efficiency at cruise.

Apart from the mixing line, the water and ice saturation pressures curves, determine the regions for the different water phases, as indicated in Figure 2-3. Equations (2-5) and (2-6) allow for the calculation of the saturated water pressure and saturated ice pressure, respectively, using only the ambient temperature (Padfield n.d.). The saturated water pressure formula is known as Clausius-Clapeyron relation.

$$P_s^w = 610.78\, e^{\left[17.2694\, \frac{(T-273.16)}{(T-34.86)}\right]} \quad \textbf{(2-5)}$$

$$P_s^{ice} = e^{\left[28.916 - \frac{6140.4}{(T-0.16)}\right]} \quad \textbf{(2-6)}$$

Once the water phase diagram and the mixing line are explained, their relationship enables the contrail formation forecast in accordance with Schmidt-Appleman criteria. On the one hand, for given ambient conditions, if the mixing line crosses the water saturation pressure curve, droplets are formed, and consequently, contrails. This is the case of the dashed line in Figure 2-3. On the other hand, for the same ambient conditions, if the exhaust gases are hotter or have a lower water content, the mixing line will not cross the water saturation pressure curve, and hence, contrails are not formed. The dotted line in Figure 2-3 represents this case. According to Schmidt-Appleman criteria, aircraft flying at the same altitude can produce or not contrails depending on the conditions of exhaust gases. This phenomenon can be observed in Figure 2-4.

Figure 2-4: Airbus A340 producing contrails and Boeing B707 without contrails flying at 10.5 km altitude (Schumann 2000)

Based on the previous explanation, if a line tangent to the water saturation pressure curve at point C is defined for given ambient conditions, it can be concluded that if the mixing line is steeper than the tangent, contrail formation will occur. This tangent line is known as critical mixing line, and it is represented in Figure 2-3 as a solid line. The slope of the critical mixing line, G_{cri}, is calculated joining the ambient point B and the tangency point C. Therefore, G_{cri} only depends on environmental conditions as can be observed in equation (2-7) (Lasa Carrillo 2014). In this equation T_{cri} is the critical temperature, which corresponds to the temperature of the tangency point C, and $P_s^w(T_{cri})$ is the water saturation pressure at the critical temperature.

$$G_{cri} = \frac{P_s^w(T_{cri}) - P_{amb}}{T_{cri} - T_{amb}} \quad \textbf{(2-7)}$$

Persistence of contrails depends on the ambient ice saturation. Hence, given the ambient conditions, if the ambient water vapour pressure exceeds the ice saturation pressure, the contrail formed will be persistent. Graphically, this means

that the point of the environmental conditions (B) is above the ice saturation line in Figure 2-3. According to reference (Schumann 2005), contrails are short-lived if the ambient is dry. Consequently, if the ambient point (B) is below this line, ice crystals will sublimate, and the contrail will vanish. These two situations are known as persistent contrails and non-persistent or threshold contrails respectively, and they are represented in Figure 2-5. Persistent contrails are represented by the mixing line III, while the threshold contrail corresponds to the mixing line IV. Mixing line II is the critical mixing for ambient conditions T, and finally, the case I represents no contrail formation.

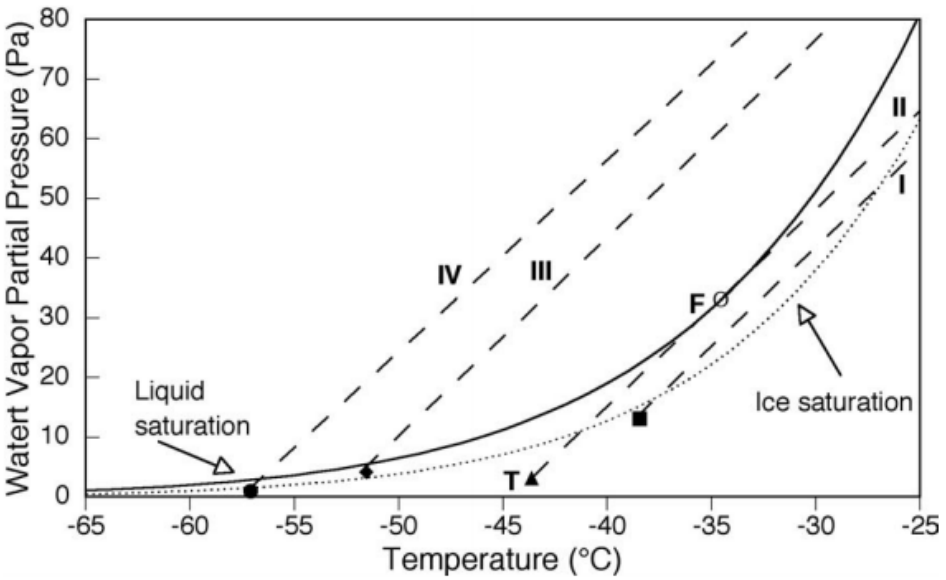

Figure 2-5: Water phase diagram with different mixing lines with different ambient conditions (Minnis 2003)

2.2 Global Warming

Nowadays, the growing environmental awareness has led to the implantation of regulations such as emission limitation to prevent, or at least to reduce, greenhouse effect, and consequently, Global Warming.

The present section analyses the impact of anthropogenic emissions in Global Warming (GW). It is divided in two subsections. The first one describes different GW metrics including the advantages and disadvantages of applying them to

aircraft emissions. The second subsection explains the impact of aircraft emissions in Global Warming, focusing mainly on the impact of contrails.

2.2.1 Quantification of Global Warming impact

The quantification of the Global Warming effect of pollutants is necessary for the assessment of Global Warming. Thus, GW metrics are used to identify, quantify and compare contribution to Global Warming of different pollutants. According to reference (Shine et al. 2005), the impact of emission can be regarded as the following chain: Emissions → Concentration changes → Radiative forcing → Climate impacts → Societal and ecosystem impact → Economic damage. It has been recognised that the further down the chain, the greater becomes the relevance of the impacts. However, the complexity and uncertainty in computational techniques increase. This chain can be applied to aviation emissions as shown in Figure 2-6.

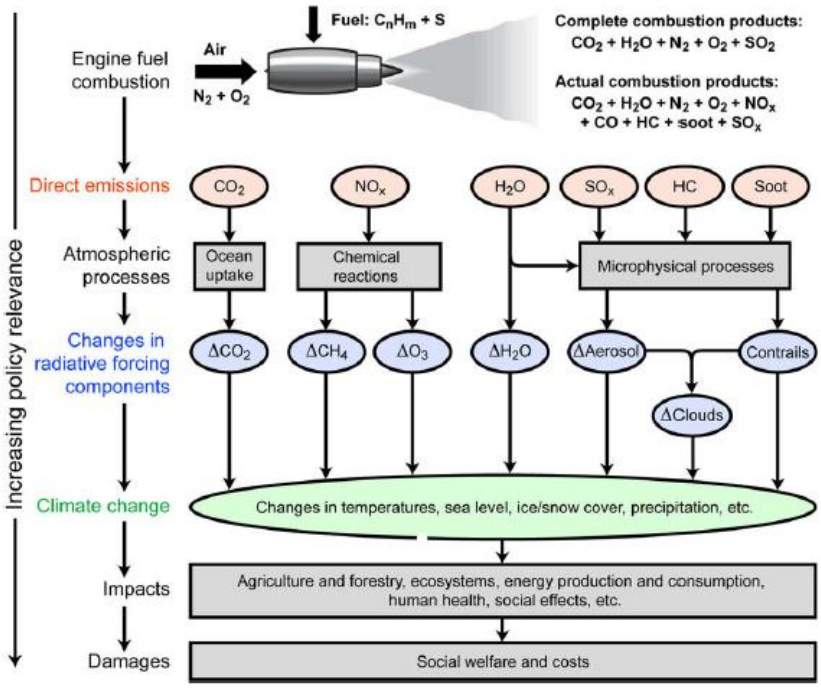

Figure 2-6: Aircraft emissions and climate change (Lee et al. 2009)

Nowadays, the objective is to find an appropriate metric reflecting the societal and economic impact. However, given the current state of climate models, it is hard to achieve the desired metric. In fact, there is an ongoing discussion about

which metric can best quantify GW impact. The most important metrics used today are discussed in the following subsections.

2.2.1.1 Radiative forcing

Radiative forcing, RF, is a standard metric commonly used to compare the contribution of variations in individual ambient constituents to the Earth energy imbalance since pre-industrial times (CCC 2009). Some pollutants, like Greenhouse gases, disturb the equilibrium state of the Earth radiation budget absorbing additional heat energy, which will remain within Earth system. This additionally absorbed heat energy is known as Radiative forcing.

As Radiative forcing increases, more heat is absorbed and consequently, the Earth's average surface temperature increases. The temperature will continue to rise until the radiation input and output of the atmosphere are in equilibrium again. To conclude, a positive radiative forcing will result in a temperature rise, while a negative value will lead to a temperature drop (Noppel 2007).

The surface temperature rise is not only affected by the radiative forcing but also by the climate sensitivity parameter, λ. Then, the surface temperature rise, ΔT_{surf}, is defined as provided in equation (2-8) (Penner et al. 1999). RF is expressed in [W m^{-2}], the temperature rise in [K], and the climate feedback parameter in [K W^{-1} m^2].

$$\Delta T_{surf} = \lambda \, RF \qquad \textbf{(2-8)}$$

Radiative forcing of atmospheric constituents measures the current concentration of past emissions. As a result, long-lived pollutants, such as CO_2 and CH_4, cause a radiative forcing that will persist for several decades after emitted. In the case of short-lived emissions, such as contrails, the induced radiative forcing will diminish to zero only some hours after emission. Additionally, according to reference (Shine and Forster 1999), radiative forcing of a particular pollutant is dependent on its spatial distribution and interaction with radiation, whether solar or terrestrial. The global radiative forcing in 2005 for the principal components is shown in Figure 2-7. The geographic spatial scale of the RF from each pollutant

and the Level Of Scientific Understanding (LOSU) are included on the right of the figure.

The main disadvantage of this metric is that it only indicates the current impact, and hence, imbalance of past emissions. Therefore, this parameter does not show how current emissions will affect future climate change. This is because, as explained before, emissions with long residence times will keep their radiative forcing effect for much longer than emissions with short residence times. Although RF presents this disadvantage, it is a standard metric because it is easy to use and understand.

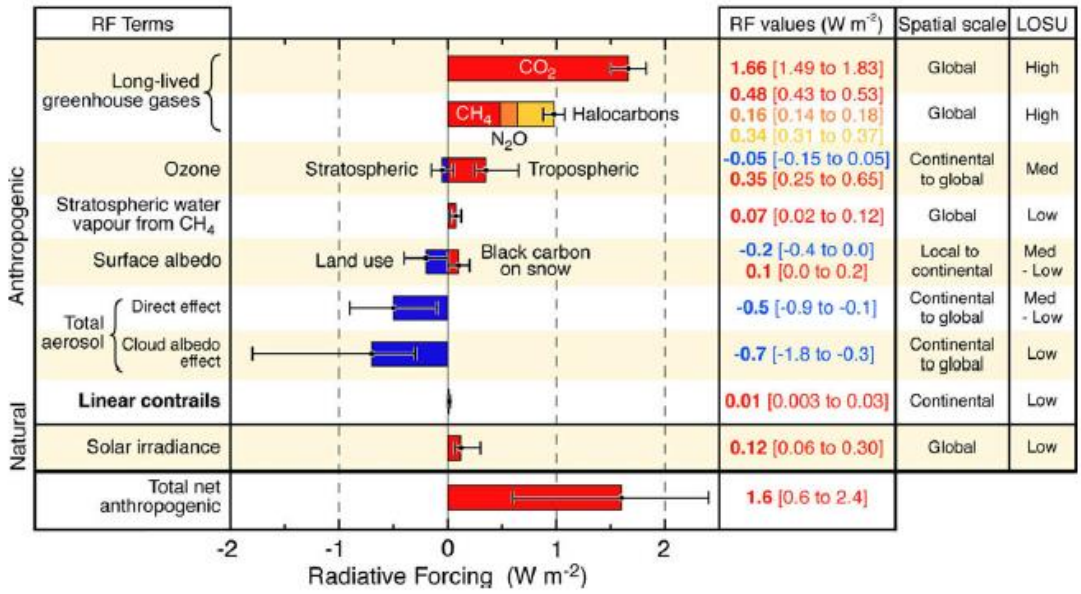

Figure 2-7: Global radiative components in 2005 (Lee et al. 2009)

Focusing on aviation, an alternative metric based on RF is the radiative forcing index, RFI, which compares aviation's total radiative forcing with that of aviation CO_2 emissions (Gössling and Upham 2009). This metric presents the same disadvantages as radiative forcing.

2.2.1.2 Global Warming Potential

The Global Warming Potential, GWP, is a metric that measures the contribution of different pollutants to Global Warming. It can be defined as "the time-integrated radiative forcing due to a pulse emission of a particular gas relative to a pulse emission of a reference gas over a time horizon" (Shine et al. 2005). The

reference gas is commonly CO_2. The usual time period chosen is 100 years, as in Kyoto Protocol, but shorter and longer timescales can be employed.

The main disadvantage of this approach is that it only works correctly for long-lived emissions, whose concentration does not depend on location or altitude as they are well mixed on a global scale. For this reason, short-lived pollutants, such as contrails and NO_x, are not suitably measured with this metric as their occurrence is limited to certain locations and altitudes. For this reason, GWP is not a suitable approach for measuring the influence of aviation emissions in Global Warming.

2.2.1.3 Global Temperature Potential

The Global Temperature Potential, GTP, is another metric analogous to the GWP that calculates the average surface temperature response due to the release of a particular gas relative to the release of a reference gas at some specific future point in time. According to reference (Shine et al. 2005), there are two different ways to calculate GTP, considering pulsed emissions (GTPP) or considering sustained emissions (GTPS). Obviously, depending on the kind of emission selected, the result will be different.

As climate impact can be forecasted, both metrics, GTPP and GTPS, are one step further down in the chain given in Section 2.2.1 than radiative forcing and GWP. However, a workshop of the IPCC (IPCC 2009) concluded that it would be inappropriate to replace GWP by GTP at the current time as more research is required on the performance of GTP.

2.2.2 Global Warming impact of aircraft emissions

This section focuses on the impact of aircraft emissions in Global Warming. The chart in Figure 2-8 shows the radiative forcing of aviation emissions in 2005, and their geographic spatial scale and LOSU. As can be observed, CO_2, Aviation Induced Cirrus (AIC) and O_3 are the main contributors to Global Warming induced by aircraft. In the case of AIC, a very low level of scientific understanding has been achieved and consequently, there is a high uncertainty on its RF value. For

this reason, two total aviation RF are usually presented, including and excluding aircraft induced cirrus.

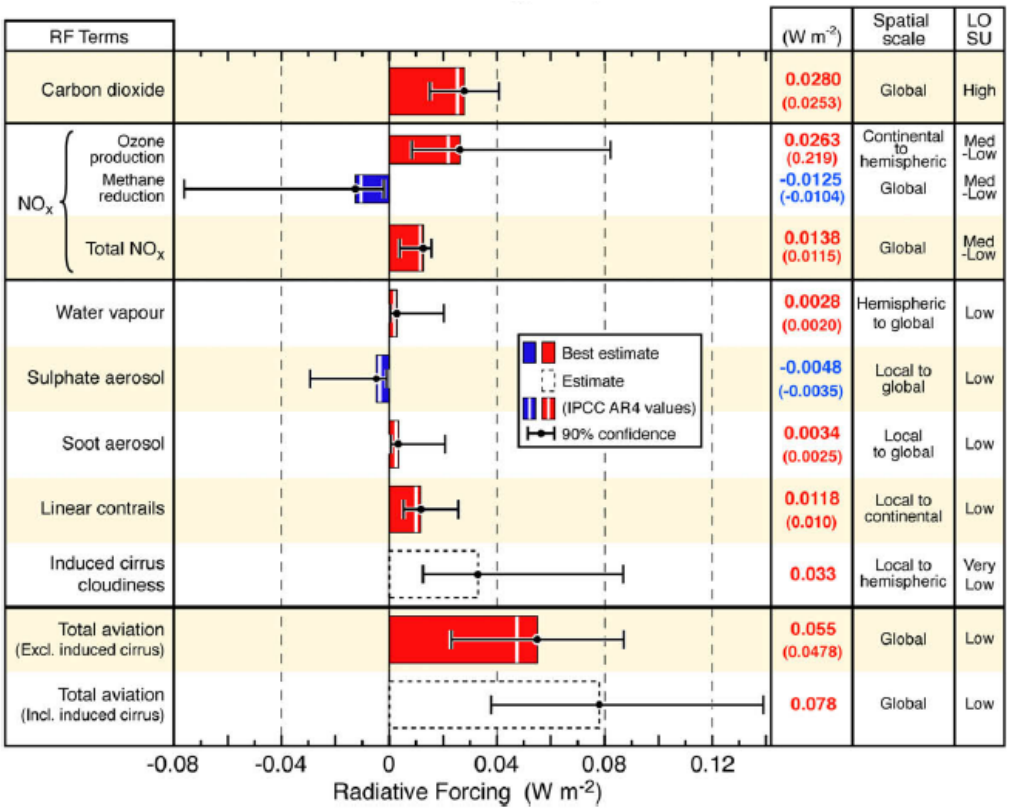

Figure 2-8: Aviation Radiative Forcing Components in 2005 (Lee et al. 2009)

Regarding contrails, their warming impact is expected to be lower than that of the main contributors described above, but it is still considerable. The LOSU of contrails is low, as well as the LOSU of water vapour and aerosols. Moreover, a cooling effect caused by aviation is expected due to the emission of sulphate aerosols and the reduction in atmospheric methane.

Finally, if a more global impact overview is required, the effect of aviation emissions on climate change is represented in Figure 2-6.

2.2.2.1 Global Warming impact of contrails

Contrails have a direct impact on climate as explained in the previous section. However, although some research has been performed in this field, the impact of contrails is still difficult to describe and measure accurately. This is because properties of contrails vary widely depending on ambient conditions, contrails coverage and their optical depth. Contrails that persist long enough spread

forming cirrus clouds. During this transition, the properties of contrails vary progressively, making the quantification of contrails impact even more challenging. Due to all these reasons, nowadays there are still considerable uncertainties about the GW impact of contrails and aircraft induced cirrus.

Nonetheless, a radiative forcing analysis of contrails can be conducted considering shortwave radiative forcing, RF_{SW}, and longwave radiative forcing, RF_{LW}. On the one hand, the shortwave radiative forcing refers to the solar energy flux not allowed to enter the Earth's atmosphere, what results in a negative RF, and thus, a cooling effect. On the other hand, the longwave radiative forcing corresponds to the heat flux from the ground prevented from leaving the Earth's atmosphere, leading to a positive RF, and consequently, a warming effect. The net radiative forcing, RF_{total}, can be expressed as the sum of these two effects.

$$RF_{total} = RF_{LW} + RF_{SW} \quad \textbf{(2-9)}$$

The net radiative forcing achieves its maximum value at night because shortwave RF is zero, resulting only in longwave RF, which has a warming effect. In conclusion, the net effect of contrails radiative forcing is generally positive, and according to reference (Meerkötter et al. 1999), a warming net effect is induced by contrails.

Radiative forcing of contrails and cirrus clouds depends mainly on coverage and optical depth. Focusing on contrail and cirrus clouds coverage, Table 2-1 provides coverage data over Europe, USA and east coast Southeast Asia. These values were extracted from reference (Burkhardt and Kärcher 2011), and they represent the maximum values of contrail cirrus coverage over some zones of the analysed areas. The average contrail cirrus coverage on a global scale is also included in the last column of Table 2-1.

	Europe	***USA***	***Southeast Asia***	***Global***
Contrails	2%	1%	0.2%	0.07%
Cirrus clouds	10%	6%	1%	0.61%

Table 2-1: Contrail-Cirrus coverage over different areas and globally

2.3 Contrail avoidance strategies

Since the 90s, several researches have been conducted with the challenge of achieving a better understanding of the environmental impact of contrails and how to reduce their formation. Although there has been much progress in this field, much remains to be done.

In the present section, different contrail avoidance strategies are presented. Currently, the most analysed strategy consists on planning flight routes or flight altitudes in a way that contrail formation can be reduced. The second approach presented consists on water condensation and collection from the core exhaust for contrail prevention. Finally, other technologies used for contrail mitigation are described.

2.3.1 Air traffic adjustment

Air traffic adjustment strategy consists on the avoidance of regions where the formation of persistent contrails is enhanced. The aim of this strategy is to mitigate the Global Warming impact of contrails by reducing the radiative forcing. If the contrail is formed, its persistence depends on ambient conditions, which differ depending on altitude and geographical location. A study conducted in reference (Noppel 2007) shows how the probability of contrail formation changes depending on height and location. From this study, it is concluded that in the mid-latitudes (30ºN-60ºN), the probability of contrail formation is very high at altitudes of the upper troposphere (around 10 km). For the purpose of avoiding these high probability contrail formation regions, two kinds of air traffic adjustment strategies are presented: temporal and spatial.

As explained previously in Section 2.2.2.1, the net radiative forcing of contrails achieves its maximum value at night. Consequently, to avoid this effect, temporal air traffic adjustments were developed. According to reference (Stuber et al. 2006), most of the radiative forcing caused by contrails during winter is a result of flying at night. A solution to this problem was provided in reference (Myhre and Stordal 2001), who suggested that if the flight density increases during sunrise and sunset, a reduction of the contrails radiative forcing could be experienced.

However, this solution does not consider the fact that contrail induced cirrus clouds formed during the evening can persist during night, causing a greater radiative forcing impact (Mannstein and Schumann 2005). From an economical point of view, the limitation of air traffic to morning and evening is impractical. Additionally, the fact of restricting the time of flights can lead to air traffic congestion.

The alternative option to temporal air traffic adjustments is the application of spatial adjustments. The basis of this method is that aircraft avoid atmospheric regions where the formation of persistent contrails is promoted. These regions can be avoided by changing the flight path of the aircraft horizontally or changing the cruise altitude. On the one hand, the horizontal deviation would imply an increase in fuel consumption as the length of the flight increases. On the other hand, the variation in altitude would also mean an increase in fuel consumed as the aircraft is not flying at the optimised cruise altitude.

According to reference (Noppel 2007), three different approaches were identified for the mitigation of contrail formation by adjusting air traffic spatially. The first method consists of a global variation of the cruise altitude. If the cruise altitude is displaced downwards on a global scale, a decrease in contrail coverage is achieved, and hence, in the contrails radiative forcing. An associated fuel burn penalty is expected (Fichter et al. 2005). The minimum altitude at which contrails formation occurs depends on ambient conditions, in particular, on relative humidity. The minimum altitude varies between 8.8 km and 10.4 km depending on whether RH is supersaturated (100%) or dry (0%) respectively (Filippone 2010).

The second approach is based on the restriction of cruise altitudes depending on the current atmospheric conditions for some areas. The idea of this method is to reallocate cruise altitudes in 6-hour intervals depending on ambient conditions, what results in a contrail coverage decrease of 65-95%. Consequently, the decline in contrail formation results in a fuel consumption penalty of 2.6-7.0% (Williams and Noland 2005).

The last approach consists on a variation of the aircraft cruise altitude depending on ambient conditions. Weather forecast data or in-flight measurements can be used to produce an optimised flight path that mitigates contrail formation. Reference (Noppel 2007) suggests that this approach reaches 78% decrease in contrail formation with a 0.8% fuel burn penalty associated, which is lower than for the first and second methods.

Apart from the associated fuel burn penalty, which is a distinct disadvantage of air traffic spatial adjustments, the complexity of the air traffic management and safety would be very high.

2.3.2 Clean exhaust engine concept

The clean exhaust engine concept, CEEC, is a novel engine concept that was first introduced by Dr F. Noppel. The potential of this engine is that it offers the possibility to reduce all aircraft emissions simultaneously. Additionally, this engine has a significant increase thermal efficiency as stated in reference (Noppel et al. 2009).

This novel engine concept could operate with hydrogen or any hydrocarbon based fuel. For the present analysis, only kerosene is considered. Accordingly, the combustion process of this fuel is analysed. After this, a water collection, storage and handling analysis is presented to understand more in detail the behaviour of this concept.

2.3.2.1 Kerosene combustion process

Before analysing the combustion process of kerosene, a brief introduction of different types of kerosene-based jet fuels is included. Reference (Chevron 2007) states that three types of kerosene are currently used by commercial aircraft industry: Jet A, Jet A-1 and Jet B.

The most used kerosene-type fuels in the world are Jet A and Jet A-1. Jet A is used in the USA while Jet A-1 is used in most of the rest of the world. The main difference between these two fuels is that Jet A-1 has a lower freezing point than Jet A, -47ºC and -40ºC, respectively. For this reason, Jet A-1 is more suitable for long international flights, particularly on polar routes in winter. However, the

reasons why USA chooses Jet A are fuel price and availability. Wide-cut fuel, also known as Jet B, is used only in some parts of Canada and Alaska due to its suitability for cold climates (Chevron 2007).

The most common aviation turbine fuel (avtur) is consequently Jet A-1. The average formula of avtur is not accurately defined as its composition can change depending on the distillation process of the jet fuel. Reference (Goodger 2014) suggested that the average formula of avtur is $C_{12.5}H_{24.4}$, which has a similar C-H ratio to the average formula $C_{11}H_{21}$ provided in reference (Lefebvre and Ballal 2010). Therefore, the average formula of avtur suggested by Goodger is selected. The combustion process of the kerosene with this composition is presented in equation (2-10).

$$C_{12.5}H_{24.4} + 18.6\,(O_2 + 3.76\,N_2) \rightarrow 12.2\,H_20 + 12.5\,CO_2 + 69.936\,N_2 \qquad \textbf{(2-10)}$$

This equation has been defined considering stoichiometric fuel-air mixture. The sulphur content in the fuel is not taken into account for the combustion process. Additionally, NO_x, CO and aerosol emissions are not considered as combustion products as the combustion is assumed to be complete. In Figure 2-6 the complete combustion products and actual combustion products are provided.

Using the stoichiometric equation (2-10), the emission indexes for water and carbon dioxide can be calculated. The emission index of a gas, EI, is defined as the mass produced of a selected gas per kg of fuel burnt. It is a mass ratio between the selected gas and the fuel. According to equation (2-10), the emission index of water vapour, EI_w, is 1.2592 kg water/kg fuel, and the emission index of carbon dioxide, EI_{CO_2} is 3.1537 kg CO_2/kg fuel. The values obtained for both emission indexes have been verified and compared with other documents. One of these documents is provided in reference (Schwartz Dallara, Kroo, and Waitz 2011), and the specified emission index values are 1.26 and 3.16 for water vapour and carbon dioxide, respectively.

In conclusion, the emission index is a useful tool to calculate an accurate value of aircraft emissions if fuel burnt is known.

2.3.2.2 Water collection, storage and handling

The clean exhaust engine concept consists of an intercooled recuperated configuration engine in which a dehumidifier is introduced to condense water vapour at the core exhaust of the engine. For more information about engine performance of CEEC, see references (Noppel 2007) and (Noppel et al. 2009).

To condense water vapour inside the engine, the temperature of the water has to be lower than the critical temperature, 647 K, according to water phase diagram. Consequently, a temperature reduction of the mass flow is considered in CEEC after the low-pressure turbine using a heat exchanger, the recuperator. This temperature reduction helps the dehumidifier condense water during different flight phases.

Reference (Qureshi 2016) has developed a contrail-free engine through the design of a turbomachinery that condenses the water vapour content at the core exhaust within the engine. This device separates and collects the water before releasing the remaining exhaust gases into the atmosphere through the core exhaust nozzle. Once water is condensed, it can be stored on the aircraft or released into the atmosphere (Noppel et al. 2009).

Focusing on the water storage on the aircraft, from 1 kg of fuel, 1.26 kg of water are produced according to the emission index provided in the previous section. This result implies that the aircraft weight will increase when water condensation occurs if all the water is collected and then stored. A fuel consumption penalty is expected due to this increase in weight.

The volume of the water produced compared to the volume of fuel burnt can be calculated with the water and avtur emission indexes and densities. Assuming standard conditions, the water density is 1 kg/dm^3 and the avtur density is $0.8kg/dm^3$. Then, the volume ratio between water produced and fuel consumed can be calculated, and it is 1.00736. This result implies that the volume of water produced is similar to the volume of fuel burnt. Accordingly, fuel tanks could be used to store water using a membrane that separates both liquids.

The possibility of releasing liquid water into the atmosphere was also considered in CEEC. Liquid water can be discharged into the atmosphere during its collection with a different size or different state, reducing its Global Warming impact. The main disadvantage of this approach is that a better understanding of contrails and cirrus clouds is required. Another possibility consists on releasing liquid water at a lower altitude after having carried it during cruise phase for a period of time. An option to release liquid water is during the descent after the whole cruise flight phase. Releasing water at a lower altitude would prevent the formation of contrails and hence, the contrails radiative forcing would fade. The main disadvantage of carrying the water during cruise phase and then releasing at a lower altitude is that a fuel consumption penalty is associated.

In addition to the release of liquid water into the atmosphere, different aircraft or engine uses can be given to the condensed water. Collected water can be injected into the combustion chamber reducing the NO_x formation. An 80% reduction in NO_x can be achieved, as stated in reference (Lefebvre and Ballal 2010). Moreover, part of the condensed water can be used for aircraft systems.

2.3.3 Other technologies

Apart from the two contrail avoidance strategies described, several techniques have been designed with the same purpose over the last years. One of this techniques was based on chemical devices (Singh 1988). The objective of these chemical devices was to use additions to the aircraft plume to alleviate the saturation pressure of water required for condensation. Detergents or surfactants are injected into the plume to suppress the contrail formation. The consequences of carrying these detergents during the flight mission are weight and fuel consumption penalties.

Other process, known as sonication, prevents contrail formation with an ultrasound device (Noppel, Singh, and Taylor 2012). The process consists on the application of ultrasound on water droplets emissions reducing their pressure, what results in droplets vaporisation. This method can be an attractive contrail avoidance technique, but it has a weight and fuel consumption penalty.

3 AIRCRAFT AND ENGINE MODELS

The main objective of the current project was to study the effect of storing the water condensed from engine core exhaust for contrail prevention during cruise. In this chapter, the selection and creation of aircraft and engine baseline models used to analyse the aircraft performance are presented.

Regarding the selection of the aircraft and engine models, a large wide-body four-engine aircraft was chosen because the amount of stored water would be high enough to obtain unambiguous results. Between large wide-body four-engine aircraft a combination of an airframe inspired the Airbus A380 and a three-spool high bypass turbofan engine inspired by the Rolls-Royce Trent 900 was selected. It was the chosen option because it had already been employed in previous investigations of this contrail avoidance technique (Qureshi 2016).

A conventional turbofan engine was selected even though the concept in reference (Noppel 2007) suggested that an intercooled recuperated engine had to be used to condense the water at the engine core exhaust. However, the engine performance analysis conducted in reference (Qureshi 2016) suggests that the performance of the turbofan and the intercooled recuperated engines are similar. Accordingly, for simplicity, a three-spool high bypass turbofan inspired by the Roll-Royce Trent 900 was considered instead of an intercooled recuperated configuration engine.

For the creation of the aircraft baseline, firstly, an optimised model of the engine was designed with the software Turbomatch, and later, the aircraft model was created with the software Hermes, in which Turbomatch generates an engine input. A brief explanation of each software is provided in sections in which they are used.

Each model is presented in a different section. A brief introduction of the model, the assumptions considered, the model development, and finally, the model validation are included in both sections.

3.1 Three-spool high bypass turbofan engine

The three-spool high bypass turbofan engine was inspired by the Rolls-Royce (RR) Trent 900 because it is one of the possible options for the Airbus A380. It has been very successful as over half of operators selected this engine for the A380 instead of the other option, the Engine Alliance GP7000. According to ICAO, the RR Trent 900 engine also has lower NO_x emissions than the competitor (Rolls-Royce 2016).

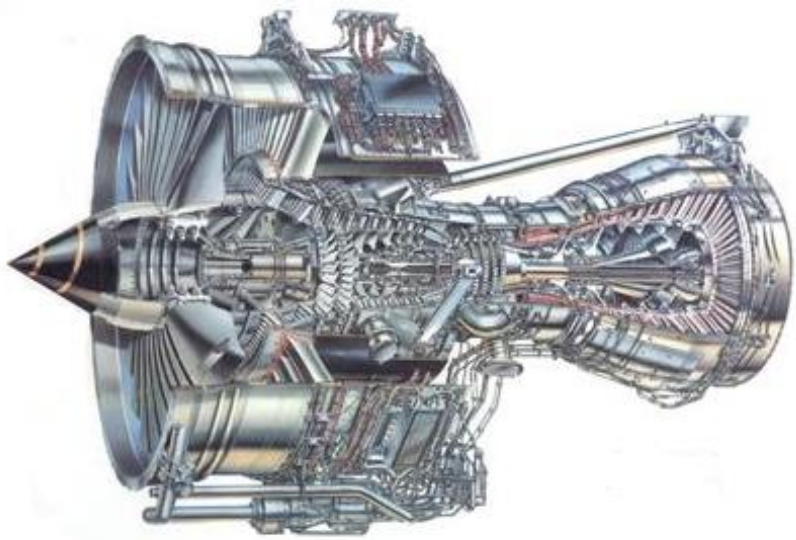

Figure 3-1: Rolls-Royce Trent 900 engines series cutaway (McAlpine 2016)

3.1.1 Engine specifications

RR Trent 900 has been defined so far as an engine, but it corresponds to an engine series. A cutaway of Trent 900 engines series is illustrated in Figure 3-1. According to reference (EASA 2013), seven different engines are classified as Trent 900. Thus, one of these engines had to be selected to design it according to the available data of the model. The chosen engine was RR Trent 970-84 because more data of this engine and of the corresponding aircraft model were available. However, the creation of a model completely identical to the original was not possible as engine manufacturers do not provide all the engine parameters data. As a result, the model was designed as similar as possible to the original engine with the available data, which are gathered in Table 3-1 with their corresponding source.

Cruise conditions (ISA)		
Altitude	10,670 m	(Daly 2011)
Mach number	0.85	(Daly 2011)
Thrust	65.4 kN	(Daly 2011)
SFC	14.665 mg/(N s)	(Daly 2011)
Take off (T/O) conditions (S/L)		
Mass flow	1,204-1,245 kg/s	(Daly 2011)
Bypass ratio (BPR)	8.5-8.7	(Daly 2011)
Pressure ratio	38.5	(Daly 2011)
Maximum COT	1,820 K	(EASA 2013)
Thrust	334.29 kN	(EASA 2013)
Fuel flow	2.6 kg/s	(ICAO 2013a)

Table 3-1: Trent 970-84 data for cruise and T/O conditions

Additionally, reference (EASA 2013) provided information about the compressor and turbine stages, and about bleed air extraction of the Trent 900 engines. The number of stages is presented in Table 3-2. Regarding the bleed air extraction, at normal operating conditions, there are 4 air bleeds apart from the combustor cooling bleed. The first bleed is located at the fan outlet to cool the air of the cabin system pre-cooler. The second bleed is taken off the HP turbine for the nacelle thermal anti-icing flow demand. Finally, air is bled from IP or HP compressor, depending on the port pressure in the compressors. No information about combustion chamber cooling bleed is given. For more details about Trent 900 series engines bleeds, see reference (EASA 2013).

	Compressor	***Turbine***
Low pressure (LP)	Single stage	5 stages
Intermediate pressure (IP)	8 stages	Single stage
High pressure (HP)	6 stages	Single stage

Table 3-2: Compressor and turbine stages of the Trent 900 series engines (EASA 2013)

3.1.2 Assumptions

Some assumptions were considered to facilitate the creation and design process of the engine. These assumptions are presented below.

- ISA conditions were considered during the whole flight mission.
- Pressure recovery was 99% for all the different flight phases.
- Compressors and turbines efficiencies were defined according to the current technology level.
- Pressure ratios of the different compressors were determined considering the data available.
- Stators angle was assumed to remain constant during the whole flight mission.
- Degradation of the components was neglected.
- Pressure losses in all ducts were 1%, except in the case of the combustor, in which a 6% pressure loss was used.
- Combustion efficiency was 99.8% throughout the whole mission.
- Air bled for combustion chamber cooling was assumed to be 19%.
- Only 2 of the 4 compressor bleeds of the original engine were taken into consideration. Nacelle thermal anti-ice bleed and IP compressor customer bleed were neglected for simplicity of the engine.
- Air bleeds located into a compressor were assumed to be situated before it.

3.1.3 Engine model design

The design of the engine model was carried out using the latest version of the software Turbomatch. This software has been developed by Cranfield University to simulate the performance of gas turbines in a non-linear steady state. In this software, the different components or parts of the engine are defined as bricks, and their corresponding parameters are known as brick data. In order to link the bricks, the utilisation of station vectors is required. Each station vector comprises the different properties of the gas at that station. For further details, refer to (Nikolaidis 2015).

Bearing in mind the data and assumptions stated before, the design of a three-spool high bypass turbofan engine inspired by the Trent 970-84 engine was conducted using the software Turbomatch. The first step was the creation of a schematic representation of the three-spool high bypass engine, which is illustrated in Figure 3-2. In this illustration, all the selected engine components and station numbers for the model are represented. Station numbering should have been defined according to SAE nomenclature (SAE 2004). However, as can be observed, this nomenclature was not followed in Figure 3-2 because it was assigned in accordance with the numbering used in Turbomatch input file, for easier understanding.

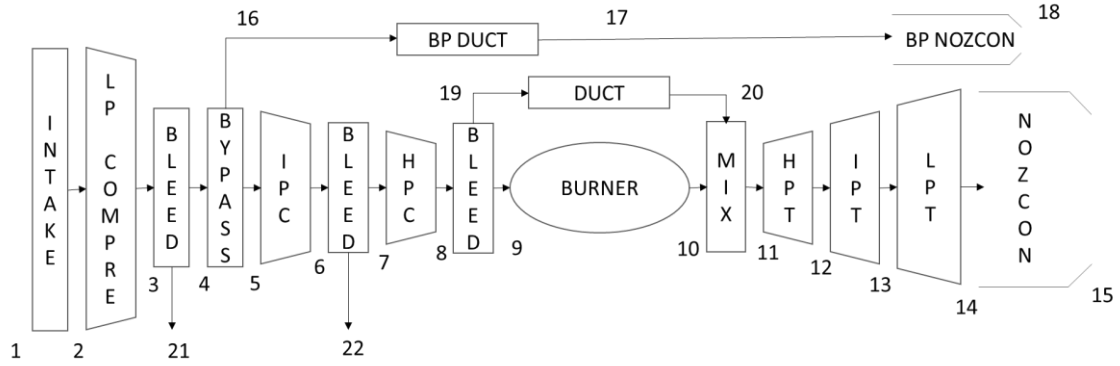

Figure 3-2: Scheme of the three-spool high bypass turbofan engine

The scheme represented in Figure 3-2 served as a basis to create the Turbomatch input code, which is given in Appendix A.1. The selected components and station numbers in this input code were the same as in Figure 3-2. In the Turbomatch input file cruise and take-off conditions are used to create an engine model as similar as possible to the RR Trent 970-84. The design point (DP) of the engine corresponds to cruise and the take-off condition was used to create an off design point (OD).

An optimisation of the values of turbomachinery DP efficiencies, compressors DP pressure ratios (PR), bypass ratio (BPR), DP and OD combustor outlet temperature (COT), DP mass flow and DP bleeds was carried out in Matlab to obtain thrust and SFC values at cruise and take-off conditions as close as possible to the data specified in Table 3-1. In addition to thrust and SFC, OD

mass flow and OD overall PR were outputs of the optimisation. The results of the optimisation are provided in Table 3-3.

Parameter	Optimised value
Fan DP efficiency	0.90
IP compressor DP efficiency	0.90
HP compressor DP efficiency	0.90
LP turbine DP efficiency	0.93
IP turbine DP efficiency	0.91
HP turbine DP efficiency	0.92
Fan DP PR	1.66
IP DP PR	4.00
HP DP PR	6.44
DP Bypass ratio	8.68
DP COT	1,603 K
OD COT	1,743 K
DP mass flow	518.76 kg/s
Bleed after fan	0.003
Bleed after IP compressor	0.02
Combustor cooling bleed	0.19

Table 3-3: Optimised values for Turbomatch input file

The brick data of the Turbomatch input file were defined in accordance with the values given in Table 3-3. The optimisation enabled the achievement of an engine model that works in a similar way to the RR Trent 970-84.

3.1.4 Engine model validation

In this section, the validation of the engine model inspired by the Trent RR 970-84 is presented. The validation was conducted comparing the results obtained in Turbomatch with the available data of the engine provided in Section 3.1.1. The engine model was designed with the primary goal of getting the Turbomatch results of the considered parameters as similar as possible to the datum. The

comparison between the values obtained from the Turbomatch model and the datum values/intervals is provided in Table 3-4.

Parameter	Value obtained from Turbomatch model	Datum value/interval	Deviation
DP Thrust	65,664 N	65,400 N	0.40%
DP SFC	15.53 mg/(N s)	14.67 mg/(N s)	5.86%
T/O Thrust	337,518 N	334,290 N	0.97%
T/O fuel flow	2.6 kg/s	2.6 kg/s	0.00%
T/O mass flow	1,203 kg/s	1,204-1,245 kg/s	0.08%
T/O BPR	8.71	8.5-8.7	0.12%
T/O overall PR	38.6	38.5	0.26%

Table 3-4: Validation of engine model results

As can be observed from this table, all the outcome parameters fitted appropriately to the datum value or interval with a deviation of less than 1%, except the cruise (design point) SFC. This deviation was quite high, almost 6%, what would result in a fuel over-consumption during cruise, which is the longest flight phase. This deviation might have been caused by the fact that several assumptions have been stated for this engine, so the performance of the engine model changed slightly from the original engine. Additionally, fuel consumption tests are commonly carried out in a low consumption environment and with a low consumption engine setting. Despite this slight deviation on DP SFC, as the other values adjusted appropriately to datum, the model was considered accurate and valid for the upcoming analyses.

Finally, this engine model inspired by the RR Trent 970-84 was included in the Turbomatch engine library of Cranfield University.

3.2 Large wide-body aircraft

The large wide-body aircraft was inspired by the Airbus A380 as stated in the introduction of this chapter. The Airbus A380 aircraft is the largest commercial aircraft flying nowadays, with a capacity from 544 to 853 passengers, depending

on the class configuration. The double-deck configuration offers 50% more floor surface than the next largest aircraft. The long ranges of more than 15,200 km that this aircraft can achieved also alleviate traffic congestion (Airbus 2016).

Figure 3-3: Airbus A380 (Airbus 2016)

3.2.1 Aircraft specifications

The Airbus aircraft model that corresponds to the engine selected in the previous section is the Airbus A380-841, according to reference (Jane's 2015). This aircraft configuration belongs to A380-800 series and the available weight data about it are gathered in Table 3-5, with their corresponding source. External dimensions data were also provided in reference (Jane's 2015).

Parameter	Value	Source
Aircraft empty weight	270,010 kg	(Jane's 2015)
Maximum T/O weight	560,000 kg	(Jane's 2015)
Maximum landing weight	389,995 kg	(Jane's 2015)
Maximum payload weight	83,700 kg	(Airbus 2014)
Maximum fuel weight	259,465 kg	(Jane's 2015)

Table 3-5: Weight specification data of Airbus A380

Regarding the mission specification data, the A380 cruising altitude is 10,670 m according to reference (Jane's 2015). This value is in line with the Trent 970-84

cruise altitude specified in Table 3-1. Reference (Jane's 2015) states that the economy Mach number of the A380 is 0.82 while the Mach number specified in engine data is 0.85 (Daly 2011). As the economy Mach number suggested for the aircraft, 0.82, corresponds to the A380 model with Engine Alliance GP 7000 installed, a Mach number of 0.85 was selected in accordance with the engine data.

Finally, the A380 payload-range diagram is represented in Figure 3-4. Assumptions are included at the bottom left of the chart. As can be observed, the maximum payload coincides with the value stated in Table 3-5. The maximum achievable range by the A380 is around 17,600 km with no payload.

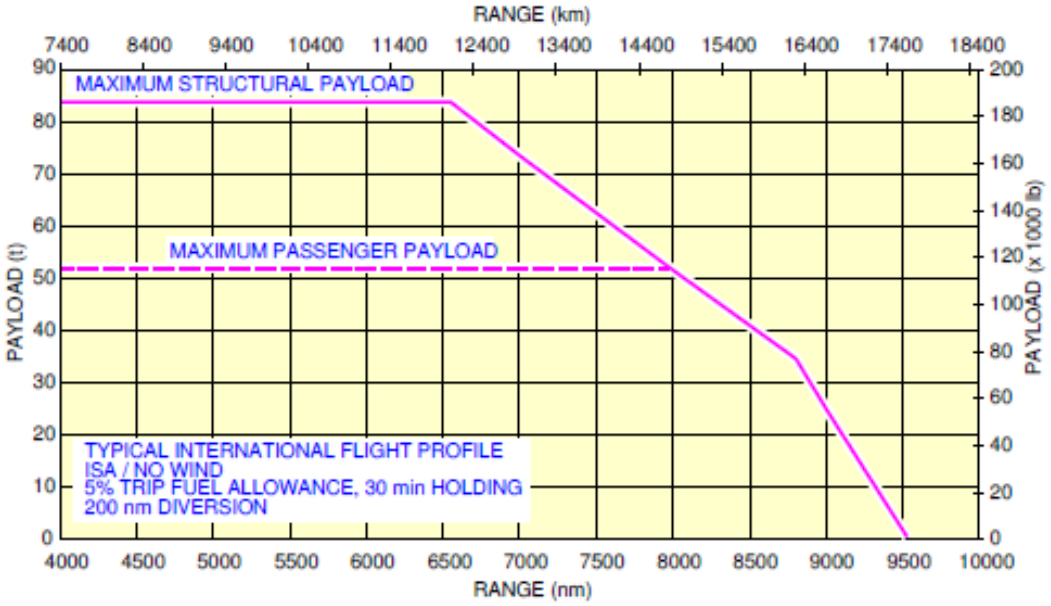

Figure 3-4: A380 Payload-Range diagram (Airbus 2014)

3.2.2 Assumptions and considerations

Some assumptions and considerations to facilitate the creation and design process of the aircraft are presented below.

- Constant altitude and Mach number during the cruise phase.
- No diversion was considered during the flight mission.
- No ambient temperature deviation from ISA and zero wind was assumed.
- Relative contingency fuel to remain after landing was 5%.
- Holding altitude was 457 m and hold time was 30 min.

The first three assumptions were stated for a simplification of the aircraft design. The other two assumptions were held in accordance with conventional reserves used for fuel planning (Jenkinson, Simpkin, and Rhodes 1999). The contingency fuel is carried in case of deviations from the expected fuel consumption data, from meteorological conditions or from planned routes/altitudes occur (Laskaridis, Pilidis, and Kotsiopoulos 2005).

3.2.3 Aircraft model design

The design of the aircraft model was conducted using the software Hermes. This software has been developed by Cranfield University, and it simulates the performance of aircraft, including the engine performance using the software Turbomatch. The creation of the aircraft model using Hermes is based on a modular layout, so that the modules can be easily altered and integrated for different analysis. The six different modules are: shape and geometry data, mission profile, atmospheric data, engine data, aerodynamic data, and aircraft performance (Laskaridis et al. 2005).

Hermes input files consist of the geometry, mission, and engine specification data (GeomMissionEngineSpec input) and the engine performance data (EngPerfData input). The GeomMissionEngineSpec input comprises four sets of data:

1. Shape and geometry data
2. Mission/weight specification data
3. Mission profile specification data
4. Engine specification data

The GeomMissionEngineSpec file of this project was designed using the same input created in reference (Qureshi 2016) as a baseline. Qureshi's input was created for an aircraft model inspired by the A380-800. Therefore, some modifications are carried out in Qureshi's file to adapt the input for the aircraft model inspired by the A380-841. The created GeomMissionEngineSpec Hermes input is provided in Appendix B.1. The shape and geometry data are the same

except for the engine length and diameter. The new engine dimensions data are taken from reference (EASA 2013).

The mission/weight specification data were modified according to the assumptions stated in the previous subsection and the weight data specified in Table 3-5. The engine weight is also adjusted in accordance with reference (EASA 2013). Finally, either the range or the fuel weight must be defined as an input of this data set. For the present study, the range was selected as input. The value of the input range corresponds to the DP range, which is the maximum range that can be reached with the maximum payload.

The mission profile specification data set of the present input file was the same as in Qureshi's file. In this data set the duration of landing and taxi phase were in line with allowances stated by reference (Jenkinson et al. 1999). Landing phase typical duration is 6 min both for domestic and for international flights. However, characteristic duration of the taxi phase is 9 min for domestic flights and 12 minutes for international flights. Consequently, as long and short haul flights were considered during the analysis an intermediate value of 10 min was selected.

Lastly, the engine specification data had to be defined to complete the GeomMissionEngineSpec input file. In this data set, information from the Turbomatch input code, described previously in Section 3.1, is required. One of these inputs, the COT interval for each flight phase, must be selected carefully because it is the major source of convergence issues in Hermes. If the intervals are selected arbitrarily without taking into account the operation of the engine model throughout the whole flight path, the interval could be too low to the aircraft to climb or too high so that the aircraft cannot descend.

This last data set of the GeomMissionEngineSpec input file is not read by Hermes, and it is only used, accompanied with the DP Trent 970-84 engine code, for the creation of the other Hermes input file, EngPerfData, using Turbomatch. The version of the Turbomatch software linked with Hermes is not the latest version utilised for the engine creation. Therefore, the EngPerfData input was generated manually using the most recent version of Turbomatch to ensure consistency of the results. The Hermes output files comprise the aircraft

performance and the engine performance data. For further information about Hermes refer to the user manual (Cranfield University 2009).

3.2.4 Aircraft model validation

In this section, the validation of the aircraft model inspired by the Airbus A380-841 was conducted comparing between the payload-range diagram of the aircraft model obtained from Hermes and the A380 payload-range diagram adopted from Airbus datasheet (Airbus 2014).

The payload-range diagram of the model was represented changing the payload-range setting of the aircraft design in Hermes. This diagram takes into account the maximum T/O weight and the maximum fuel weight.

Both payload-range diagrams were calculated for the same flight characteristics, and they are represented in Figure 3-5.

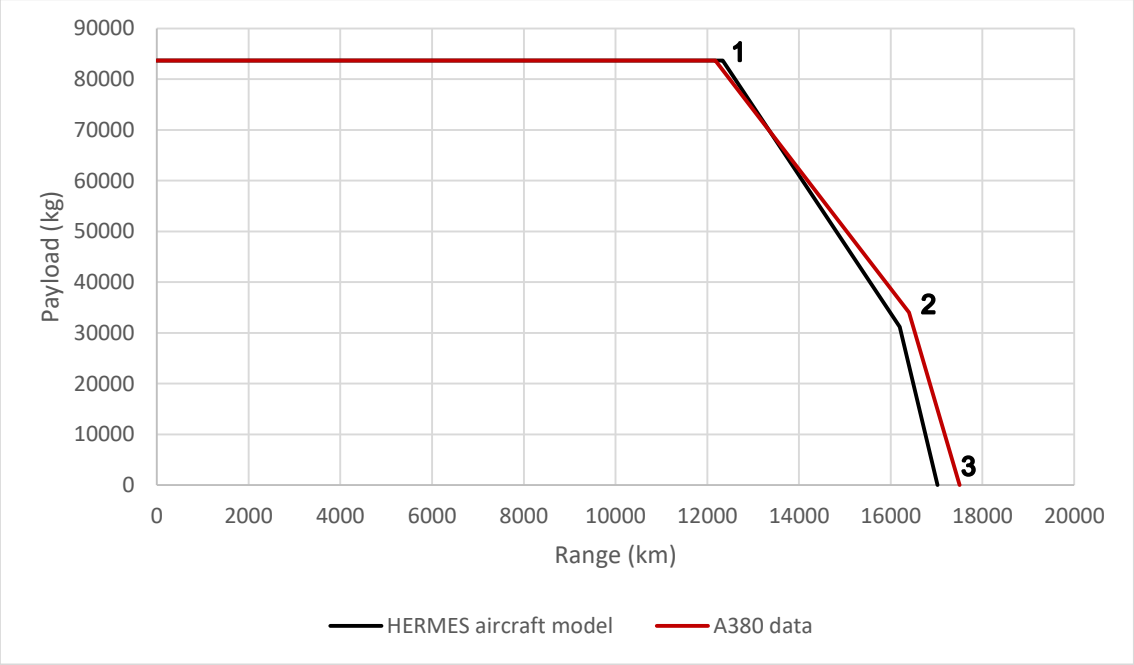

Figure 3-5: Payload-range diagram of Hermes aircraft model and A380

In this chart, the black line illustrates the aircraft model designed with Hermes and the red line shows the A380 diagram. As can be observed, the design point of the Hermes diagram is very similar to the DP of the original A380 curve (point

1). After the DP, the curve slope changes because the maximum T/O weight cannot be exceeded. Then, this slope varies again after point 2 due to another limitation, the maximum fuel weight. Finally, the point 3 represents the maximum range point, in which the payload carried is null.

The range deviation of the Hermes aircraft model with regard to the A380 at the marked points of the chart is presented in Table 3-6. The range deviations of the three points were below 3%. The payload-range deviation could be caused by the higher SFC at cruise of the created engine model and the differences in the aircraft performance. Taking into account the similar pattern of both diagrams and low deviation of the points, the aircraft model was accepted.

Point number	Range deviation
Point 1	1.27%
Point 2	1.22%
Point 3	2.74%

Table 3-6: Range and payload deviations of the Hermes model

Finally, due to the satisfactory results of the aircraft baseline model inspired by the A380-Trent 900 configuration, the model was considered valid for the current work.

4 AIRCRAFT PERFORMANCE ASSESSMENT WITH WATER STORAGE

In this chapter the methodology to study the aircraft performance with water storage for contrail prevention during cruise is described. It also includes the steps to conduct a global warming analysis can be with the results of the aircraft performance.

4.1 Aircraft performance analysis

Once the model inspired by A380-Trent 900 was built with the software Hermes, the next step of the present study was the implementation of the contrail avoidance strategy suggested in reference (Noppel 2007) to the aircraft baseline model. The contrail avoidance technique consists in the water condensation at the engine core exhaust. The condensed water can be stored on the aircraft or it can be released into the atmosphere. The current study focuses only on water storage during cruise, and water release was assumed to happen after this flight phase. For this reason, the storing water aircraft was simulated only during cruise.

To conduct this analysis, the aircraft baseline model and the aircraft model carrying water during cruise were compared. The model of the water-carrying aircraft during cruise was made with the software Matlab. In this case, Hermes was not used because it cannot change the aircraft weight due to the collection and storage of water during the cruise phase. In order to use the same software for the final comparison analysis between the baseline model and the water-carrying aircraft, the baseline model was also built with Matlab, in accordance with the Hermes results. A validation process of the baseline model in Matlab was conducted to verify that the Matlab aircraft performance was similar to the Hermes aircraft performance.

Throughout this section, the below-mentioned points are followed.

- Assumptions of water storage aircraft
- Aircraft baseline model algorithm
- Water storage model algorithm

- Water storage model implementation in Matlab
- Validation of the Matlab model

4.1.1 Assumptions and considerations

Some assumptions and considerations were stated to facilitate the creation of the water storage aircraft model. These assumptions are presented below.

- Water was only stored during the cruise phase, and it was released once this phase is completed. It was assumed that contrails are only formed during cruise.
- According to the water emission index, 1.2592 kg of water were produced per 1 kg of fuel burn.
- All the water produced was stored on the aircraft.
- Constant altitude and Mach number during the cruise phase.
- No ambient temperature deviation from ISA and zero wind.

These assumptions were implemented in the water storage analysis. Only the last two assumptions needed to be applied to the aircraft baseline model.

4.1.2 Aircraft baseline model algorithm

In this section, the algorithm to create the Matlab baseline model is presented. This algorithm is very similar to the one that was used in the water storage case, and only minor modifications were applied in the water storage model.

First of all, the Matlab model was developed during cruise condition because contrails were assumed to form only at that phase. The Matlab algorithm of the aircraft baseline model was created in accordance with Hermes algorithm. Consequently, some results of the Hermes simulation were required by the Matlab model for a similar aircraft performance. In Hermes, the whole cruise phase is divided into small segments and the same operations are repeated in each segment to obtain the aircraft and engine performances during cruise. The Matlab model followed the same method, splitting the cruise phase in the same number of segments as Hermes. The operations in each segment were defined

emulating the Hermes simulation. The Matlab algorithm of each cruise segment is represented in Figure 4-1.

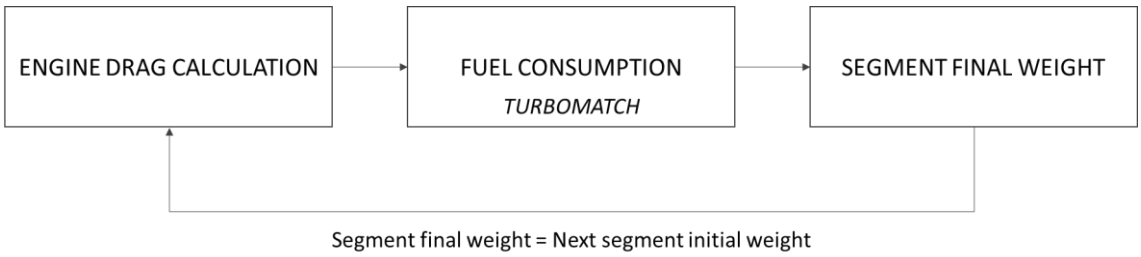

Figure 4-1: Scheme of the cruise segment algorithm

This scheme illustrates the three main calculations of the Matlab aircraft performance simulation. The cruise initial weight is required to start the simulation of the algorithm. Then, the algorithm is repeated for all the cruise segments. The final weight of one cruise segment is used as the initial weight of the following segment. The three primary calculations of the algorithm are detailed and explained thoroughly in the following subsections.

4.1.2.1 Engine drag calculation

The objective of this calculation was to obtain the engine drag of the corresponding segment initial weight. The required operations are summarised in Figure 4-2 and detailed in this section.

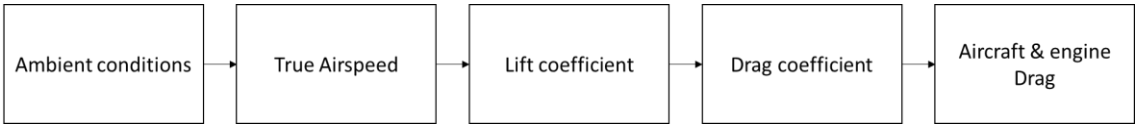

Figure 4-2: Algorithm to calculate engine drag

First of all, the ambient conditions must be defined to calculate the density of air at the cruise altitude, which was set as 10,670 m. The ambient pressure and temperature are defined in equations (4-1) and (4-2). These equations were extracted from reference (Cavcar 2014), and they enable the ambient conditions calculation for a given altitude h. Sea level (S/L) pressure and temperature must be known. Then, air density can be estimated with the ambient pressure and

temperature, as provided in equation (4-3). SI units must be used in these formulae.

$$T_{amb(h)} = T_{S/L} - 6.5\ \frac{h}{1000} \quad \textbf{(4-1)}$$

$$P_{amb(h)} = P_{S/L}\left(1 - 0.0065\ \frac{h}{T_{S/L}}\right)^{5.2561} \quad \textbf{(4-2)}$$

$$\rho_{amb(h)} = \frac{P_{amb(h)}}{R\ T_{amb(h)}} \quad \textbf{(4-3)}$$

Furthermore, True Airspeed (TAS) must be calculated for the Mach number M selected for the cruise mission, which was 0.85. TAS calculation is provided in equation (4-4) and it was extracted from reference (Lawson 2016). In this equation, the ratio of specific heat γ, Mach number M, the ideal gas constant R and the ambient temperature at cruise altitude $T_{amb(h)}$ are used for TAS calculation. A constant value of 1.4 was assumed for the ratio of specific heat. SI units must be used in this formula.

$$TAS = M\sqrt{\gamma\ R\ T_{amb(h)}} \quad \textbf{(4-4)}$$

The ambient cruise temperature, pressure, density and the TAS are required parameters during the whole segment algorithm. Once these values are determined, the lift coefficient and drag coefficient of the aircraft can be estimated as shown in equations (4-5) and (4-6). These formulae are provided in reference (Eurocontrol 2011).

Looking at the lift coefficient formula, initial weight W_i, gravity acceleration g, air density ρ at cruise altitude, True Airspeed TAS and wing reference area S are necessary for the lift coefficient C_L calculation. The wing reference area of the A380 aircraft is 845 m^2 (Jane's 2015). The drag coefficient of the aircraft model inspired by the A380 was determined with the lift coefficient. The profile drag coefficient C_{D0} and the lift dependent coefficient C_{Dl} are constants and their value can be obtained from documents like reference (BADA 2011). In this document, the values of C_{D0} and C_{Dl} for the different flight phases are given. However,

Hermes calculates these values in a different way and it does not give them as results. Consequently, they were determined using the lift and drag coefficients of the aircraft performance Hermes output file. The resultant values of C_{D0} and C_{Dl} were 0.1601 and 0.04479, respectively. Despite having data on the public domain, the calculated values were used to ensure that the Matlab model was similar to the Hermes model.

$$C_L = \frac{2\, W_i\, g}{\rho\, TAS^2\, S} \quad \textbf{(4-5)}$$

$$C_D = C_{D0} + C_{Dl}\,(C_L)^2 \quad \textbf{(4-6)}$$

Finally, the aircraft and engine drag are calculated with the drag coefficient as shown in equations (4-7) and (4-8). The aircraft drag calculation formula was extracted from reference (Eurocontrol 2011). In this formula drag coefficient C_D and other parameters detailed before were used. Once the aircraft drag is determined, the engine drag is calculated just dividing the aircraft drag by the number of engines, which was 4 in this case.

$$D_{A/C} = \frac{C_D\, \rho\, (TAS)^2\, S}{2} \quad \textbf{(4-7)}$$

$$D_{eng} = \frac{D_{A/C}}{4} \quad \textbf{(4-8)}$$

4.1.2.2 Fuel consumption calculation

This section presents the calculation procedure of the fuel consumption of the aircraft using the engine drag calculated as explained in the previous section. The operations are summarised in Figure 4-3 and detailed in this section.

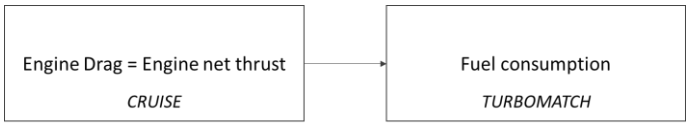

Figure 4-3: Algorithm to calculate engine fuel consumption

The engine net thrust is equal to the engine drag during cruise phase if straight and level flight path is assumed. Then, the fuel consumption of the engine is given

by Turbomatch defining the net thrust, cruise altitude, and Mach number as inputs. The result of this calculation is different for each cruise segment because drag changes with the segment initial weight.

4.1.2.3 Segment final weight calculation

The fuel consumption estimated by Turbomatch is required to determine the segment final weight of the aircraft. The operations to achieve this objective are summarised in Figure 4-4 and detailed in the present section.

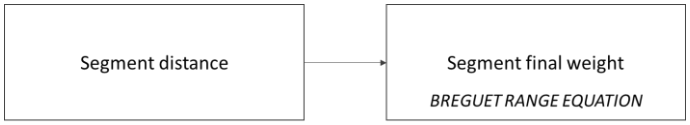

Figure 4-4: Algorithm to calculate segment final weight

First of all, the distance of each segment is calculated by dividing the cruise total range by the number of segments. Then, the Breguet Range equation is used to calculate the segment final weight of the aircraft with the segment distance, as shown in equation (4-9). This mathematical statement was provided in reference (Waitz 2008).

$$dist_{seg} = \frac{TAS\ (L/D)}{g\ SFC}\ ln\left(\frac{W_{initial}}{W_{final}}\right) \quad \textbf{(4-9)}$$

In the Breguet Range equation the segment distance $dist_{seg}$, the True Airspeed TAS, the lift to drag ratio L/D, the gravity acceleration g, the SFC and the segment initial weight $W_{initial}$ are known parameters, so the segment final weight W_{final} can be determined. The lift coefficient to drag coefficient ratio C_L/C_D is used instead of the lift to drag ratio L/D. This operation is consistent because C_L/C_D is a simplification of L/D.

4.1.3 Water storage model algorithm

The algorithm used in Matlab for the water storage model is very similar to the baseline model as only one operation must be added. The first two main calculations, engine drag, and fuel consumption are the same. But the segment final weight calculation changes because the water weight must be introduced in

this operation. Consequently, the algorithm of the segment final weight is modified as shown in Figure 4-5.

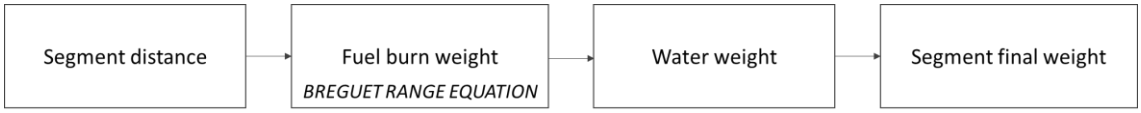

Figure 4-5: Algorithm to calculate segment final weight in water storage model

The Breguet range equation gives the final weight of a segment. The fuel burn weight can be calculated as the difference between the segment initial weight and the final weight given by the Breguet range equation for the same segment. Then, the weight of the water produced from the combustion during the segment is calculated multiplying the fuel burn weight and the emission index, as shown in equation (4-10). The difference between the water and fuel burn weight is added to the segment initial weight to determine the final weight of the segment. This operation is presented in equation (4-11).

$$W_w = EI_w W_{fuel} \quad \textbf{(4-10)}$$

$$W_{final} = W_{initial} + (W_w - W_{fuel}) \quad \textbf{(4-11)}$$

Using this methodology, two aircraft performance analyses can be conducted:

- A range comparison between the baseline and the water storage model using the same amount of fuel to observe the range reduction because of carrying the water
- A fuel burn penalty comparison between the baseline and the water storage model flying the same distance

4.1.3.1 Range reduction analysis

In the range reduction analysis, the Matlab baseline model is simulated using the payload-range diagram of the baseline aircraft as a reference.

The fuel burnt by the baseline model during the cruise phase is set as a limitation in the water storage simulation, as the engine cannot burn more fuel than what is carrying. Consequently, a reduction in the cruise range is experienced by the water storage aircraft due to the fuel overconsumption. The fuel restriction is not

the only limitation, as the maximum take-off weight cannot be exceeded during cruise either.

Considering these limitations, the range reduction during cruise of the DP (maximum range for the maximum payload) can be determined. Then, the climb and descent distances are assumed to be the same in both models. Consequently, the cruise range reduction is equal to the mission range reduction. This way, the payload-range diagram of the water storage model can be represented considering all the restrictions. The new payload-range diagram should look similar to the red dashed line of the diagram in Figure 4-6. The blue line is taken from Figure 3-5 to represent the baseline aircraft. The range reduction should result in the design point moving to the left, from DP to DP'.

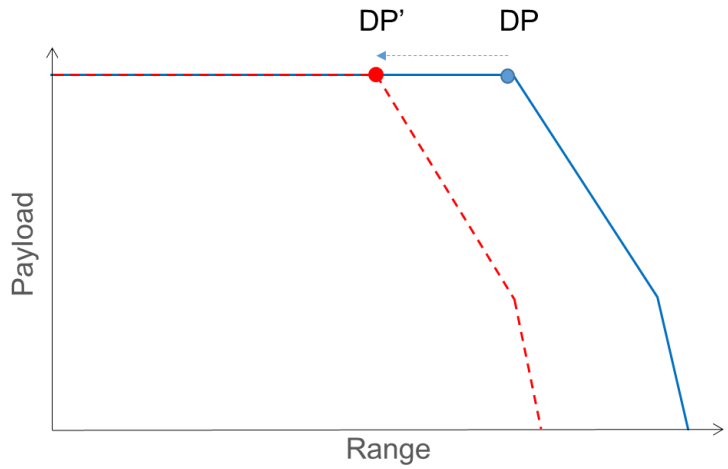

Figure 4-6: Expected behaviour of the water-storing aircraft range.

4.1.3.2 Fuel burn penalty

As seen in the previous section, a payload-range diagram showing a different design point is generated from the range reduction analysis. The new design point given by that diagram is used to calculate the fuel burnt of the baseline and the water storage models. Comparing the results of both models, the fuel burn penalty is obtained.

The fuel burnt by the baseline model can be calculated in Matlab, adopting the cruise initial weight, number of segments and cruise range directly from Hermes. The water storing aircraft should have a higher cruise initial weight than the

baseline because it needs to carry more fuel to complete the same range, due to the fuel overconsumption. This fact makes the calculation of the fuel burnt by the water storing aircraft slightly more complex than for the case of the baseline aircraft.

The procedure to calculate the fuel burn penalty of the water storing aircraft is as follows:

1. Using Hermes, the range of the conventional aircraft is increased, consequently increasing the amount of fuel that it requires for the mission, what gives an augmented cruise initial weight.
2. With the new cruise initial conditions, a range reduction analysis is conducted. This is done to verify that the range introduced in Hermes for the conventional aircraft produces the DP' range in the water storing aircraft.
3. If the range reduction analysis proves that the range introduced in Hermes was correct, the fuel burn penalty can be calculated. If, however, the range reduction analysis provides a value of the range different to DP', the procedure must be repeated from step 1.

Once the answer to step 3 is positive, the fuel burn penalty is calculated comparing the weight of the fuel burnt of the baseline and water storing models at the end of cruise.

4.1.4 Water storage model implementation

The implementation of the water storage model in Matlab is explained in this section. Different functions were created to include the algorithms and analyses presented before. In the following subsections, each function is described. For further details of the algorithms, see Sections 4.1.2 and 4.1.3.

4.1.4.1 Engine Drag

The Engine Drag function calculates the engine drag from the segment initial weight. The algorithm with the different inputs and outputs is provided in Figure 4-7. Inputs are represented as entering arrows and outputs as exiting arrows. The cruise initial weight is only required for the first loop.

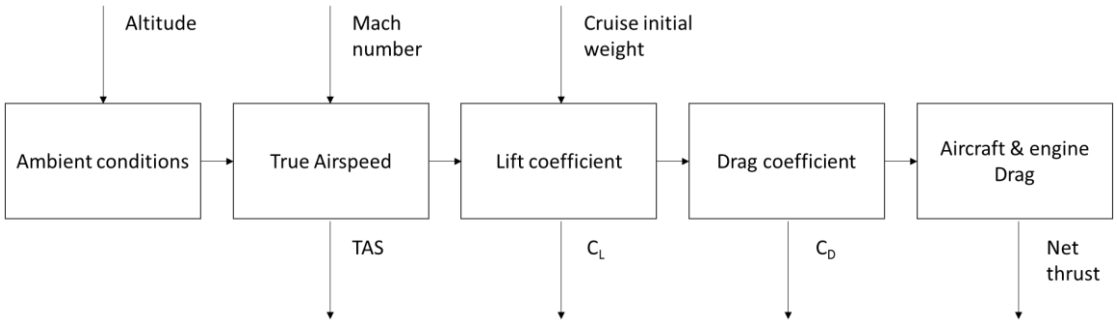

Figure 4-7: Algorithm of engine drag calculation with inputs/outputs

4.1.4.2 Fuel consumption

The fuel consumption function determines the engine SFC taking the cruise altitude, Mach number, and net thrust as inputs. This Matlab function calls the Turbomatch software and introduces the cruise altitude, Mach number and net thrust, obtaining the engine SFC as an output. The algorithm of this function with the corresponding inputs and outputs is represented in Figure 4-8.

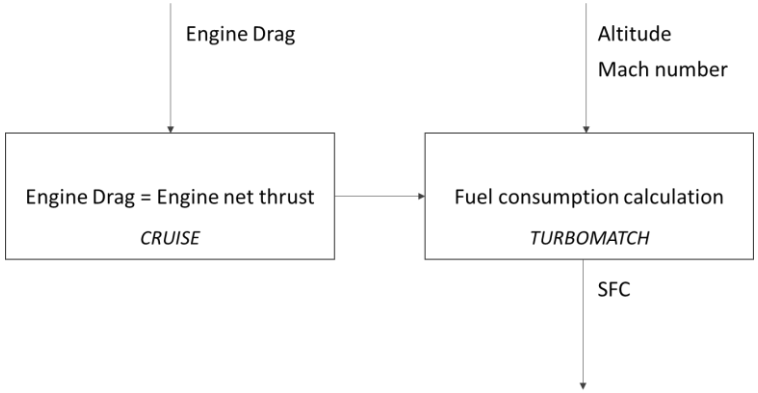

Figure 4-8: Algorithm of the fuel consumption calculation with inputs/outputs

4.1.4.3 Segment distance

A simple function to calculate the distance of each cruise segment was created. Only the cruise range and the total number of segments are needed to calculate this distance. Hermes simulation considers that the distance of the first and the last cruise segments is half the length of the other segments. Consequently, a new input is required in this function, the segment number. The inputs and outputs are represented in Figure 4-9.

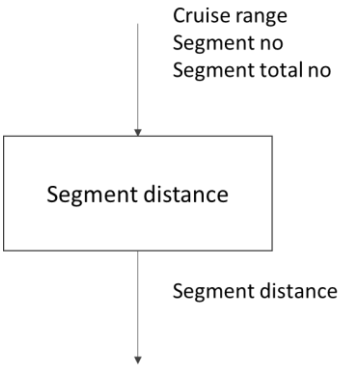

Figure 4-9: Inputs/Outputs for the segment distance calculation

4.1.4.4 Segment final weight

This function calculates the segment final weight from the engine fuel consumption. The algorithm with the different inputs and outputs is provided in Figure 4-10.

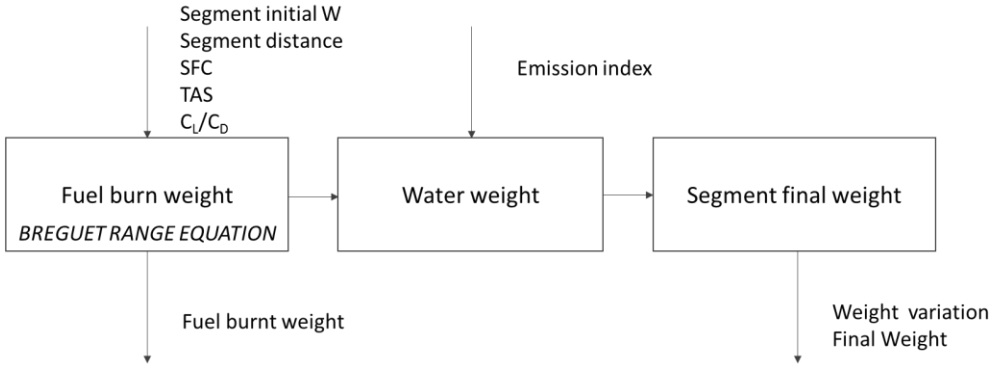

Figure 4-10: Algorithm of the segment final weight calculation with inputs/outputs

In this case, the emission index input indicates the quantity of water per kilogramme of fuel burnt that is stored on the aircraft. In the baseline case, the value 0 is used for this input, because even though water is produced in the combustion process, none of it is stored.

4.1.4.5 Range reduction analysis

This Matlab function determines the range reduction experienced by the water storage model with reference to baseline model using the same amount of fuel. This function brings together all the previous ones.

Firstly, a loop is implemented to obtain the aircraft baseline model during cruise. Then, taking the total fuel burnt of this simulation as a reference, another loop calculates the cruise range reduction due to the water-carrying of the aircraft. The climb and descent distances are assumed to be the same as in the baseline case. This assumption enables the calculation of the total reduced range of the water storage aircraft.

This analysis requires many inputs and produces several outputs. There are two kinds of outputs: Excel outputs and Matlab outputs. The Excel outputs are saved in a matrix that has the same number of rows as number of segments and the same number of columns as the number of excel outputs. This array is written in an Excel file at the end of the loop. As there are two loops in this function, one for each model, two arrays are generated and then written in different cells in the same Excel sheet.

Inputs	Outputs
Cruise altitude	Segment number (*Ex*)
Mach number	Cumulated time (*Ex*)
Cruise initial weight (*He*)	Net thrust (*Ex*)
Cruise range (*He*)	SFC (*Ex*)
Climb distance (*He*)	Aircraft total weight (*Ex*)
Descent distance (*He*)	Cruise segment fuel burn weight (*Ex*)
Segment total number (*He*)	Cumulated fuel burn weight (*Ex*)
	Segment distance (*Ex*)
	Cruise covered distance (*Ex*)
	Drag coefficient (*Ex*)
	Lift coefficient (*Ex*)
	Total reduced range
	Validation variable

Table 4-1: Inputs/Outputs of the range reduction function

Two extra outputs are given by the Matlab function: the total reduced range of the water storage model and a variable that informs if maximum T/O weight is

exceeded or not during cruise. All the inputs and outputs used in this function are presented in Table 4-1.

The inputs marked with a *He* are extracted from Hermes aircraft performance output. Furthermore, the outputs marked with an *Ex* are excel outputs, and they are used in the comparison between the baseline and the water storage model.

4.1.4.6 Fuel burn penalty analysis

This Matlab function calculates the fuel burn penalty experienced by the water storage model with reference to the baseline model that covers the same flying distance. This function brings together the first four functions presented before.

Only one loop is implemented in this function to simulate the fuel burn penalty of both the baseline and the water storage models during cruise. This loop is simulated for the baseline model if the emission index input is defined as 0. If the emission index input is set as 1.2592, the loop is simulated for the water storage model. The meaning of the emission index input is explained in Section 4.1.4.4.

Inputs	Outputs
Cruise altitude	Segment number
Mach number	Cumulated time
Cruise initial weight (*He*)	Net thrust
Emission index input	SFC
Cruise range (*He*)	Aircraft total weight
Segment total number (*He*)	Cruise segment fuel burn weight
	Cumulated fuel burn weight
	Segment distance
	Cruise covered distance
	Drag coefficient
	Lift coefficient

Table 4-2: Inputs/Outputs of the fuel burn penalty analysis

This analysis requires many inputs and produces several outputs that are saved in a matrix that has the same number of rows as number of segments and the

same number of columns as the number of excel outputs. This matrix is written in Excel at the end of the loop, and it is written in different cells in the same Excel sheet depending on the model simulated. All the inputs and outputs are provided in Table 4-2. The inputs marked with a *He* are extracted from Hermes aircraft performance output.

4.1.5 Matlab model validation

This subsection presents the validation of the baseline mode simulated with Matlab with respect to the Hermes baseline model. As it was explained in the methodology, the Matlab model only simulates the aircraft performance during cruise. Thus, the results obtained during cruise performance for both models were compared, analysing the deviation between them.

The Matlab baseline model during cruise was created imitating the method of the software Hermes. For this reason, the cruise phase was divided into small segments, as stated in the methodology. Then, both simulations were conducted considering the DP of the payload-range diagram as the reference point. With this aircraft payload-range combination, the performance outputs were calculated for each cruise segment in the way specified in Section 4.1.4.6. The maximum deviation of the different output parameters between Hermes and Matlab results during cruise phase is presented in Table 4-3.

On the basis of these results, it could be concluded that the aircraft simulation designed with Matlab was very accurate as the deviation of all parameters was below or equal to 0.33%. The largest deviation corresponded to the cumulated time. This deviation value was obtained in the first cruise segment because Hermes does not use as many decimals as Matlab. During the cruise phase, this error stabilised and reduced to values around 0.05%. This deviation is considered a systematic error.

The deviation of the drag coefficient was random, and consequently, the drag coefficient deviation is considered a random error. In the cases of the SCF and cruise segment fuel burnt, the largest deviation value was obtained at the last cruise segment. As it was expected, these results demonstrate that both

parameters are related. The error experienced by these two parameters is systematic. The deviations of the other parameters were very low and they are systematic errors.

Parameter	Deviation
Cumulated time	0.33%
Net thrust	0.04%
SFC	0.24%
Aircraft total weight	0.01%
Cruise segment fuel burn weight	0.22%
Cumulated fuel burn weight	0.02%
Segment distance	0.00%
Cruise covered distance	0.00%
Drag coefficient	0.27%
Lift coefficient	0.10%

Table 4-3: Validation of Matlab model

In conclusion, the Matlab model was considered valid due to its accuracy in relation to the Hermes software performance results during cruise.

4.2 Global Warming analysis

The main objective of the Global Warming analysis was to assess if the contrail prevention counteracts the additionally emitted carbon dioxide. This additional CO_2 is emitted because of the fuel burn penalty. The value of this penalty was obtained from the aircraft performance simulation carrying water.

To conduct this assessment, a Global Warming metric was selected. As the residence time of CO_2 and contrails is completely different, the selection process was not an easy task. For this reason, in this section, firstly, the GW metric selection is discussed and secondly, the model to analyse the GW impact of contrails and CO_2 with the selected metric is described.

4.2.1 Global Warming metric selection

Nowadays, the selection of a proper metric to assess the aviation Global Warming impact is still an issue. As stated above, this is due to the different residence time of aircraft emissions.

The different metrics that can measure the GW impact of aviation are defined and explained in Section 2.2.1. These metrics are Radiative Forcing (RF), Global Warming Potential (GWP) and Global Warming Temperature (GWT). The advantages and disadvantages of each metric are presented in Table 4-4.

	Advantages	Disadvantages
RF	Easily usable and understandable metric	Backward looking metric only based on current concentrations
GWP	It analyses the GW impact of emissions on a timescale	Short-lived pollutants, whose occurrence is limited to some locations, is not suitably measured
GWT	The average surface temperature response to an emission is measured at a specific future point in time	More research is required on this metric

Table 4-4: Advantages and disadvantages of different GW metrics

Considering the information provided in Table 4-4, it was concluded that GWP was not a proper metric to determine the GW impact of aviation, as emissions with a short residence time are not suitably measured. Regarding GWT metric, it is expected to replace GWP in the future, but further research on the metric is required. Consequently, radiative forcing (RF) was selected as the metric to measure the GW impact of aviation, even though it determines the current imbalance of past emissions.

4.2.2 Global Warming impact of contrails and CO_2

The procedure to assess the Global Warming impact of contrails and CO_2 is described in this section. This analysis was conducted to verify if the fuel burn penalty due to the avoidance of contrails was beneficial for Global Warming.

A model to analyse the Global Warming impact of contrails and CO_2 was developed using the selected metric, radiative forcing. This model consists of a 1 m^2 surface, and the global average emissions of aviation per sq m are located on it. The average value was used because the occurrence of some emissions is limited to some altitudes and latitudes. This model enables the analysis of the radiative forcing of each individual aircraft pollutant.

Current values of radiative forcing only are not enough to measure the GW impact of avoiding contrails. This is because radiative forcing is a backward looking metric, and it only measures the current imbalance of past emissions. For this reason, future scenarios of radiative forcing were considered to analyse the GW effect of contrails avoidance. The radiative forcing values of 2005, 2020 and 2050 were extracted from reference (Lee et al. 2009) and presented in Appendix C.1. With the RF forecast, the 1 m^2 surface model could be used to determine if the fuel burn penalty due to the avoidance of contrails was beneficial. But first, the assumptions considered when contrails are prevented must be introduced:

- Radiative forcing of contrails, cirrus clouds and water vapour are zero.
- CO_2 radiative forcing rate increases according to the fuel burn penalty of the contrail prevention technique.

In this study, it was assumed that all the water produced by the fuel combustion during cruise phase was collected and stored on the aircraft. This stored water was then released at a lower altitude after the cruise phase. Consequently, contrails and aircraft induced cirrus clouds formation was prevented during cruise phase and their RF could be assumed zero. However, water vapour release was not avoided as all the water collected was emitted at a lower altitude. According to reference (Frömming et al. 2012), the global mean net RF of water vapour reduces as the flight altitude decreases. In addition, if the water vapour is released at a low altitude, in which weather clouds are present, H_2O emissions may condense. In this context, the radiative properties of water vapour can be neglected.

In view of these assumptions, three different cases were defined to carry out the Global Warming analysis of preventing contrails:

- Contrails are not avoided
- Contrails are prevented in 2005
- Contrails are prevented in 2020

Obviously, the second case is technically impossible as the technology has not been implemented yet. The same happens with the third case as this contrail avoidance technique is insufficiently mature to be implemented in 2020. However, the three cases were considered because they allowed for calculating the net radiative forcing impact of avoiding contrails. In addition, the effect of avoiding contrails in different years could also be studied.

5 RESULTS AND DISCUSSION

In the first section of this chapter the water-carrying aircraft performance results are presented and discussed. Then, the second section provides the results of the Global Warming analysis conducted with the previous results. Finally, a general discussion of the results is carried out.

5.1 Aircraft performance

This simulation studied the effect of water storage on aircraft, with respect to the baseline aircraft. To achieve this purpose, two analyses were conducted. The first one consisted in analysing the range reduction of the water storage model in relation to the baseline model using the same amount of fuel. The second analysis measured the fuel burn penalty of the water storage model with regard to the baseline model for the same covered range. In the following sections, the results of these two analyses are provided.

5.1.1 Range reduction analysis

To analyse the range reduction experienced by the water storage aircraft, the payload-range diagram of the baseline aircraft, which is illustrated in Figure 3-5, was used as the reference curve. Then, the payload-range diagram of the water storage model was obtained applying the methodology and implementation in Matlab provided in Sections 4.1.3.1 and 4.1.4.5. The range reduction was only measured during cruise so that the same amount of fuel was burnt in both models during this flight phase. Climb and descent distances were assumed to be equal for the baseline and the water storage aircraft models.

The range reduction experienced by the water storage compared to the baseline aircraft is illustrated in Figure 5-1. In this diagram, three different curves were represented.

The black curve represents the payload-range of the baseline model, taking into account the typical weight restrictions:

- Maximum payload weight, which produced the horizontal line from 0 to 1.

- Maximum T/O weight, which produced the slope between 1 and 2. The maximum T/O weight represents the mechanical integrity limits of aircraft structures. As in conventional aircraft the maximum weight occurs at the beginning of the mission, this weight limitation is known as T/O weight.
- Maximum fuel that could be stored in the fuel tanks of the aircraft, which produced the slope between 2 and 3.

The blue curve illustrates the range reduction experienced by the water storage aircraft when the same amount of fuel was used in both baseline and water storage aircraft. The limitations for the blue curve were the same as for the black curve.

However, when water is stored on the aircraft, the weight increases during cruise phase. This way, it could be possible to exceed the maximum T/O weight during cruise, so that this limitation, instead of being considered only for T/O, must be considered for the cruise phase too. This way, the red line was produced, which is the actual payload-range curve of the water-storing aircraft.

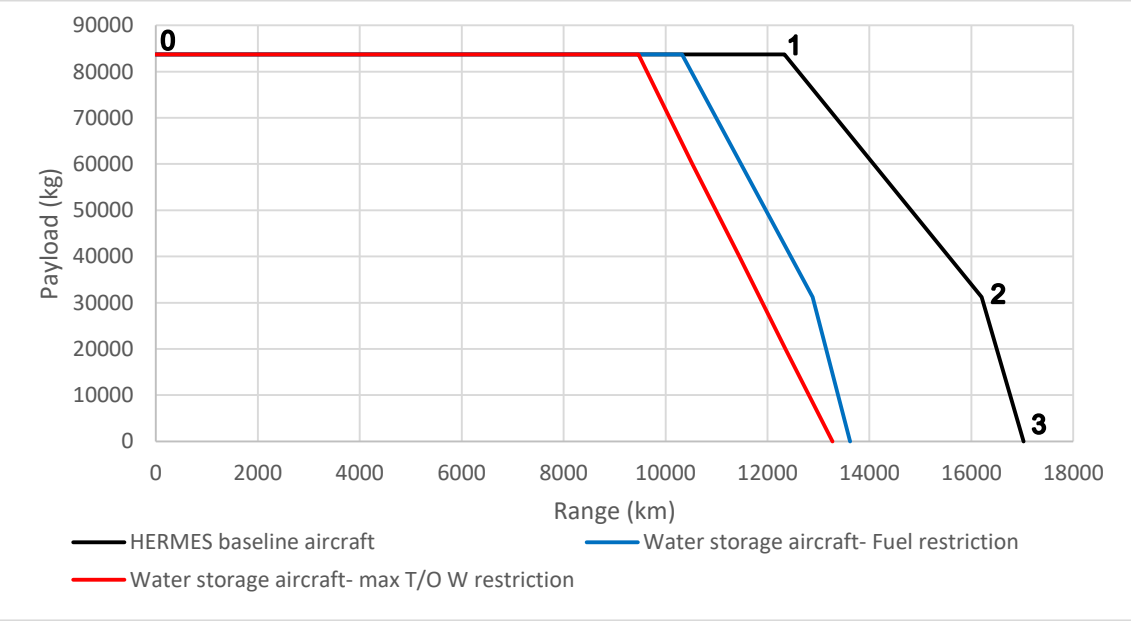

Figure 5-1: Baseline aircraft payload-range diagram and different limitations of the water storage aircraft payload-range diagram

The range reduction of points 1, 2 and 3 is shown in Table 5-1. The most interesting point of this analysis is point 1, as it corresponds to the DP of the

aircraft model. The range reduction that occurred at DP was quite high, due to the large amount of water stored on the aircraft during this long range configuration. In addition, the relative range reduction in percentage increased until point 2, where the maximum reduction was achieved, and then decreased until point 3.

Point	Baseline range	Water storage range	Deviation
Point 1	12,335 km	9,469 km	23.23%
Point 2	16,200 km	11,845 km	26.88%
Point 3	17,021 km	13,276 km	22.00%

Table 5-1: Range reduction analysis

Based on this data, it was concluded that the longest the range of the baseline aircraft, the higher the range reduction. This conclusion is only valid until point 2. From this point, the range difference between both models decreased in magnitude and consequently, in relative values. The final representation of the baseline aircraft and the final water storage aircraft payload-range diagrams is provided in Figure 5-2.

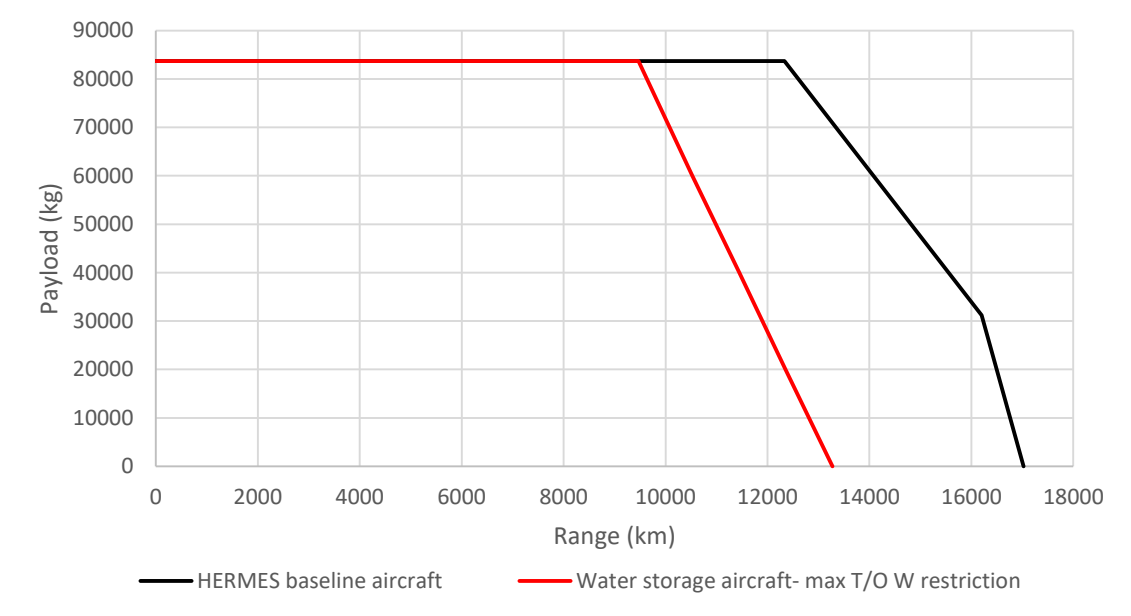

Figure 5-2: Baseline aircraft and water storage aircraft payload-range diagrams

5.1.2 Fuel burn penalty analysis

Once the previous analysis was performed, the DP of the water storage aircraft payload-range diagram was selected for the fuel burn penalty analysis. The DP point corresponded to the maximum range with the maximum possible payload weight. The fuel burn penalty was calculated comparing the fuel burnt by the baseline and water storage models following the methodology and implementation explained in Sections 4.1.3.2 and 4.1.4.6.

In the previous analysis, it was assumed that the climb and descent distances in both models were the same because they were carrying the same amount of fuel. In this case, however, to be able to fly the same range as the baseline model, the water-storing aircraft must carry more fuel. As a consequence, the weight of the water storage aircraft was higher, what implies that the descent and climb distances are different for the two models. If the aircraft is heavier, it would need a longer distance to climb to the same altitude than a lighter aircraft. For the descent, the opposite effect occurs.

In the following charts, the results of aircraft weight, thrust, SFC and finally, fuel burnt of both aircraft models are illustrated.

5.1.2.1 Aircraft total weight comparative analysis

The total weight of the water storage aircraft increased during the cruise phase, as can be observed in Figure 5-3 below. This pattern was the expected result because the emission index of water is higher than 1, so per 1 kg of fuel burnt more than 1 kg of water was produced and stored.

The aircraft total weight difference at the initial point of cruise arose because the extra fuel burnt by the water storage aircraft was considered and introduced on the aircraft. As can be seen in the chart, this deviation was not very high. However, the difference on aircraft weight was seen to significantly grow at the end of the cruise phase. The reason behind this growth was that, at that point of the phase, all the water that had been produced was stored on the aircraft. Finally, although the weight change during the cruise phase seemed linear in both cases, only the water storage aircraft weight varies in an almost linear manner.

The baseline aircraft weight curve was not a perfect line. This fact is clarified later with the fuel burnt chart.

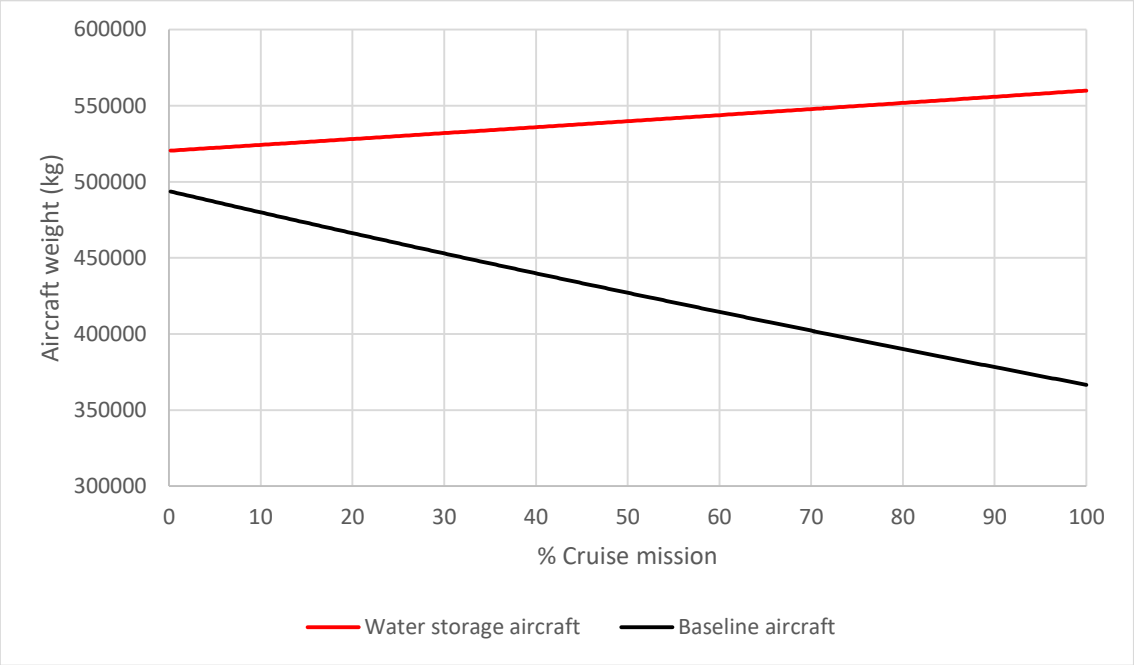

Figure 5-3: Aircraft total weight variation during cruise

In Table 5-2, the initial and final aircraft weight during weights are presented, as well as the percentage deviation between them.

	Baseline aircraft	**Water storage aircraft**	**Deviation**
Initial value	493,658 kg	520,517 kg	5.44%
Final value	366,593 kg	559,998 kg	52.76%

Table 5-2: Initial and final values of aircraft total weight during cruise

5.1.2.2 Thrust comparative analysis

According to thrust analysis, as can be observed in Figure 5-4, the thrust required during cruise decreased in the baseline case, where the altitude and Mach number were held constant. This is the usual performance of conventional aircraft. The thrust requirement of the water storage aircraft, however, increased during cruise. This thrust variation also followed the expected behaviour, as the aircraft weight was increasing during this flight phase because of the increasing amount of stored water.

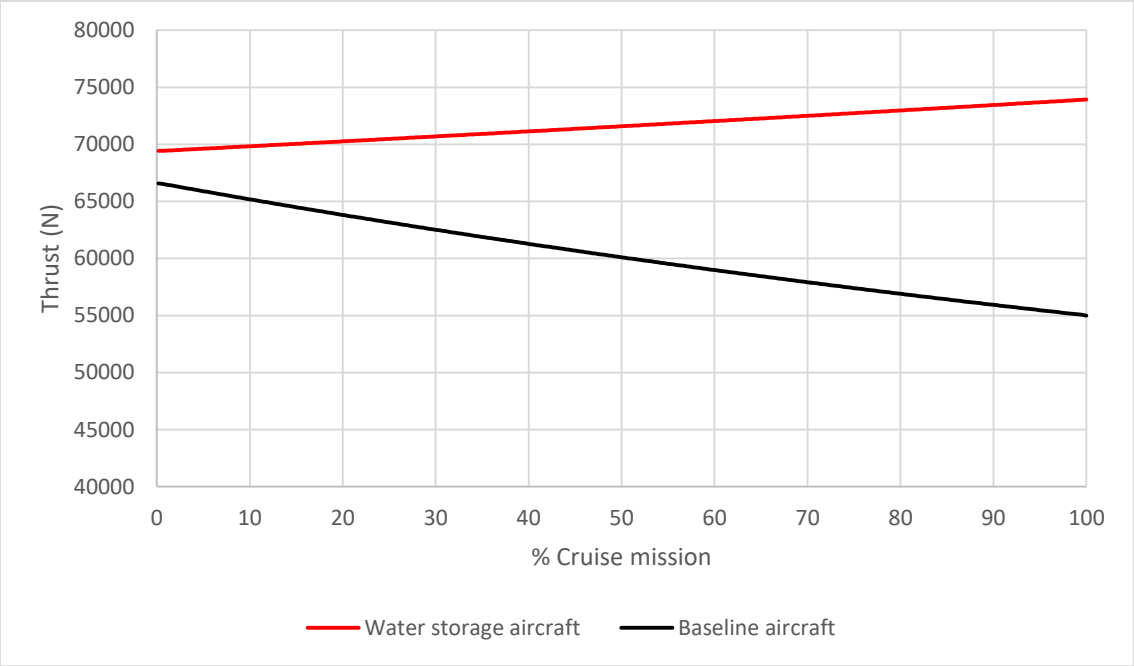

Figure 5-4: Thrust required variation during cruise

In Table 5-3, the initial and final values of thrust during cruise are presented, with the percentage deviation between them. The thrust difference at the initial point of cruise was caused because of the additional amount of fuel required by the water storage aircraft to complete the flight mission. The rise of thrust difference between both models at the end of the cruise phase was provoked by the aircraft total weight increase due to the stored water during cruise. Although the thrust variation seems linear in both models, the water storage thrust aircraft curve has a more linear pattern than the baseline case.

	Baseline aircraft	**Water storage aircraft**	**Deviation**
Initial value	66.57 kN	69.43 kN	4.30%
Final value	55 kN	73.94 kN	34.43%

Table 5-3: Initial and final values of thrust during cruise

5.1.2.3 SFC comparative analysis

Regarding the SFC variation of both models during cruise, a similar result to those seen for weight and thrust was obtained, as can be seen in Figure 5-5. The SFC of the baseline aircraft decreased during the cruise phase because of the

decrease in weight and, consequently, decrease in thrust requirements. The SFC of the water storage aircraft, on the contrary, increased due to the continuous collection of water. A small discontinuity was observed in the water storage aircraft at around 10% of the cruise mission. As can be observed in Figure 5-4, the thrust required during cruise did not present any irregularity during cruise. Consequently, as the SFC is the fuel flow to thrust ratio, the discontinuity must had been caused because Turbomatch calculated a slightly high value of the fuel flow.

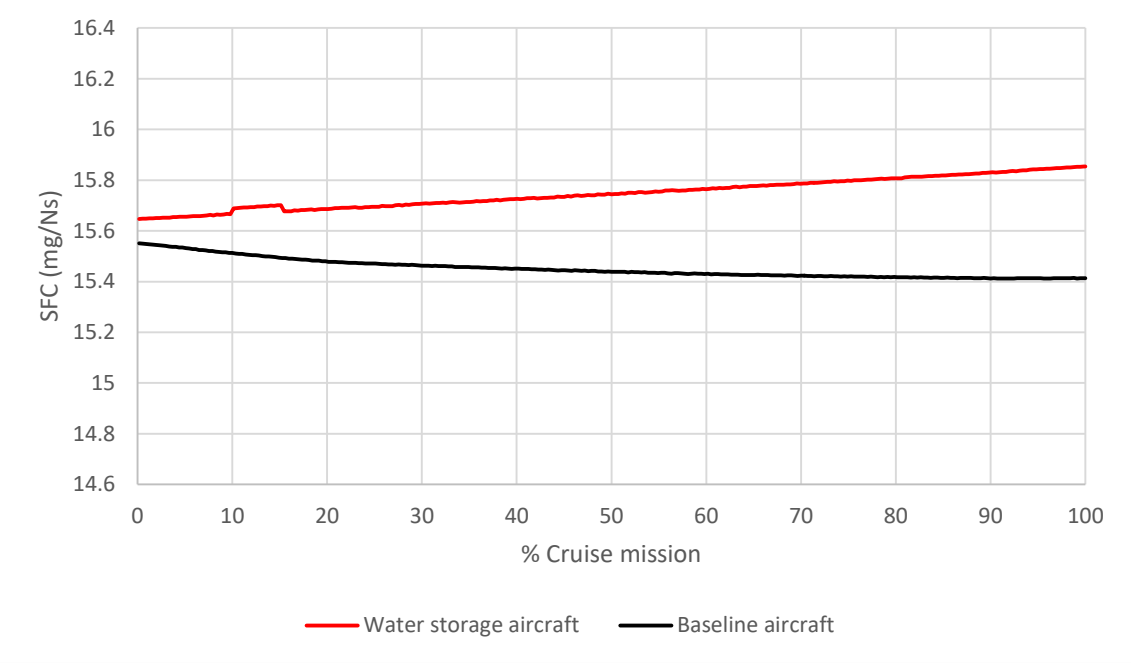

Figure 5-5: SFC variation during cruise

As can be observed in Table 5-4, the deviation of the SFC at the beginning and at the end of the cruise phase was smaller than for aircraft weight and thrust. This is because the SFC is a fuel flow to thrust ratio, and the reduction in one was almost compensated by the reduction of the other, so the relationship between them did not change much.

	Baseline aircraft	**Water storage aircraft**	**Deviation**
Initial value	15.55 mg/(N s)	15.65 mg/(N s)	0.64%
Final value	15.41 mg/(N s)	15.85 mg/(N s)	2.86%

Table 5-4: Initial and final values of SFC during cruise

The SFC of the water storage aircraft varied in a linear manner, except for the irregularity. The baseline aircraft SFC, however, decreased and achieved a minimum value at the last segments of the cruise phase, showing a non-linear pattern. This is the typical behaviour of conventional aircraft: there is a point during the cruise phase at which a minimum SFC value is achieved, and after that point, it increases. This increase happens because the engine is operating at low power settings. From the minimum point, the fuel flow does not decrease as fast as the thrust, so the SFC increases. This behaviour can be further studied in reference (Cohen, Rogers, and Saravanamuttoo 1996).

5.1.2.4 Fuel burnt comparative analysis

Finally, the fuel burnt results during cruise, which allow for the fuel burn penalty calculation, are provided in Figure 5-6. The ordinate axis represents the amount of fuel burnt between the beginning and the specified fraction of cruise. As can be observed, the water storage aircraft had consumed more fuel at the end of cruise than the baseline aircraft. This was the expected performance as the aircraft total weight, the thrust and the SFC were higher in the case of the water storage aircraft, what resulted in a higher fuel consumption.

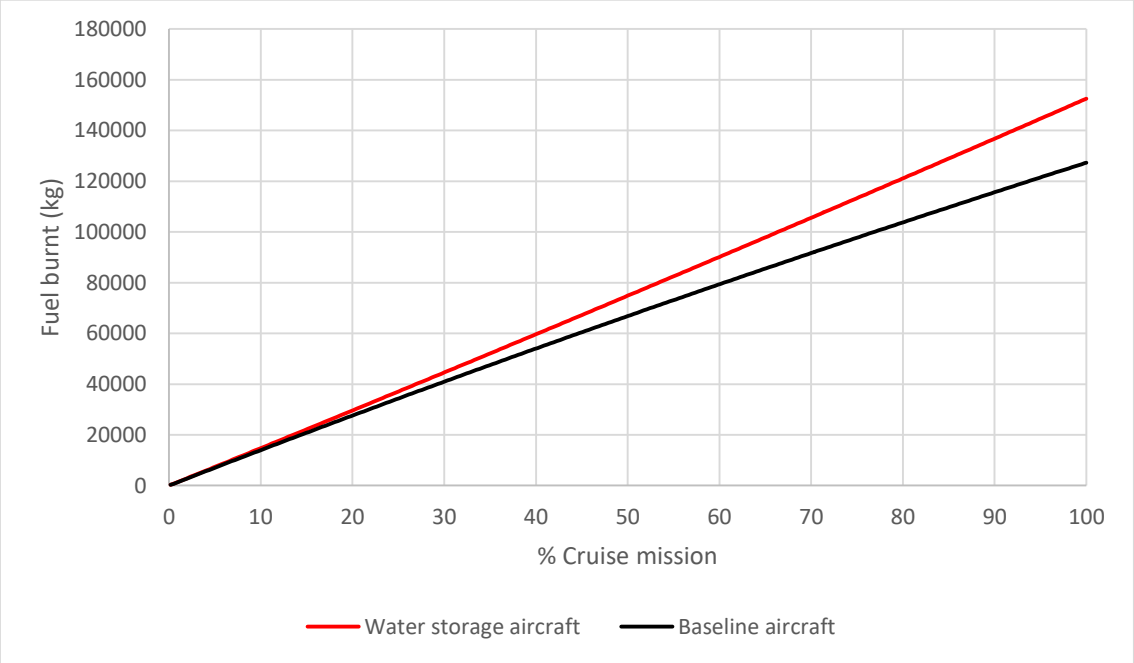

Figure 5-6: Total fuel burnt during cruise

Both curves started from the coordinate origin, and they increased until they reached the final values stated in Table 5-5. The final cruise difference and deviation of the total fuel burnt represents the overconsumed fuel and the fuel burn penalty of the water storage aircraft, respectively, in comparison to the baseline aircraft during the cruise phase. In this case the irregularity observed in the SFC curve did not have a notable effect, despite the relationship between the SFC and the fuel burn weight. This is because the irregularity was so small that when calculating the cumulative value, it was not appreciated.

The total fuel burnt curve in the case of the water storage aircraft followed an almost linear pattern, while the baseline aircraft total fuel burnt variation slightly decreased during the cruise mission. For this reason, the aircraft total weight of the baseline aircraft described before did not vary in a linear manner. In addition, it can be observed that the distance between both curves increases as the cruise distance covered by the aircraft increases.

	Baseline aircraft	**Water storage aircraft**	**Deviation**
Initial value	0 kg	0 kg	0 %
Final value	127,314 kg	152,581 kg	19.85%

Table 5-5: Initial and final values of total fuel burnt during cruise

The water storing aircraft consumed a total of 25,267 kg more fuel than the baseline aircraft, which represented a 19.85% of fuel burn penalty during cruise. If the total fuel weight difference is multiplied by the CO_2 emission index, which was specified in the literature survey, the total weight of the extra emitted CO_2 resulted in 79,687 kg.

To conclude this section, the specified fuel burn penalty was only applied to the cruise phase. The fuel burn penalty of the whole flight mission was measured dividing the weight of the overconsumed fuel during the cruise phase by the weight of the fuel burnt to complete the whole mission. From this calculation, the fuel burn penalty of introducing this contrail prevention technique was estimated to be of 17.35% for the DP payload-range.

5.2 Global Warming analysis

The main purpose of the Global Warming analysis was to assess if the net balance between the positive effect of avoiding contrails and the negative effect of the additionally emitted CO_2 is beneficial. In this section, the results of the Global Warming analysis are presented.

The methodology of this analysis was detailed in Section 4.2.2. As explained there, this study was carried out with the results of the aircraft performance. Therefore, the DP of the payload-range diagram obtained for the water storage aircraft, was used as the reference point. This way, a 17.35% mission fuel burn penalty was considered, what is the same as considering a 17.35% increase in CO_2 emission.

As stated in the methodology, RF future scenarios[1] were used as a basis for the three assumed cases proposed for this analysis:

- Contrails are not avoided before 2050
- Contrails are avoided in 2005
- Contrails are avoided in 2020

The RF values of the first assumed case are provided in Appendix C.1. The RF values of the two cases where contrails are avoided are provided in Appendices C.2 and C.3. To discuss these results, three bar charts were made to measure the RF of the contaminants during different years for the three difference cases:

- Radiative forcing of CO_2
- Total aviation RF without including aircraft induced cirrus (AIC)
- Total aviation RF including aircraft induced cirrus (AIC)

5.2.1 Analysis of the radiative forcing of CO_2

Figure 5-7 was created with the CO_2 results given in Appendix C.4. The CO_2 radiative forcing is represented on the y axis, while the different years and

[1] There are five different future scenarios. One corresponds to year 2020. The other four correspond to different possibilities of year 2050.For more information, refer to Appendix C.1.

scenarios are introduced in the x axis. The three assumed cases are presented with colour bars on each year scenario.

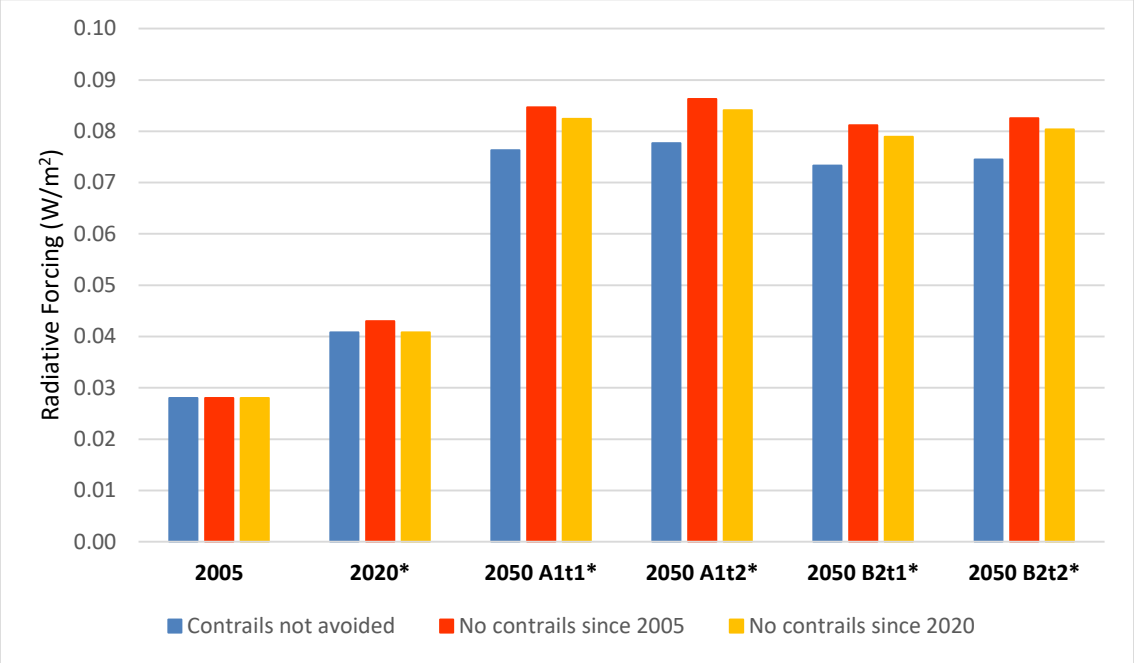

Figure 5-7: CO_2 radiative forcing of the different scenarios for the three assumed cases

The blue bar was taken directly from the public domain information and it was taken as a reference to which the other cases were compared. The red bar corresponded to the case in which contrails are avoided in 2005, and the yellow bar corresponded to the case of avoiding contrails in 2020. The variation of these bars from the blue one was determined using the 17.35% increase in the CO_2 emissions since the year contrails were avoided. For example, if the radiative forcing without contrail avoidance (blue bar) was predicted to increase x%, if the contrail avoiding technique was implemented, the increase in the RF would be of 1.1735*x%. The relative changes of the red and yellow bars with respect to the blue one for the five future scenarios are provided in Appendix C.4.

Looking at Figure 5-7, a slight rise of the CO_2 radiative forcing of year 2020 was observed in the case contrails were avoided in 2005. The radiative forcing of CO_2 of year 2050 increased much more notably, as the contrail avoidance technique would have been operative for a longer time, increasing the amount of CO_2 in the

atmosphere. As can be observed in the blue bars, the first two scenarios of 2050 consider a high amount of CO_2 in the atmosphere because they are really optimistic about the future aviation growth, while the last ones are more conservative. In addition, the difference between both technology levels can be also appreciated because the *t2* case was more focused on reducing NO_x to the CO_2 detriment. Consequently, the radiative forcing of CO_2 is higher with a *t2* option than with a *t1* option.

Furthermore, it could be concluded from Figure 5-7 that the later the contrail avoidance technique based on water collection and storage is implemented, the lower the environmental impact of CO_2.

5.2.2 Analysis of the radiative forcing of total aviation without AIC

For this section, the radiative forcing of all the aviation pollutants were considered, except for the AIC, because of the high uncertainty of the mean RF value of AIC.

The chart represented in Figure 5-8 was created with the total aviation radiative forcing given in Appendix C.4. The axes and bars represent the same as is the chart of the previous section. The variation of the red and yellow bar was determined considering the changes in CO_2, water vapour and contrails radiative forcing, as the other pollutants do not change with the inclusion of the water storing technique. The relative changes of the red and yellow bars with respect to the blue one for the different scenarios are provided in Appendix C.4.

A huge drop of the total aviation radiative forcing would occur for 2020 in the case contrails were avoided in 2005. For the year 2050 scenarios, the total aviation RF in both contrail avoidance cases would decrease vastly too, due to the importance of contrails and water vapour in total aviation RF, even though CO_2 radiative forcing would increase, as shown in Figure 5-7. As can be observed in the tables given in Appendix C.4, the RF reduction in the first two scenarios of 2050 would be larger than in the last ones. In addition, the reduction with the *t2* setting would be higher than with the *t1* setting. The reason for this is that even though the CO_2

RF would increase, the total aviation RF would lower with *t2* because the influence of contrails and water vapour in the total RF is greater.

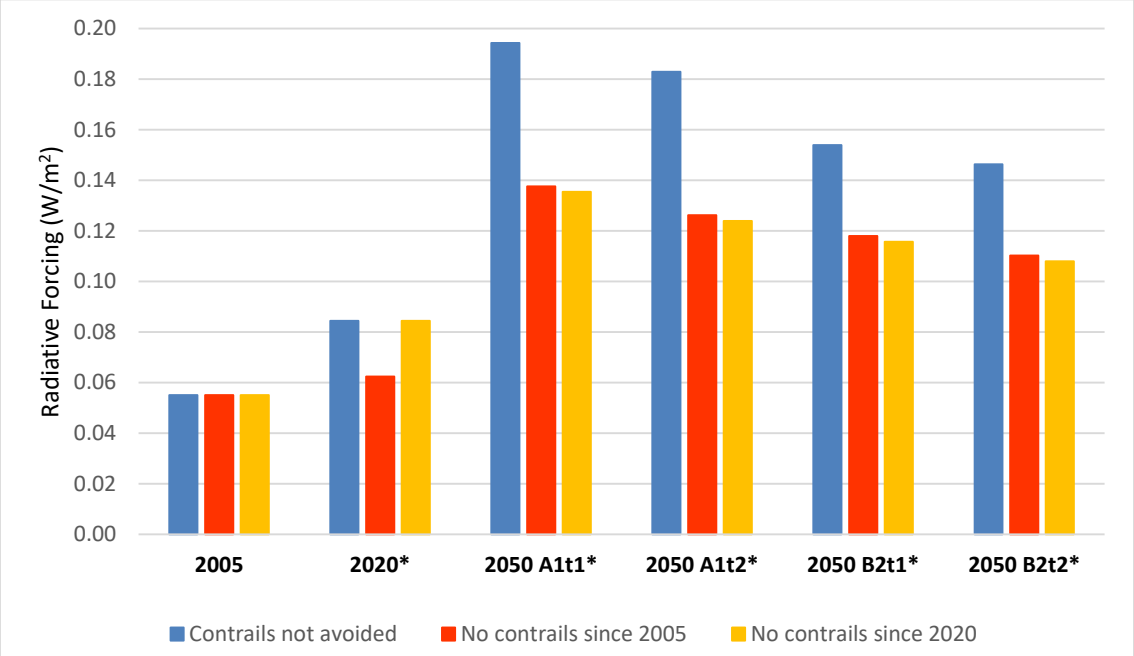

Figure 5-8: Total aviation radiative forcing of the different scenarios for the three assumed cases (AIC not considered)

It can be concluded from Figure 5-8 that the later the contrail avoidance technique based on water collection and storage is implemented, the lower the environmental impact of aviation. This conclusion is a consequence of the final comment suggested at the end of the CO_2 analysis. The reason for this difference between the red and yellow bars in the different 2050 scenarios is the CO_2 emitted from 2005 to 2020. Finally, the reduction of total aviation radiative forcing due to the studied prevention technique varies between around 23% and 33% in 2050 when AIC were not considered.

5.2.3 Analysis of the radiative forcing of total aviation with AIC

The chart represented in Figure 5-9 was created considering the total aviation radiative forcing given in Appendix C.4. In this case, AIC were included in the RF analysis. Despite the great uncertainty of the mean RF value of AIC, the effect of aviation induced cirrus is present and it had to be considered. The axis and bars configuration is the same as explained in the previous charts. The variation of the

red and yellow bar was determined considering the changes in CO_2, water vapour, contrails and AIC radiative forcing. The percentage changes between the blue and the red and yellow bars for the different scenarios are provided in Appendix C.4.

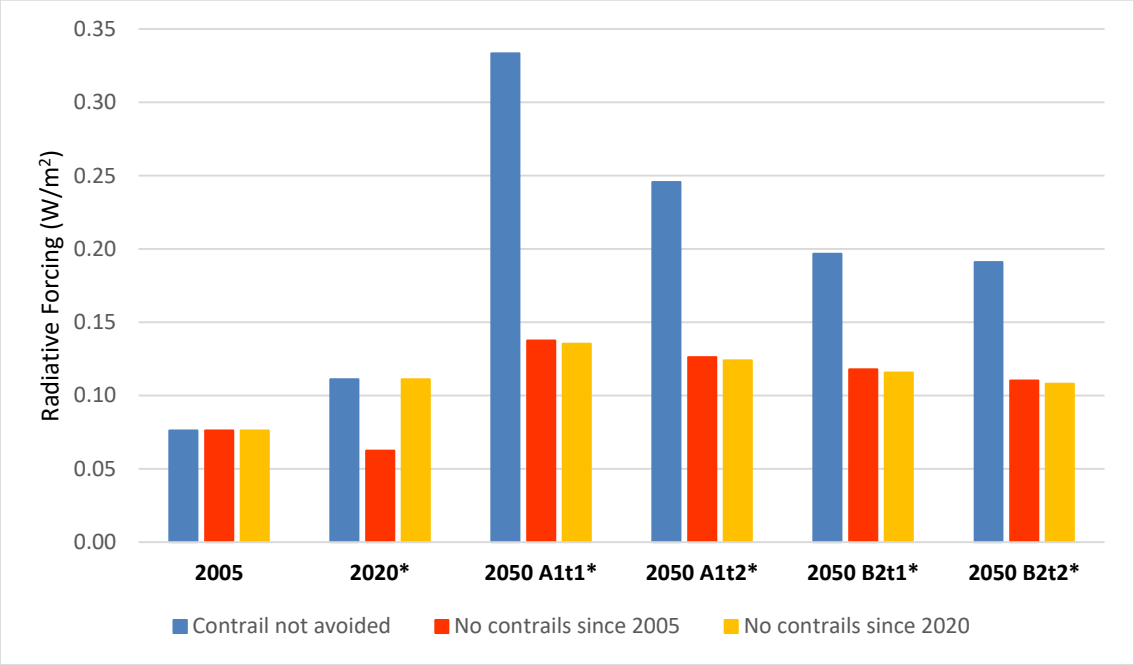

Figure 5-9: Total aviation radiative forcing of the different scenarios for the three assumed cases (AIC considered)

Considering the AIC did not have any effect on the 2050 scenarios for the cases of contrail avoidance, because the aircraft induced cirrus radiative forcing is null in those cases. AIC do have an effect on blue bars, because their RF is taken into account, increasing the total RF. Consequently, all the RF reductions experienced in this chart are greater than in the previous one.

The pattern obtained in Figure 5-9 is very similar to the one in Figure 5-8 but with greater RF reductions. For this reason, the comments and discussion of the previous analysis can be also applied to this one. Finally, the reduction of total aviation radiative forcing due to the studied prevention technique varies between around 40% and 50% in 2050 if AIC were included in the calculation.

In conclusion, according to the results obtained from this analysis, the net effect of this contrail avoidance technique would be positive from a radiative forcing

point of view. This is because the positive effect of avoiding contrails would larger than the negative effect of emitting more CO_2.

5.3 Discussion of results

In this section, the previously explained results are further discussed so that the conclusions of this project are built on a solid foundation. The section is divided into two subsections: aircraft performance and Global Warming analysis.

5.3.1 Aircraft performance

The results obtained of the aircraft performance, both for range reduction and for fuel burn penalty were as expected. These results did not only provide a numerical value of the penalties of the contrail avoidance technique based on water storage, but also proved that the methodology was valid and could be applied to different projects in the future.

The range reduction experienced by the water storage aircraft was significant in comparison to the range of the baseline aircraft. This reduction varied between 22% and 26.88% for points in the diagonal lines of the payload-range diagram of Figure 5-2. Looking at this chart, it can be seen that the payload-range curves of the baseline and water-storing aircraft separate with increasing range of the baseline model, until the maximum fuel weight limitation of the diagram is reached (point 2). This implies that the longer the range of the baseline aircraft, the higher the range reduction experienced by the water storage aircraft (only up to point 2). Then the lines start to get closer. This conclusion was stated only analysing the DP and points 2 and 3, which were on the right side of the DP. For this reason, to verify that this statement was correct, an additional range reduction analysis was conducted, considering the design point and points to the left and to the right of the DP. The points used for this analysis were on the curve of the payload-range diagram.

The results, given in Table 5-6, demonstrated that the previous statement was correct, as the range difference between both aircraft models increased until 16200km in the baseline model (point 2), and then decreased. Moreover, from this analysis, it was concluded that the range limitation of the water storage

aircraft for short and mid-ranges is the fuel restriction and not the maximum T/O weight during cruise, which was the case of long-ranges. This is because for long ranges it is necessary to carry more fuel, so that more water is generated in cruise. Finally, an important point to keep in mind is that for short and mid-ranges the deviation is not very high. Hence, the avoidance technique does not have a great impact on the performance of the aircraft.

Baseline aircraft range (km)/ *Payload (kg)*	**3,000**/ *83,700*	**6,000**/ *83,700*	**9,000**/ *83,700*	**12,335**/ *83,700*	**16,200**/ *31,207*	**17,020.9**/ *0*
Water storage aircraft range (km)	2,954.6	5,651.4	8,048	9,469	11,845.2	13,276
Difference (km)	45.4	348.6	952	2,866	4,354.8	3,744.9
Deviation	1.51%	5.81%	10.58%	23.23%	26.88%	22.00%

Table 5-6: Range reduction in magnitude and in percentage terms

Another point to discuss regarding the range reduction analysis is the assumption of considering the climb and descent distances the same for the baseline and water storage aircraft models. In addition, the same aircraft and engine weights were considered for both cases, but in reality, the water storage would have an extra weight because more devices would be required for water condensation. Based on these considerations, the climb distance would be similar for both cases as their fuel weight would almost equal in a real situation, and only a small variation of engine and aircraft weight should be considered. However, the descent distance may change drastically in the water storage model as the aircraft weight is much higher due to the water collected and stored during cruise. Furthermore, the water would be released during the descent phase, so the aircraft performance would change even more. The descent performance of the aircraft was not included in the scope of the present thesis and for this reason, the assumption of considering the same distances as in the baseline case was stated.

Regarding the fuel burnt analysis, the climb and descent distances were not the same for the baseline and water storage aircraft models, as the water storage aircraft required more fuel than the baseline aircraft for the same range. As the baseline aircraft was lighter than the water storage aircraft during climb, the climb distance and the fuel consumption were smaller than in the baseline case. The descent performance, on the contrary, was facilitated for the heavier water-storing aircraft, what reduced the descent distance and fuel consumption of the aircraft during descent.

Focusing on the graphical results of the fuel burnt analysis, the cause of the aircraft total weight difference between water storage and baseline aircraft at the beginning of cruise might seem to be the extra fuel burnt by the water storage model during the cruise phase. However, not only the extra fuel burn affect this difference, but also the contingency of this extra fuel and the different fuel consumption during the descent phase.

Another interesting point to discuss around the fuel burnt analysis is the final result. A 17.35% increase in fuel consumption was experienced by the water storage aircraft during cruise at DP payload-range configuration. The analysis was conducted only for one point of the payload-range diagram. Consequently, in Section 5.3.1.1, the results of a fuel burnt sensitivity analysis developed for lower range and payload settings are provided. The maximum fuel burn penalty of the water storage technique is also included in Section 5.3.1.1.

Both range reduction and fuel burn penalty analyses were carried out assuming that all the water produced from the fuel combustion process was collected and stored. The condensation device designed in reference (Qureshi 2016) enables the whole condensation of water. However, this is the extreme situation of collecting and storing the water, because maybe not all the water needs to be condensed to avoid contrails. Therefore, the aircraft performance results represented the maximum penalties for range and fuel burnt of this contrail avoidance technique. An analysis considering different amounts of collected water is carried out in Section 5.3.1.2. Valuable conclusions were extracted from

this analysis, which may be useful for future work about this contrail avoidance technique.

Furthermore, not only different amounts of collected water should be considered, but also that maybe water storage on the aircraft is not necessary. It could be possible to recirculate the condensed water could in the aircraft and then, emit it into the atmosphere in a different state and with different particle properties. The purpose of this process would be to reduce, not eliminate, the radiative forcing of contrails, and consequently, of aircraft induced cirrus clouds.

5.3.1.1 Fuel burnt sensitivity analysis

The fuel burnt analysis was only performed for the DP payload-range setting. To consider lower range and payload settings, a sensitivity analysis of the fuel burnt was carried out. Only lower range and payload setting were selected because the design point corresponds to the maximum range for the maximum possible payload.

Before performing the sensitivity analysis, the fuel burn penalty of different situations had to be calculated. Firstly, points with shorter ranges and DP payload were selected. And secondly, points with lighter payload and DP range were chosen. The methodology of this calculations was the same as in the case of the fuel burn penalty analysis.

The fuel burn penalty results of points with shorter range and points with smaller payload are provided in Table 5-7 and Table 5-8, respectively. The fuel burn penalty was measured in both cases during cruise and during the flight mission.

Range (km)	**2,367.25**	**4,734.5**	**7,101.75**	**9,469**
Fuel burn penalty during cruise	2.06%	5.99%	11.27%	19.85%
Fuel burn penalty (Mission)	1.29%	4.74%	9.56%	17.35%

Table 5-7: Fuel burn penalty of points with shorter range and DP payload

Payload (kg)	20,925	41,850	62,775	83,700
Fuel burn penalty during cruise	14.56%	16.12%	17.86%	19.85%
Fuel burn penalty (Mission)	12.85%	14.20%	15.68%	17.35%

Table 5-8: Fuel burn penalty of points with smaller payload and DP range

From these results, a sensitivity analysis of the mission fuel burn penalty was conducted comparing how a reduction of range and a reduction in payload affect to the main parameter, the mission fuel burn penalty. This comparison is represented in Figure 5-10.

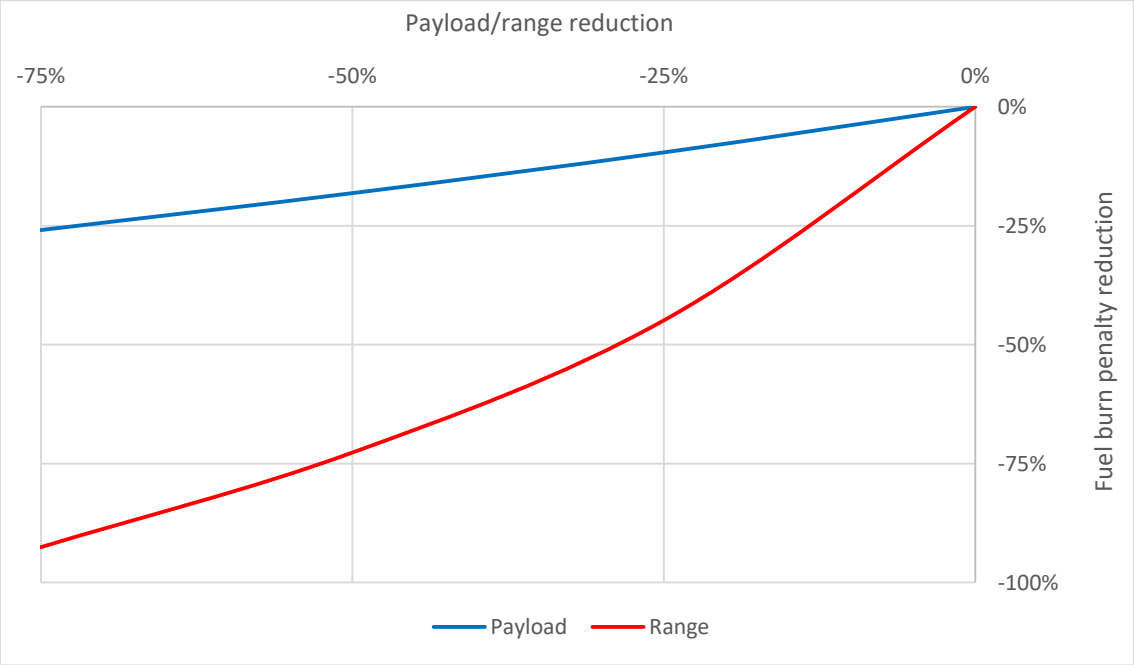

Figure 5-10: Fuel burn penalty sensitivity analysis

This figure demonstrates that range changes have a greater impact on the fuel burn penalty than changes in payload. This analysis confirms that this contrails avoidance technique does not have a great impact on the aircraft performance for short and mid-ranges, because the reduction in fuel burn penalty with respect to DP is very high for short ranges. For instance, it can be observed from Table 5-7 that the fuel burn penalty of a mission that covers 4734.5 km is 4.74%. However, when the covered distance extends to 7101.75 km, the fuel burn

penalty increases to 9.56%. As can be observed in Table 5-8, the impact of payload in the fuel burn penalty of the mission is not as important as the impact of range.

In the current analysis, the fuel burn penalties are lower than the DP value because shorter ranges are studied. The maximum fuel burn penalty of the payload-range diagram corresponds to the maximum range point. In this point a 29.26% and a 26.56% fuel burn penalties are obtained during cruise and during the mission respectively.

Regarding the shape of the curves in Figure 5-10, the payload curve is nearly linear, while the range curve is more similar to a parabolic curve. The reason for obtaining different patterns is that the reduction of payload produces a drop in the fuel consumption during the mission, so less fuel has to be carried. The relationship between this reduction of mission fuel weight and the decrease of payload is almost linear, what results in a linear relationship between payload reduction and fuel burn penalty reduction.

The relationship between range reduction and mission fuel weight is not linear. This is because the smaller the range, the lesser the importance of the cruise phase. Hence, the water collected and stored on the aircraft is low for short hauls, so range changes do not significantly affect to the fuel consumption of the aircraft. For this reason, the slope of the range curve in Figure 5-10 is less steep in short hauls. In the case of long hauls, the amount of water collected and stored on the aircraft is much higher than in short hauls. Consequently, the aircraft fuel consumption increases enormously in this case. Thus, the slope of the range curve is steeper in long than in short hauls. All this explanation justifies the parabolic shape of the range curve in Figure 5-10.

Finally, it can be concluded from this sensitivity analysis that the impact of range on the fuel burn penalty of this contrail avoidance technique is noteworthy. This analysis enhances the statement that the implementation of this contrail avoidance technique is attractive for short and mid-ranges.

5.3.1.2 Water collection analysis

In the present MSc project, the calculations presented in the results section considered that all the water produced by the combustion process was collected and stored. But maybe the condensation of all the produced water was not required for contrail prevention. Accordingly, an analysis considering different amounts of collected water was conducted. The methodology of this calculation was the same as in the range reduction analysis. In Figure 5-11, the payload-range diagrams of the baseline aircraft and different collection configurations of the water storage aircraft are represented, for the same amount of fuel. In this figure, the black and red curves represent the baseline and water storage aircraft. The other water storage curves calculated represent aircraft that, while having the contrail prevention technique implemented, do not store all the water produced.

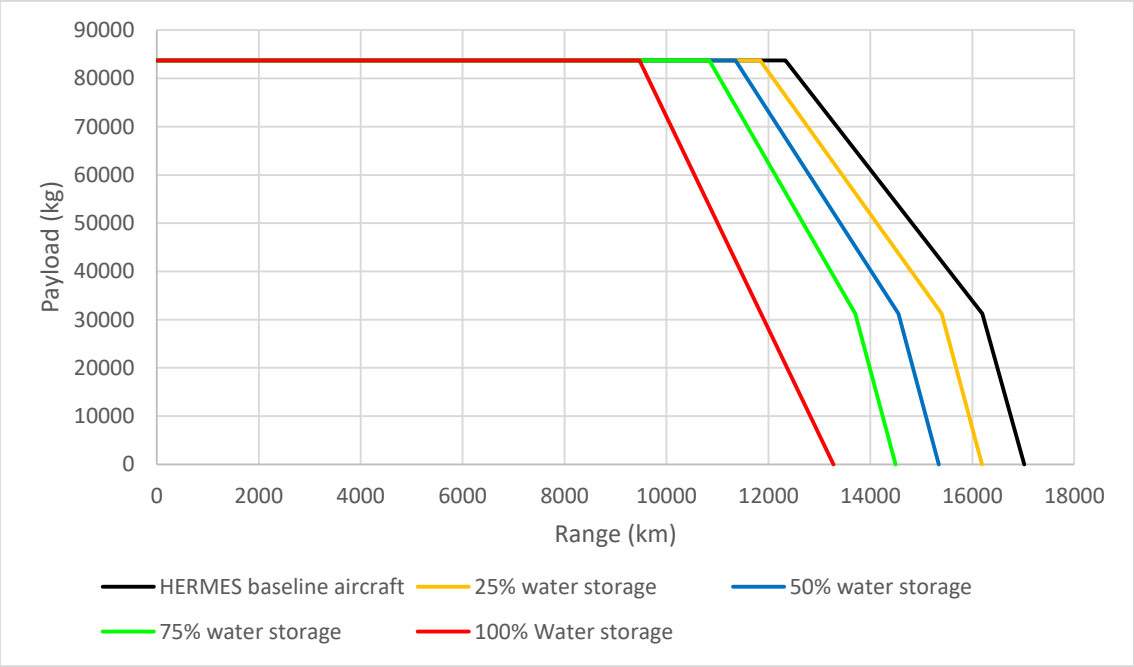

Figure 5-11: Payload-range diagrams of the baseline aircraft and different water storage configuration aircraft for the same amount of fuel

This figure shows that the shapes of the 25%, 50% and 75% water storage diagrams are more similar to the baseline diagram shape than to the 100% water storage aircraft. The reason for this is that the limitations applied for the generation of these curves were the same. These limitations were the maximum

T/O weight and the maximum fuel weight. Recalling from Section 5.1.1, the red curve, which corresponds to the 100% water storage aircraft, has another pattern because it considered that the maximum T/O weight could not be exceeded during the cruise phase. The maximum T/O weight limitation during cruise must only be considered if the weight of the stored water exceeds the fuel burn weight.

For the weight of the stored water to exceed the fuel burn weight it is necessary to store at least 79.4% of the water produced. To calculate this limit value, the condition is that the weight at the beginning and end of cruise is the same. This happens when the weight of the stored water is equal to the weight of the fuel burnt. To calculate the weight of the stored water, the total weight of the fuel is multiplied by the product of the emission index and the percentage of the stored water. If this product is higher than one (which happens for percentages above 79.4%) the weight of the aircraft will increase.

The range reduction depending on the amount of stored water is provided in Table 5-9. As can be observed, the lesser the water stored, the smaller the range reduction. Moreover, an almost linear pattern is observed between the range reduction and the amount of stored water, except for the 100% water storage aircraft. This is because the maximum T/O weight cannot be exceeded during cruise and the range is even more restricted than in the other cases.

	Baseline range	**Water storage range**	**Deviation**
25% Water storage	12,335 km	11,836 km	4.05%
50% Water storage	12,335 km	11,353 km	7.96%
75% Water storage	12,335 km	10,839 km	12.13%
100% Water storage	12,335 km	9,469 km	23.23%

Table 5-9: DP range reduction of the water storage configurations on the payload-range diagram

Using the payload-range design point of each water storage configuration, the fuel burn penalty analysis of the different water storage configurations during cruise and the whole mission was conducted and the results are represented in

Table 5-10. The methodology of this calculation was the same as in the fuel burnt analysis. From this table, it is demonstrated that the lesser the water stored, the lower the fuel burn penalty due to the water storage technique during both cruise and flight mission. In addition, a parabolic relationship is observed between the fuel burn penalty and the amount of stored water, except again for the 100% water storage aircraft. This is because the range of this water storage aircraft did not follow the sequence in the previous table, so the result in this table is accordingly altered.

	25% Water storage	**50% Water storage**	**75% Water storage**	**100% Water storage**
Fuel burn penalty during cruise	4.91%	10.40%	16.63%	19.85%
Fuel burn penalty (mission)	4.33%	9.17%	14.65%	17.35%

Table 5-10: Fuel burn penalty of the water storage configurations

To sum up, the most valuable conclusions about the water storage technique are repeated here. On the one hand, the maximum T/O weight limitation must only be considered during cruise when the stored water weight is higher than the fuel burn weight. On the other hand, the lesser the water stored, the smaller the range reduction and the lower the fuel burn penalty.

5.3.2 Global Warming analysis

In the global warming analysis a comparison between the GW positive effect of avoiding contrails and the GW negative effect of the extra CO_2 emitted to the atmosphere was conducted. In this section, before focusing on the results, the great disadvantage of the implementation of the studied contrail avoidance technique is discussed.

The aim of the water storage technique is to avoid the contrail formation. When the formation of contrails is avoided, the radiative forcing of contrails, AIC and water vapour become zero a few hours after they are banned. However, this contrail avoidance technique is accompanied with an increase in CO_2 emissions. These emissions could remain in the atmosphere between 5 and 200 years

(IPCC 2007). Consequently, it is not justified to implement contrail avoidance techniques in the near future even though a positive radiative forcing balance is obtained. Additionally, nowadays the CO_2 policies are very restrictive, and an increase in CO_2 emissions is not contemplated. Therefore, contrail avoidance techniques must be introduced in the distant future if the fuel burn penalty is less significant.

Moreover, it was concluded from the GW analysis that the later the contrail avoidance technique based on water collection and storage is implemented, the lower the environmental impact of aviation. Hence, this conclusion of the GW analysis goes hand in hand with the comments previously stated.

Focusing on the calculations carried out in the GW analysis, a point to highlight is the total aviation radiative forcing calculation considering the aircraft induced cirrus. The mean RF value of AIC presents a great uncertainty. Nevertheless, the effect of aviation induced cirrus is present in the atmosphere and it has to be considered. The high uncertainty in the radiative forcing of cirrus clouds is due to their coverage, which varies enormously depending on the latitude. Consequently, to study this uncertainty, a sensitivity analysis is conducted in Section 5.3.2.1 below.

Regarding the final results of the Global Warming analysis, it was concluded that a net positive effect was achieved due to the implementation of the studied contrails avoidance technique. This final result was stated using the radiative forcing to measure the net balance between the positive effect of avoiding contrails and the negative effect of emitting more CO_2. However, as it was stated in the GW metric selection in the methodology, the radiative forcing only measures the current imbalance of past aviation emissions, and does not account for the impact that long-lived pollutants will have in the future. This disadvantage remains even if future scenarios are introduced in the analysis. In the year 2050 scenario, for example, the RF would be accounting for the pollutants emitted until that moment, but not for the effect that those pollutants will have after year 2050. For this reason, the results of this analysis do not reflect the environmental impact of some emissions after year 2050, e.g. carbon dioxide. To study even further

future scenarios, it should be necessary to estimate the RF of further years 2100, 2150, etc. which is not viable. In conclusion, a better metric is required in aviation to measure the real GW impact of the emissions.

5.3.2.1 AIC radiative forcing sensitivity analysis

The obtained results of the radiative forcing of total aviation showed that the RF reduction due to the studied contrails prevention technique varies between around 40% and 50% in 2050 if aircraft induced cirrus clouds were included in the calculation. However, the radiative forcing of AIC presents the highest uncertainty of the aviation emissions. Consequently, in this section, this uncertainty is analysed. The purpose of this analysis was to determine the RF reduction experienced by the total aviation radiative forcing due to the water storage technique considering a 90% confidence range of the AIC radiative forcing.

The maximum and minimum values of 90% confidence range of the AIC radiative forcing were used to calculate the radiative forcing of total aviation for the three assumed cases. The followed methodology was the same as in the Global Warming analysis. The results of the calculation are given in Appendix C.5.

From these results, depending on the future scenario, the total aviation radiative forcing could be reduced between 18% and 72% in 2050 thanks to the water storage technique. This result can be shocking because the minimum reduction value of this sensitivity analysis (18%) is lower than the minimum reduction value of the analysis when AIC are not considered (23.4%), which was explained using Figure 5-8. However, the reason for this is that the radiative forcing of contrails is included in the AIC radiative forcing. Hence, also the contrails uncertainty is considered in the current sensitivity analysis.

6 CONCLUSIONS AND FUTURE WORK

In this chapter, the conclusions based on the previous discussion of the results and future work of the project are presented.

6.1 Conclusions

First of all, the implementation of the contrail prevention technique based on water storage is feasible as the condensed water volume can be stored in the fuel tanks using a membrane to separate both liquids. The possibility of using this technology arises because the condensed water volume is almost equal to the fuel burnt volume, 1.00736 m^3 of water are produced per m^3 of fuel burnt.

Regarding the aircraft performance results, the water storage technique implementation results in a 23.23% range reduction between baseline and water-storing aircraft if both of them use the same amount of fuel, and a 17.35% fuel burn penalty if both of them cover the same range. The limitation that restricts the payload-range diagram of the water storage aircraft is the maximum T/O weight during cruise. This limitation must be considered during cruise only if the weight of the stored water exceeds the fuel burn weight, which happens when more than 79.4% of the produced water is stored. This is the case of the present analysis, in which a 100% of the water is stored.

From the discussion of these results, it has been concluded that the range of the baseline aircraft is a decisive factor in range reduction and fuel burn penalty of the water-storing aircraft. On the one hand, for long range aircraft, the range reduction is very significant, as the DP range is reduced from 12,335 km to 9,469 km if the same amount of fuel is used. The fuel burn penalty of long range aircraft is also very notable, with an increase in fuel burnt of 17.35%. On the other hand, for short and mid-range aircraft the range reduction is much lower because the cruise phase is shorter. The fuel burn penalty is also lower, because the amount of water produced and stored during cruise is much lesser. From these results, it is concluded that the implementation of this contrail avoidance technique is most attractive for short and mid-ranges.

Another important parameter that must be considered is the amount of water stored. This project has been carried out considering the extreme case in which all the water produced from fuel combustion is collected and stored on the aircraft. Maybe not all the water has to be stored to prevent contrails, so this possibility was also studied. For example, if only half of the total produced water is stored, a 7.96% range reduction and a 9.17% fuel burn penalty are produced due to the contrail avoidance technique implementation. Hence, it is concluded that the amount of water collected and stored by the aircraft must be as small as possible to enable both the prevention of contrails and the minimisation of the penalties.

On the basis of the results obtained from the aircraft performance analysis, the Global Warming analysis was conducted to determine the net balance of the positive effect of avoiding contrails and the negative effect of the additional CO_2 emitted. The outcome of the implementation of the water storage technique is a 40%-50% reduction in the total aviation radiative forcing in year 2050. However, the AIC present a great RF uncertainty. Then, if a 90% confidence range of the AIC radiative forcing was considered, the reduction in the total aviation radiative forcing varied between 18% and 72%.

These results showed a positive balance of the contrail prevention technique. However, the selected metric to calculate the balance, the radiative forcing, is not perfect to perform this analysis. The reason for this is that radiative forcing is based on the momentary concentrations of past emissions and cannot account for future impact of long-lived pollutant CO_2. It was still selected because a more proper metric to determine the Global Warming impact of aviation emissions has not yet been defined. Accordingly, radiative forcing analysis provides only an approximation to the impact of the contrail avoidance technique.

This project was a preliminary study to analytically assess the penalties that the water collection and storage technique involved. The purpose of the project has completely been fulfilled. Although a positive radiative forcing balance is obtained, the implementation of the contrail avoidance technique in a near future is not justified. Therefore, contrail avoidance techniques must be introduced in the distant future if it is possible to obtain lesser fuel burn penalties. The utilisation

of CO_2 reduction technologies in parallel with contrail prevention techniques could reduce the time of implantation of this technique.

Finally, although some significant research has been conducted since the contrail avoidance technique studied in this project was presented, this technology is still at an early stage. However, it is acquiring a solid analytical base so that it could be further investigated if the effect of the contrails was found to be very relevant or legislation regarding contrails formation was created.

6.2 Future work

As stated in conclusions, the investigated contrail avoidance technique is still at an early stage, so several studies and projects must be conducted in the future. In this section, some of the recommendation for future work are explained.

First of all, the implementation of the studied contrail avoidance technique was concluded to be attractive for short and mid-ranges. However, the present water storage model was based on a large wide-body aircraft, which do not usually cover short ranges. In the case an aircraft of reduced dimensions was selected to implement this technique, the range reduction and fuel burnt penalties could change in a different manner. For this reason, the same analyses performed in this work should be carried out for the smaller aircraft, to see the effect of the water storing technique.

In addition, in the current project only the kerosene was considered as fuel. The use of another fuel could also be investigated. The aircraft performance of the baseline would vary due to this change, and also the penalties due to the water storage technique. This is because each fuel has a different emission index, depending on their composition, and consequently, the combustion of each of them would produce different amounts of water to be collected and stored on the aircraft. A preliminary study of fuels was conducted in reference (Noppel 2007).

In the current project, the aircraft performance due to the contrails avoidance technique was studied only during cruise. After this flight phase, the water was assumed to be released at a lower altitude. This means that the aircraft must descend some distance before releasing the stored water, which could have

critical effects on the aircraft performance. The study of this phase of the descent has to be carefully analysed because of the extra weight carried by the aircraft. Hence, new models must be developed for this descent phase.

Furthermore, a contrail prediction analysis to estimate the amount of water that needs to be stored to prevent contrails should be produced. This is because the penalties of the water storing technique decrease a lot if the amount of the stored water is lower.

The release of the liquid water was not covered in the present thesis and it was assumed that this release occurred at a lower altitude. However, it is necessary to achieve a good understanding of how the different physical properties of water particles affect to the environment when released at different altitudes. This investigation would facilitate the decision of which altitude is the best to release the water. Moreover, another possibility to the storage of water during cruise is the water treatment and release into the atmosphere with different physical properties. This study can be included in the altitude release analysis.

Finally, focusing again on the water storage case, a fraction of the collected water could be utilised for another aircraft or engine purposes. For example, some water could be used for aircraft systems, or for a reduction of the NO_x emission by injection of the condensed water into the combustion chamber of the engine. This would be an interesting analysis to carry out as the penalties of the water storage technique would be reduced, improving the NO_x emissions too.

REFERENCES

Airbus. 2014. *Aircraft Characteristics for Airport and Maintenance Planning-A380*.

Airbus. 2015. “Flying By Numbers.” 1–27.

Airbus. 2016. “Airbus A380.” Retrieved July 21, 2016 (http://www.airbus.com/aircraftfamilies/passengeraircraft/a380family/).

Appleman, H. 1953. “The Formation of Exhaust Condensation Trails by Jet Aircraft.” *American Meteorological Society*.

BADA. 2011. *Aircraft Performance Operational File - A388_.OPF*.

BEACON. n.d. “The Greenhouse Effect - BErkeley Atmospheric CO2 Observation Network.” *The Greenhouse Effect*. Retrieved June 26, 2016 (http://beacon.berkeley.edu/GHGs.aspx).

Burkhardt, Ulrike and Bernd Kärcher. 2011. “Global Radiative Forcing from Contrail Cirrus.” *Nature Climate Change* 1(1):54–58.

Cavcar, Mustafa. 2014. “The International Standard Atmosphere (ISA).” Retrieved July 1, 2016 (http://home.anadolu.edu.tr/~mcavcar/common/ISAweb.pdf).

CCC, Committee on Climate Change. 2009. “Meeting the UK Aviation Target—Options for Reducing Emissions to 2050.” *International Civil Aviation Organization* (December).

Chen, Chih-chieh and Andrew Gettelman. 2016. “Simulated 2050 Aviation Radiative Forcing from Contrails and Aerosols.” *Atmospheric Chemistry and Physics* 7317–33.

Chevron. 2007. *Aviation Fuels- Technical Review*. San Ramón, CA. Retrieved (http://books.google.co.uk/books/about/Aviation_Fuels.html?id=Eyp2QgAACAAJ&pgis=1).

Cohen, H., G. F. C. Rogers, and H. I. H. Saravanamuttoo. 1996. *Gas Turbine Theory*.

College of Dupage. n.d. “Cloud Physics- Collision/Coalescence; The Bergeron Process.”

Cranfield University. 2009. “Hermes V5 & TmatchCalls V3 - User Manual.”

Daly, Mark. 2011. “Rolls-Royce Trent 900.” in *IHS Jane’s Aero Engines 2011*.

EASA, European Aviation Safety Agency. 2013. *Type-Certificate Data Sheet-Trent 900 Series Engines*.

Eurocontrol. 2011. *User Manual for the Base of Aircraft Data (BADA) Revision 3.9*.

Fichter, Christine, Susanne Marquart, Robert Sausen, and David S. Lee. 2005. “The Impact of Cruise Altitude on Contrails and Related Radiative Forcing.” *Meteorologische Zeitschrift* 14(4):563–72.

Filippone, Antonio. 2010. “Cruise Altitude Flexibility of Jet Transport Aircraft.” *Aerospace Science and Technology* 14(4):283–94.

Frömming, C. et al. 2012. “Aviation-Induced Radiative Forcing and Surface Temperature Change in Dependency of the Emission Altitude.” *Journal of Geophysical Research Atmospheres* 117(19):1–15.

Galvin, K. P. 2005. “A Conceptually Simple Derivation of the Kelvin Equation.” *Chemical Engineering Science* 60(16):4659–60.

Garrett, Tim. 2016. “The Kelvin Equation : Why Does a Droplet Form ?” *University of Utah* 1–4. Retrieved June 26, 2016 (http://www.inscc.utah.edu/~tgarrett/5200/Notes/Kelvin.pdf).

Goodger, Eric M. 2014. “Gas Turbine Combustors- Fuels (Cranfield University Class Notes).” 5.

Gössling, Stefan and Paul Upham. 2009. *Climate Change and Aviation: Issues, Challenges and Solutions*.

ICAO. 2013a. *ICAO Engine Exhaust Emissions Data Bank- Subsonic Engines-Trent 970-84*.

ICAO. 2013b. “ICAO Environmental Report 2013.” *ICAO Environmental Report 2013* 1–224.

IPCC. 2007. *Mitigation of Climate Change: Contribution of Working Group III to the Fourth Assessment Report of the Intergovernmental Panel on Climate Change*.

IPCC. 2009. *Summary Report of the IPCC Expert Meeting on the Science of Alternative Metrics*. Oslo, Norway.

Jane’s. 2015. “Airbus A380.” in *IHS Jane’s All the World's Aircraft*.

Jenkinson, L. R., P. Simpkin, and D. Rhodes. 1999. *Civil Jet Aircraft Design*. Butterworth Heinemann.

Lasa Carrillo, M. 2014. “Preliminary Performance and Contrail Formation Assessments of a HWB Aircraft Using Distributed Propulsion System with LH2 Fuel.” (August):2013–14.

Laskaridis, Panagiotis, Pericles Pilidis, and Petros Kotsiopoulos. 2005. “An Integrated Engine--Aircraft Perfomance Platform for Assessing New Technologies in Aeronautics.” *Isabe 2005* 1–13.

Lawson, C. 2016. “Introduction to Aircraft Performance.” in *Propulsion Systems Performance and Intengration Vol 2*. Cranfield University.

Lee, David S. et al. 2009. “Aviation and Global Climate Change in the 21st Century.” *Atmospheric Environment* 43(22-23):3520–37.

Lefebvre, A. H. and D. R. Ballal. 2010. *Gas Turbine Combustion: Alternative Fuels and Emissions*. Third.

Mannstein, Hermann and Ulrich Schumann. 2005. “Aircraft Induced Contrail Cirrus over Europe.” *Meteorologische Zeitschrift* 14(4):549–54.

McAlpine, Alan. 2016. “‘Buzz-Saw’ noise and Nonlinear Acoustics.” Retrieved July 12, 2016 (http://www.southampton.ac.uk/engineering/research/projects/buzz_saw_noise_and_non_linear_acoustics.page#project_overview).

Meerkötter, R. et al. 1999. “Radiative Forcing by Contrails.” *Annales Geophysicae* 17(8):1080–94.

Minnis, P. 2003. “Contrails.” *Elsevier Science* 509–20.

Myhre, Gunnar and F. Stordal. 2001. “On the Tradeoff of the Solar and Thermal Infrared Radiative Impacts of Contrails.” *Geophysical Research Letters* 28(16):3119–22.

Nikolaidis, Theoklis. 2015. *The Turbomatch Scheme*. 1.1 for v2. Cranfield University.

Noppel, F. G., D. Lucisano, and R. Singh. 2009. “Performance of the Clean Exhaust Engine Concept.” *Journal of Engineering for Gas Turbines and Power* 131(3):031201.

Noppel, F. G., R. Singh, and D. Taylor. 2012. “Method and Apparatus for Suppressing AeroEngine Contrails.” (594/2012).

Noppel, Frank G. 2007. “Contrail and Cirrus Cloud Avoidance Technology.” Cranfield University.

Padfield, Tim. n.d. “Equations Describing the Physical Properties of Moist Air - Conservation Physics.” Retrieved July 2, 2016 (http://www.conservationphysics.org/atmcalc/atmoclc2.pdf).

Paoli, Roberto and Karim Shariff. 2016. “Contrail Modeling and Simulation.” *Annual Review of Fluid Mechanics* 48(1):393–427.

Penner, Joyce E., David H. Lister, David J. Griggs, David J. Dokken, and Mack McFarland. 1999. “Aviation and the Global Atmosphere: A Special Report of IPCC Working Groups ....” 373.

Qureshi, Sarah. 2016. “Contrail-Free Aero-Engines (Unpublished).” Cranfield University.

Riebeek, Holli. 2010. “Global Warming.” *NASA- Earth Observatory*. Retrieved June 26, 2016 (http://earthobservatory.nasa.gov/Features/GlobalWarming).

Roig Medina, Marcel. 2014. “Contrail Avoidance Technologies- The Use of Liquid Hydrogen in Aero Gas Turbines.”

Rolls-Royce. 2016. “Trent 900 Overview.” Retrieved July 12, 2016 (http://www.rolls-royce.com/products-and-services/civil-aerospace/products/civil-large-engines/trent-900.aspx#overview).

Runge-Metzger, Artur. 2011. “Aviation and Emissions Trading.” *ICAO Council Briefing* (September). Retrieved June 26, 2016 (http://ec.europa.eu/clima/policies/transport/aviation/docs/presentation_icao_en.pdf).

SAE, Society of Automotive Engineers. 2004. *Aircraft Propulsion System Performance Station Designation and Nomenclature - Aerospace Standard AS755*.

Schrader, ML. 1997. “Calculations of Aircraft Contrail Formation Critical Temperatures.” *Journal of Applied Meteorology* 1725–29.

Schumann, Ulrich. 1996. “On Conditions for Contrail Formation from Aircraft Exhausts.” *Meteorol. Zeitschrift* 5:4–23.

Schumann, Ulrich. 2000. “Influence of Propulsion Efficiency on Contrail Formation.” *Aerospace Science Technology* 4:391–401.

Schumann, Ulrich. 2005. “Formation, Properties and Climatic Effects of Contrails.” *Comptes Rendus Physique* 6(4-5 SPEC. ISS.):549–65.

Schwartz Dallara, Emily, Ilan M. Kroo, and Ian A. Waitz. 2011. “Metric for Comparing Lifetime Average Climate Impact of Aircraft.” *AIAA Journal* 49(8):1600–1613.

Shine, Keith P. and Piers M. De F. Forster. 1999. “The Effect of Human Activity on Radiative Forcing of Climate Change: A Review of Recent Developments.” *Global and Planetary Change* 20(4):205–25.

Shine, Keith P., Jan S. Fuglestvedt, Kinfe Hailemariam, and Nicola Stuber. 2005. “Alternatives to the Global Warming Potential for Comparing Climate Impacts

of Emissions of Greenhouse Gases." *Climatic Change* 68(3):281–302.

Singh, S. 1988. "Method of Suppressing Formation of Contrails and Dilutions Therefor."

Stuber, Nicola, Piers Forster, Gaby Rädel, and Keith Shine. 2006. "The Importance of the Diurnal and Annual Cycle of Air Traffic for Contrail Radiative Forcing." *Nature* 441(7095):864–67.

Turgut, E. T. and M. A. Rosen. 2011. "Emission Assessment of Aviation." Pp. 20–72 in *Technology Engineering and Management in Aviation: Advancements and Discoveries*.

Waitz, Ian A. 2008. *The Breguet Range Equation - MIT*.

Williams, Victoria and Robert B. Noland. 2005. "Variability of Contrail Formation Conditions and the Implications for Policies to Reduce the Climate Impacts of Aviation." *Transportation Research Part D: Transport and Environment* 10(4):269–80.

Williams, Victoria, Robert B. Noland, and Ralf Toumi. 2002. "Reducing the Climate Change Impacts of Aviation by Restricting Cruise Altitudes." *Transportation Research Part D: Transport and Environment* 7(6):451–64.

APPENDICES

Appendix A Turbomatch

In this section, the Turbomatch input code is presented, in which the design point and take-off off design point are included.

A.1 Input code

```
HIGH BYPASS TURBOFAN ENGINE PERFORMANCE SIMULATION
Rolls-Royce THREE - SPOOL Trent 970-84
Modelled by: Fernando Lartategui Atela
Date: 01-May-2016

////
OD SI KE VA FP
-1
-1
INTAKE      S1,2          D1-6          R200
COMPRE      S2,3          D7-18         R202          V7  V8
PREMAS      S3,4,21       D19-22
PREMAS      S4,5,16       D23-26                      V23
DUCTER      S16,17        D27-31        R204
NOZCON      S17,18,1      D32-33        R206
COMPRE      S5,6          D34-45        R208          V34 V35
PREMAS      S6,7,22       D46-49
COMPRE      S7,8          D50-61        R210          V50 V51
PREMAS      S8,9,19       D62-65
DUCTER      S19,20        D66-70        R211
BURNER      S9,10         D71-78        R212
MIXEES      S10,20,11
TURBIN      S11,12        D79-93                      V80
TURBIN      S12,13        D94-108                     V95
TURBIN      S13,14        D109-123                    V110
NOZCON      S14,15,1      D124-125      R216
PERFOR      S1,0,0        D126-129,216,200,212,206,0,204,0,0,0
CODEND

DATA ITEMS ////
1 10670.0     ! INTAKE: Altitude [m]
2 0.0         ! Deviation from ISA temperature [K]
3 0.85        ! Mach number
4 0.99        ! Pressure recovery
5 0.0         ! Deviation from ISA pressure [atm]
6 0.0         ! Relative humidity [%]

7 0.85        ! FAN I: Z = (R-R[choke])/(R[surge]-R[choke])
```

```
8 1.0          ! Relative rotational speed PCN
9 1.65550      ! DP Pressure ratio
10 0.89836     ! DP ETA
11 0.0         ! Error selection
12 1.0         ! Compressor map number
13 1.0         ! Shaft number
14 1.0         ! PR degradation scaling factor
15 1.0         ! NDMF degradation scaling factor
16 1.0         ! ETA degradation scaling factor
17 -1.0        ! Effective component volume [m^3] (only for transient)
18 0.0         ! Stator angle (VSV) relative to DP

19 0.99731     ! PREMAS: LAMDA W Fan Bleed (Wout1/Win) [0.269%]
20 0.0         ! DELTA W
21 1.0         ! LAMBDA P
22 0.0         ! DELTA P

23 0.10331     ! PREMAS: LAMDA W Fan Bypass 8.68 (Wout1/Win) [1/9.68]
24 0.0         ! DELTA W
25 1.0         ! LAMBDA P
26 0.0         ! DELTA P

27 0.0         ! DUCTER: Switch 0: no reheating/intercooling
28 0.01        ! Total pressure loss:DELTA(P)/Pin=1%
29 0.0         ! Combustion efficiency (if BD(1)=1 or 2)
30 0.0         ! Limiting value for Fuel Flow: no = 100000
31 -1.0        ! Effective component volume [m^3] (only for transient)

32 -1.0        ! CONVERGENT NOZZLE: = "-1" exit area is fixed)
33 1.0         ! Scaling factor

34 0.85        ! IP COMP: I: Z = (R-R[choke])/(R[surge]-R[choke])
35 1.0         ! Relative rotational speed PCN
36 4.00000     ! DP Pressure ratio
37 0.8998      ! DP ETA
38 1.0         ! Error selection
39 4.0         ! Compressor map number
40 2.0         ! Shaft number
41 1.0         ! PR degradation scaling factor
42 1.0         ! NDMF degradation scaling factor
43 1.0         ! ETA degradation scaling factor
44 -1.0        ! Effective component volume [m^3] (only for transient)
45 0.0         ! Stator angle (VSV) relative to DP

46 0.98087     ! PREMAS: LAMDA W Customer bleed (Wout1/Win) [1.913%]
47 0.0         ! DELTA W
48 1.0         ! LAMBDA P
49 0.0         ! DELTA P
```

```
50 0.85       ! HP COMPRESSOR I: Z = (R-R[choke])/(R[surge]-R[choke])
51 1.0        ! Relative rotational speed PCN
52 6.43693    ! DP Pressure ratio
53 0.90000    ! DP ETA
54 1.0        ! Error selection
55 5.0        ! Compressor map number
56 3.0        ! Shaft number
57 1.0        ! PR degradation scaling factor
58 1.0        ! NDMF degradation scaling factor
59 1.0        ! ETA degradation scaling factor
60 -1.0       ! Effective component volume [m^3] (only for transient)
61 0.0        ! Stator angle (VSV) relative to DP

62 0.80894    ! PREMAS: LAMDA W Cooling bypass (Wout1/Win) [19.106%]
63 0.0        ! DELTA W
64 1.0        ! LAMBDA P
65 0.0        ! DELTA P

66  0.0       ! Reheat selector
67  0.01      ! Pressure loss 1%
68  0.0       ! Reheat comb efficiency
69  0.0       ! Max reheat fuel flow
70 -1.0       ! Effective component volume [m^3] (only for transient)

71 0.06       ! COMBUSTOR: Pressure loss (=DP/P inlet total)
72 0.998      ! Combustion efficiency
73 -1.0       ! Fuel flow (if -1.0, TET must be defined)
74 0.0        ! (>0) Water flow [kg s-1 or lb s-1] or (<0) WAR
75 288        ! Temperature of water stream [K]
76 0.0        ! Phase of water (0=liquid, 1=vapour)
77 1.0        ! ETA degradation scaling factor
78 -1.0       ! Effective component volume [m^3] (only for transient)

              ! MIXEES: no brick data

79 0.0        ! HP TURBINE: Auxiliary or power output [W]
80 0.8        ! Relative to max enthalpy drop to temperature ratio:ZT
81 0.6        ! Relative non-dim speed CN
82 0.92097    ! DP ETA
83 -1.0       ! Relative non-dim PCN (= -1 for compressor turbine)
84 3.0        ! Shaft Number (for power turbine, the value 0 is used)
85 5.0        ! Turbine map number
86 -1.0       ! Power law index "n" (POWER = PCN^n)
87 1.0        ! TF degradation scaling factor
88 1.0        ! DH degradation scaling factor
89 1.0        ! ETA degradation scaling factor
90 -1.0       ! Rotor rotational speed [RPS] (only for transient)
```

```
91 -1.0         ! Rotor moment of inertia [kg.m^2] (only for transient)
92 -1.0         ! Effective component volume [m^3] (only for transient)
93 0.0          ! NGV angle, relative to D.P.

94 0.0          ! IP TURBINE: Auxiliary or power output [W]
95 0.8          ! Relative to max enthalpy drop to temperature ratio:ZT
96 0.6          ! Relative non-dim speed CN
97 0.91021      ! DP ETA
98 -1.0         ! Relative non-dim PCN (= -1 for compressor turbine)
99 2.0          ! Shaft Number (for power turbine, the value 0 is used)
100 5.0         ! Turbine map number
101 -1.0        ! Power law index "n" (POWER = PCN^n)
102 1.0         ! TF degradation scaling factor
103 1.0         ! DH degradation scaling factor
104 1.0         ! ETA degradation scaling factor
105 -1.0        ! Rotor rotational speed [RPS] (only for transient)
106 -1.0        ! Rotor moment of inertia [kg.m^2] (only for transient)
107 -1.0        ! Effective component volume [m^3] (only for transient)
108 0.0         ! NGV angle, relative to D.P.

109 0.0         ! LP TURBINE: Auxiliary or power output [W]
110 0.8         ! Relative to max enthalpy drop to temperature ratio:ZT
111 0.6         ! Relative non-dim speed CN
112 0.92934     ! DP ETA
113 -1.0        ! Relative non-dim PCN (= -1 for compressor turbine)
114 1.0         ! Shaft Number (for power turbine, the value 0 is used)
115 5.0         ! Turbine map number
116 -1.0        ! Power law index "n" (POWER = PCN^n)
117 1.0         ! TF degradation scaling factor
118 1.0         ! DH degradation scaling factor
119 1.0         ! ETA degradation scaling factor
120 -1.0        ! Rotor rotational speed [RPS] (only for transient)
121 -1.0        ! Rotor moment of inertia [kg.m^2] (only for transient)
122 -1.0        ! Effective component volume [m^3] (only for transient)
123 0.0         ! NGV angle, relative to D.P.

124 -1.0        ! CONVERGENT NOZZLE: = "-1" exit area is fixed)
125 1.0         ! Scaling factor

126 -1.0        ! ENGINE RESULTS: Power output (= -1 for aero engine)
127 -1.0        ! Propeller efficiency (= -1 for turbojet/turbofan)
128 0.0         ! Scaling index ("1" = scaling, "0" = no scaling)
129 0.0         ! Only for scaling: Required DP net thrust/shaft power
-1
1 2 518.7613          ! item 2 at station 1 = Mass flow(kg/s)
10 6 1603.5774        ! item 6 at station 10 = Total temperature (K)
-1                    ! End of DP data
```

1 0.0 !Take-Off (OD Point)
3 0.0
-1
10 6 1743.38933
-1
-3

Appendix B Hermes

In this appendix, the geometric, mission and engine specification data Hermes input is presented.

B.1 Geometric, mission and engine specification data

```
!Input file for the geometric, mission and engine specifications of the aircraft
Aircraft inspired by A380-841; Engine inspired by Trent 970-84
ENGINE_SPEC: RR_Trent970-84-DP
Modelled by: Fernando Lartategui Atela – Modified from (Qureshi 2016) A380-800 input file.
Date: 14-May-2016

!GEOMETRIC DETAILS
! Wing Geometry
845             ! AcWingAInit - Wing area
7.5             ! AcWingAspr - Aspect ratio
0.203           ! AcWingCThir - Thickness chord ratio
33.5            ! AcWingSwpa - Sweep angle (in degrees)
0.26            ! AcWingTpr - Taper ratio
0.132           ! AcWingRtThir - Root thinkness ratio
0.087           ! AcWingOtThir - Outer thikness ratio
! Tailplane Geometry
222.57          ! AcTailAInit - Tailplane area
4.4             ! AcTailAspr - Aspect ratio
0.203           ! AcTailCThir - Thickness chord ratio
30              ! AcTailSwpa - Sweep angle (in degrees)
0.383           ! AcTailTpr - Taper ratio
0.132           ! AcTailRtThir - Root thinkness ratio
0.087           ! AcTailOtThir - Outer thikness ratio
! Fin Geometry
134.2           ! AcFinA - Fin area
28.99           ! AcFinSpan - Span
0.115           ! AcFinCThir - Thickness chord ratio
28.99           ! AcFinSwpa - Sweep angle (in degrees)
0.424           ! AcFinTpr - Taper ratio
0.132           ! AcFinRtThir - Root thinkness ratio
0.087           ! AcFinOtThir - Outer thikness ratio
! Fuselage Geometry
7.14            ! AcFusDia - Diameter
70.4            ! AcFusLen - Length
! Landing Gear Characteristics - ***0=default, 1=Bogie, 2=Small twin wheel***
2               ! AcLGTyp1 - Landing gear type
1               ! AcLgTyp2= 0,1,2
1               ! AcLgTyp3= 0,1,2
1               ! AcLgTyp4= 0,1,2,-1 *** -1=if the aircraft only has 3 LG
1               ! AcLgTyp5= 0,1,2,-1 *** -1=if the aircraft only has 3 LG
```

2 ! AcLGDepl - Number of segments with LG down for descent
! High lift systems
1 ! AcFlapSegTo -No of Seg with flaps deployed during TO
3 ! AcFlapSegApp - No of Seg with flaps deployed for approach
2 ! ACFlapSegLand - No of Seg with flaps deployed for Landing
1.10 ! AcExtSrTo - Wing area extension ratio TO
1.15 ! AcExtSrApp - Wing area extension ratio approach
1.20 ! AcExtSrLand - Wing area extension ratio Landing
5.0 ! AcFlapAngleTo - Flap Angle TO IN DEGREES
20.0 ! AcFlapAngleApp - Flap Angle Approach
30.0 ! AcFlapAngleLand - Flap Angle Land
1 ! AcFlapSlots - Number of Flap Slots (1-3)
! Engine Geometry
3.944 ! EngNacDiaInit - Diameter (EASA 2013)
5.4775 ! EngNacLenInit - Length (EASA 2013)
!XXXXXXXXXXXXXXXXXXXXXXXXXXXXXXXXXXXXXXXXXXXXX
!MISSION/WEIGHT SPECIFICATION DATA
245026 ! AcAfrWtInit - Airframe weight [A380-841] (Jane's 2015)
4 ! AcEngNb - Number of Engines
6246 ! EngWtInit - Engine weight, (kg/engine) (EASA 2013)
83700 ! AcPldWt - Payload weight, (kg)
100000 ! AcFuelWtInit - Fuel weight, (kg)
83700 ! AcPldWtmax - Max payload weight, kg [A380-841] (Airbus 2014)
259465 ! AcFuelWtmax - Max fuel weight, kg [standard] (Jane's 2015)
385995 !AcLandWtmax - Max landing weight, kg [A380-800] (Jane's 2015)
560000 ! AcToWtmax - Max take-off weight, kg [A380-800] (Jane's 2015)
0.0 ! DVFuelRatio - Diversion fuel weight to total fuel weight (%)
0.05 ! AcFuelContpc - Relative contingency fuel to remain after landing (%)
12335 ! AcRng - Range to be flown (km) ! Mission (2)
300. ! AcRngdv - Diversion Range to be flown (km)
2 ! AcMisType - Mission to be flown (1-fixed fuel get range) or (2-fixed range for given Pload get fuel)
1 ! DvMission - specify if diversion mission is to be run (1- NO diversion mission) or (2- YES to diversion mission)
!XXXXXXXXXXXXXXXXXXXXXXXXXXXXXXXXXXXXXXXXXXXXX
!CRUISE MAIN/DIVERSION AND HOLDING DATA
1 ! number of cruise altitudes and Mach numbers
1 ! number of cruise Temperature Deviations from ISA day (the trip is splitted equally into this number of parts. Every part has the respective DTisa)
1 ! number of diversion cruise altitudes
2 ! Cruise small segment time Interval in (min). This value affects the accuracy of the calculations, so keep it small.
10670 ! Cruise altitudes in [m] (WARNING: THE ALTITUDES CANNOT BE THE SAME)
0.85 ! Cruise Mach numbers, the same number with cruise altitudes
0 ! Cruise ambient temperature deviation from ISA, in [K]
6096 ! Diversion cruise altitudes (m)

```
0.65            ! Diversion cruise Mach numbers,
0               ! Diversion cruise ambient temperature deviation from ISA, in [K]
457.0           ! Holding altitude (m)
30.         ! Hold Time in (min)
!XXXXXXXXXXXXXXXXXXXXXXXXXXXXXXXXXXXXXXXXXXXXXXXXXXX
!CLIMB DATA
22              ! Climb segments Number
! Altitudes(m)| DTisa(K) | EAS(knots) | Power(0.-1.)
557.2           0 0.            250.            1.
900.0           0 0.            250.            1.
1500.0          0 0.            250.            1.
1981.2          0 0.            250.            1.
2438.4          0 0.            250.            1.
2743.2          0 0.            250.            1.
3048.0          0 0.            250.            1.
3048.1          0 0.            320.            1.
3657.6          0 0.            320.            1.
4267.2          0 0.            320.            1.
4876.8          0 0.            320.            1.
5486.4          0 0.            320.            1.
6096.0          0 0.            320.            1.
7620.0          0 0.            320.            1.
8077.2          0 0.            320.            1.
9144.0          0 0.            320.            1.
10058.0         0 0.            320.            1.
10668.0         0 0.            320.            1.
11227.0         0 0.            320.            1.
11887.0         0 0.            320.            1.
12000.0         0 0.            320.            1.
12496.8         0.0.            320.            1.
!XXXXXXXXXXXXXXXXXXXXXXXXXXXXXXXXXXXXXXXXXXXXXXXXXXX
!DESCENT DATA
10              ! Descent segments Number
! The altitudes are dependent on the final cruise altitude. So they are calculated
inside the code.
! DTisa(K)     | TAS(knots) | Power(0.-1.) ****Note: the last 3 power settings use
the Approach rating
0.              233.1           1.                  ! Flight Idle Rating
0.              221.5           1.                  ! Flight Idle Rating
0.              202.9           1.                  ! Flight Idle Rating
0.              195.0           1.                  ! Flight Idle Rating
0.              183.1           1.                  ! Flight Idle Rating
0.              164.7           1.                  ! Flight Idle Rating
0.              150.9           1.                  ! Flight Idle Rating
0.              140.0           1.                  ! Approach Rating
0.              135.0           1.                  ! Approach Rating
0.              135.0           1.                  ! Approach Rating
!XXXXXXXXXXXXXXXXXXXXXXXXXXXXXXXXXXXXXXXXXXXXXXXXXXX
```

```
!LANDING DATA
0.01            ! Note: Do not put final landing altitude = 0.0, use a very small value
instead.
135.00          ! Approach speed (TAS), in [m/s]
0.00            ! Deviation from standard atmosphere for Landing in [K]
6.00            ! Duration of Landing phase in [min]
!XXXXXXXXXXXXXXXXXXXXXXXXXXXXXXXXXXXXXXXXXXXXXX
!TAXI and TAKE-OFF DATA
0.02            ! AcTaxiCf1 - Runway Friction Coefficient
0.3             ! AcTaxiCf2 - Runway Friction Coefficient, BREAKES-OFF
10.0            ! AcTaxiTime - Taxi time in [min] (12mins for LR, 9mins for SR)
1.0             ! AcToTime - Take-off time in [min]
0.00            ! AcToALT - Take-off altitude in [m]
0.00            ! Take-off temperature deviation from ISA in [K]
0.0             ! TakeOff Derate (Real Values from 0 to 1, 0.0->100% of Maximum
Thrust, 1.0->0% of Maximum Thrust)
!XXXXXXXXXXXXXXXXXXXXXXXXXXXXXXXXXXXXXXXXXXXXXX
!NUMERICAL TOLERANCES AND INITIAL GUESSES
1.D-11              ! Climb and Descent internal loops relative accuracy
1.D-09              ! Main mission range relative accuracy
1.D-09              ! Diversion mission range relative accuracy
1.D-07              ! Fuel weight outer iteration loop relative accuracy
480.D00             ! Main mission duration guess 1 (for secant method, modify
it only if there is a convergence problem)
260.D00             ! Main mission duration guess 2 (for secant method, modify
it only if there is a convergence problem)
!XXXXXXXXXXXXXXXXXXXXXXXXXXXXXXXXXXXXXXXXXXXXXX
!TMATCHCALLS SPECIFICATIONS (*****HERMES DOES NOT READ THIS
PART*****)
!-------------------------------------------------------------------------
!Number of points in the Engine Design Point input file to be skipped
!before the mission profile starts (including the design point)
1
!-------------------------------------------------------------------------
!Burner exit station number
10
!-------------------------------------------------------------------------
!ENGINE TET RANGE FOR EACH PHASE
3               ! TET number for Take Off
4               ! TET number for Climb
24              ! TET number for Main and Diversion Cruise
2               ! TET number for Flight Idle (Descent) and Ground Idle
3               ! TET number for Approach
10.             ! TET step change in [K] for Take Off
10.             ! TET step change in [K] for Climb
5.              ! TET step change in [K] for Main and Diversion Cruise
25.             ! TET step change in [K] for Flight Idle (Descent) and Ground Idle
25.             ! TET step change in [K] for Approach
```

```
1750.           ! Max TET in [K] for Take Off
1740.           ! Max TET in [K] for Climb
1680.           ! Max TET in [K] for Main Mission Cruise
1250.           ! Max TET in [K] for Flight Idle (Descent) and Ground Idle
1325.           ! Max TET in [K] for Approach
!-------------------------------------------------------------------------
!ADDITIONAL ENGINE PERFORMANCE STATION VECTOR DATA (STATION, ITEM)
1               ! Number of additional engine performance station vector data
!Station | Item
10 6
!-------------------------------------------------------------------------
!ADDITIONAL ENGINE PERFORMANCE BRICK DATA (DESCRIPTION, BRICK NO, ITEM)
1               ! Number of additional engine performance brick data
!Description | BrickNo | Item        (WARNING: The BrickNo is defined according to the tabular output file of Turbomatch )
HPC_PCN 8 2
!-------------------------------------------------------------------------
!ADDITIONAL OFF DESIGN ENGINE CONFIGURATIONS (LIKE BLEEDS etc.)
!Specify additional off design specification for each flight phase (e.g. for brick data 26 "26 0.95")
0               ! Number of additional off design specifications for each flight phase
!INPUT AND OUTPUT FILE PATHS
!Engine Design Point Specification file (input to Hermes)
RR_Trent970-84-DP.dat
```

Appendix C Radiative forcing analysis

Tables of the radiative forcing model to analyse the Global Warming impact of aviation are provided in this Appendix.

C.1 Future scenarios radiative forcing

In this section, the radiative forcing of years 2005, 2020 and 2050 is provided in Table C-3. In the case of the year 2050, four different situations are presented depending on the overall aviation growth and on the engine technology level. The meaning of the abbreviation of each situation is given in Table C-1. In addition, the fuel consumption of aviation is forecasted for the future scenarios and provided in Table C-2. The data given in Table C-3 was extracted from reference (Lee et al. 2009). Although other documents, like reference (Chen and Gettelman 2016), provided the radiative forcing of contrails and AIC in future scenarios, they were not selected as they did not give RF information about CO_2 and other aviation emissions. Moreover, the RF data of aviation emissions in the year 2005 was provided in reference (Lee et al. 2009) are very accurate according to other documents. Even the RF of AIC mean value is very precise in accordance with reference (Burkhardt and Kärcher 2011). When AIC are included in the RF of total aviation, linear contrails are not considered. Finally, the percentage to the right of the columns shows the increase of radiative forcing of the emission since 2005.

A1	Upper-range overall growth of aviation
B2	Mid-range overall growth of aviation
t1	Advances in airframe and engine technology follow current trend
t2	More emphasis is placed on reducing NO_x to the CO_2 detriment

Table C-1: Abbreviation of different scenarios in 2050

Scenario	2005	2020	2050 A1t1	2050 A1t2	2050 B2t1	2050 B2t2
Fuel (Tg/year)	232.4	336	816	844.9	568.8	588.9

Table C-2: Aviation fuel consumption of the different scenarios (Lee et al. 2009)

	CO2	Ozone	Methane	Total NOx	Water vapour	Sulphate aerosol	Soot aerosol	Linear contrail	AIC (included contrails)	Total aviation (excluded AIC)	Total aviation (included AIC)
2005	0.0280	0.0263	-0.0125	0.0138	0.0028	-0.0048	0.0034	0.0118	0.0330	0.0550	0.0762
2020	0.0408 46%	0.0406 54%	-0.0192 54%	0.0214 55%	0.0040 43%	-0.0070 46%	0.0050 47%	0.0202 71%	0.0470 42%	0.0844 53%	0.1112 46%
2050 A1t1	0.0763 173%	0.1098 317%	-0.0520 316%	0.0578 319%	0.0097 246%	-0.0169 252%	0.0121 256%	0.0554 369%	0.1140 245%	0.1944 253%	0.253 232%
2050 A1t2	0.0777 178%	0.0853 224%	-0.0404 223%	0.0449 225%	0.0100 257%	-0.0175 265%	0.0125 268%	0.0554 369%	0.1180 258%	0.1830 233%	0.2456 222%
2050 B2t1	0.0733 162%	0.0765 191%	-0.0363 190%	0.0402 191%	0.0067 139%	-0.0118 146%	0.0084 147%	0.0372 215%	0.0800 142%	0.1540 180%	0.1968 158%
2050 B2t2	0.0745 166%	0.0594 126%	-0.0282 126%	0.0312 126%	0.0070 150%	-0.0122 154%	0.0087 156%	0.0372 215%	0.0820 148%	0.1464 166%	0.1912 151%

Table C-3: Radiative forcing of aviation emissions in years 2005, 2020 and 2050 Adopted from (Lee et al. 2009)

	CO2	Water vapour	Linear contrail	AIC (included contrails)	Total aviation (excluded AIC)	Total aviation (included AIC)
2005	0.0280	0.0028	0.0118	0.0330	0.0550	0.0762
2020*	0.0430 54%	0	0	0	0.0624 13%	0.0624 -18%
2050 A1t1*	0.0847 202%	0	0	0	0.1377 150%	0.1377 81%
2050 A1t2*	0.0863 208%	0	0	0	0.1262 129%	0.1262 66%
2050 B2t1*	0.0812 190%	0	0	0	0.1180 114%	0.1180 55%
2050 B2t2*	0.0826 195%	0	0	0	0.1103 100%	0.1103 45%

Table C-4: Radiative forcing of aviation emissions if contrails are prevented in 2005

	CO2	Water vapour	Linear contrail	AIC (included contrails)	Total aviation (excluded AIC)	Total aviation (included AIC)
2005	0.0280	0.0028	0.0118	0.0330	0.0550	0.0762
2020	0.0408 46%	0.0040 43%	0.0202 71%	0.0470 42%	0.0844 53%	0.1112 46%
2050 A1t1**	0.0825 194%	0	0	0	0.1355 146%	0.1355 78%
2050 A1t2**	0.0841 200%	0	0	0	0.1240 125%	0.1240 63%
2050 B2t1**	0.0789 182%	0	0	0	0.1157 110%	0.1157 52%
2050 B2t2**	0.0803 187%	0	0	0	0.1080 96%	0.1080 42%

Table C-5: Radiative forcing of aviation emission if contrails are prevented in 2020

C.2 Radiative forcing scenarios- Contrails avoided in 2005

If contrails are avoided in 2005, the radiative forcing of some emissions varies according to the assumptions stated in the methodology. The new radiative forcing of total aviation and these pollutants since 2005 is given in Table C-4. The radiative forcing of the not mentioned aviation emissions was considered constant. Finally, the percentage to the right of the columns shows the increase of radiative forcing of the emission since 2005.

C.3 Radiative forcing scenarios- Contrails avoided in 2020

If contrails are avoided in 2020, the radiative forcing of some emissions varies according to the assumptions stated in the methodology. The new radiative forcing of total aviation and these pollutants since 2020 is given in Table C-5. The radiative forcing of the not mentioned aviation emissions was considered constant. Finally, the percentage to the right of the columns shows the increase of radiative forcing of the emission since 2005.

C.4 Data for the creation of the bar charts

The data used for the creation of the bar charts is provided in this appendix section, more specifically from Table C-6 to Table C-8. In addition, the percentage change of the radiative forcing from the first case, which is contrails are not avoided, is included in the right hand column of the radiative forcing of the last two cases.

CO2	***Contrails***	***No contrails 2005***		***No contrails 2020***	
2005	0.0280	0.0280	0.0%	0.0280	0.0%
2020	0.0408	0.0430	5.4%	0.0408	0.0%
2050 A1t1	0.0763	0.0847	11.0%	0.0825	8.1%
2050 A1t2	0.0777	0.0863	11.1%	0.0841	8.2%
2050 B2t1	0.0733	0.0812	10.7%	0.0789	7.7%
2050 B2t2	0.0745	0.0826	10.8%	0.0803	7.8%

Table C-6: CO2 radiative forcing of the different future scenarios for the three assumed cases

Total (no AIC)	*Contrails*	*No contrails 2005*		*No contrails 2020*	
2005	0.0550	0.0550	0.0%	0.0550	0.0%
2020	0.0844	0.0624	-26.0%	0.0844	0.0%
2050 A1t1	0.1944	0.1377	-29.2%	0.1355	-30.3%
2050 A1t2	0.183	0.1262	-31.0%	0.1240	-32.2%
2050 B2t1	0.154	0.1180	-23.4%	0.1157	-24.8%
2050 B2t2	0.1464	0.1103	-24.7%	0.1080	-26.2%

Table C-7: Total aviation radiative forcing of the different future scenarios for the three assumed cases (AIC not considered)

Total (AIC)	*Contrails*	*No contrails 2005*		*No contrails 2020*	
2005	0.0762	0.0762	0.0%	0.0762	0.0%
2020	0.1112	0.0624	-43.9%	0.1112	0.0%
2050 A1t1	0.253	0.1377	-45.6%	0.1355	-46.5%
2050 A1t2	0.2456	0.1262	-48.6%	0.1240	-49.5%
2050 B2t1	0.1968	0.1180	-40.1%	0.1157	-41.2%
2050 B2t2	0.1912	0.1103	-42.3%	0.1080	-43.5%

Table C-8: Total aviation radiative forcing of the different future scenarios for the three assumed cases (AIC considered)

C.5 AIC radiative forcing sensitivity analysis

In this appendix, the radiative forcing of total aviation of the three assumed cases is calculated considering the minimum and maximum values of the 90% confidence range of the AIC radiative forcing. These values were extracted from reference (Lee et al. 2009). Accordingly, Table C-9 is designed using the minimum values of AIC radiative forcing, while Table C-10 is created using the maximum values of AIC radiative forcing.

In addition, the percentage change of the radiative forcing from the first case, which is contrails are not avoided, is included in the right hand column of the two last cases' radiative forcing.

Total (AIC)	*Contrails*	*No contrails 2005*		*No contrails 2020*	
2005	0.0557	0.0557	0.0%	0.0557	0.0%
2020	0.0802	0.0624	-22.2%	0.0802	0.0%
2050 A1t1	0.1770	0.1377	-22.2%	0.1355	-23.5%
2050 A1t2	0.1666	0.1262	-24.2%	0.1240	-25.6%
2050 B2t1	0.1438	0.1180	-18.0%	0.1157	-19.5%
2050 B2t2	0.1362	0.1103	-19.0%	0.1080	-20.7%

Table C-9: Total aviation radiative forcing of the different future scenarios for the three assumed cases (AIC considered) [Minimum AIC RF values]

Total (AIC)	*Contrails*	*No contrails 2005*		*No contrails 2020*	
2005	0.1299	0.1299	0.0%	0.1299	0.0%
2020	0.1892	0.0624	-67.0%	0.1892	0.0%
2050 A1t1	0.4440	0.1377	-69.0%	0.1355	-69.5%
2050 A1t2	0.4426	0.1262	-71.5%	0.1240	-72.0%
2050 B2t1	0.3288	0.1180	-64.1%	0.1157	-64.8%
2050 B2t2	0.3292	0.1103	-66.5%	0.1080	-67.2%

Table C-10: Total aviation radiative forcing of the different future scenarios for the three assumed cases (AIC considered) [Maximum AIC RF values]